ISSN 1173-5996

DESIGN OF LOADBEARING LIGHT STEEL FRAME WALLS FOR FIRE RESISTANCE

BY

J T (HANS) GERLICH

Supervised by

Dr Andrew H Buchanan

Fire Engineering Research Report 95/3
August 1995

This report was presented as a project report
as part of the M.E.(Fire) degree at the University of Canterbury

School of Engineering
University of Canterbury
Private Bag 4800
Christchurch, New Zealand

Phone 643 366-7001
Fax 643 364-2758

ABSTRACT

Light steel frame (LSF) building systems are becoming more prevalent in commercial, industrial and residential construction in New Zealand. Tested fire resistance ratings are generally available for non-loadbearing LSF drywall systems lined with gypsum plasterboard. No test information exists for loadbearing systems. Current solutions are based on limiting steel temperature.

This study investigates the parameters which affect the performance of loadbearing LSF drywall systems exposed to fire. Structural design codes for cold-formed steel members are compared. Methods are presented for calculating the reduction of steel strength and stiffness at elevated temperatures, and for predicting the deformations resulting from temperature gradients and P-Δ effects. Heat transfer modelling by computer is used to predict steel framing temperatures for systems exposed to the standard ISO834 time-temperature curve and real fires. Three full-scale furnace tests were carried out to evaluate analytical predictions.

A model is proposed for predicting the performance of loadbearing LSF systems exposed to fire. Results are within 80-90% of test results. The current practice of designing to a limiting steel temperature results in unduly conservative predictions, particularly for systems with low applied axial loads. It was also found that fire tests may give non-conservative results for systems with low stud loads due to frictional restraints.

ACKNOWLEDGEMENTS

The research described in this report was carried out at the fire research facilities of Building Technology Limited, Wellington. Financial support was provided by the Foundation for Research, Science and Technology from the Public Good Science Fund.

Completion of the project would not have been possible without the assistance of the following people and organisations.

I would like to thank my supervisor Dr Andrew Buchanan of the University of Canterbury for his inspiration, guidance and enthusiasm. Thanks also to PhD student Geoff Thomas for his assistance with TASEF heat transfer modelling.

All the staff at Building Technology Limited have been most helpful. In particular I would like to thank Dennis Waple for welcoming me and making me feel at home for the duration of the project, Peter Collier for sharing his knowledge, experience and office with me, Graham Cowles for kick-starting me on TASEF, Roger Shelton for checking the spreadsheets, and the technical staff in the structures and fire laboratories for their help with testing and data acquisition.

My employer Winstone Wallboards has been most supportive. Special thanks are due to Neil Gunn and Kevin Golding for making it all possible. Please accept my apologies for all the 'evasions' during the ME course year.

I would like to thank Wayne Carson of Steel Technology for donating the steel frames. Despite the short notice (sorry) they were always supplied on time and of outstanding quality and dimensional accuracy. Thanks to Maurice Harris and Eric MacLeod of Royds Consulting for freely sharing their knowledge of structural engineering design using cold-formed steel.

Thanks also to Charles Clifton of HERA, and Cliff Barnett and Michael Simpson of Macdonald Barnett Partners for providing information and commenting on the draft report.

Last but foremost I would like to thank my wife Annette and children Renee and Paul for their patience, support and understanding. Thanks for shifting house with me to Christchurch for the duration of the course and for putting up with a husband and father permanently glued to books or a lap-top for almost a year.

TABLE OF CONTENTS

LIST OF FIGURES AND TABLES

FIGURES page

TABLES

CHAPTER 1
INTRODUCTION

1.1 Background

The traditional method of drywall construction in New Zealand is with light timber framing and sheet material linings. The type and thickness of the linings are selected to achieve specific performance requirements such as appearance of the finished wall, impact resistance, water resistance, sound-control or fire resistance. Paper-faced gypsum plasterboard linings are most commonly used, particularly when a fire resistance rating is required.

The technology for both loadbearing and non-loadbearing cold-formed light steel frame (LSF) drywall systems is well established and has found a growing application in the USA and Australia during the 1980s. The establishment of total LSF building systems, particularly in residential construction, has led to significant market growth overseas. LSF is now estimated to hold 8% of the framing market in Australia and the steel framing industry is targeting a market share of 20% by the year 2000.

Similar growth has not been experienced in New Zealand. Although the practice of 'stick-building' non-loadbearing LSF partitioning has an established history of use in light industrial and commercial applications, total prefabricated LSF building systems have not been able to successfully compete with timber framing. This is due to the competitive pricing of framing timber on the local market combined with a reluctance to change established building practices. Reasons for the low cost of timber supply are;

- expansive forestry and an ample supply of suitable framing timber at low transportation cost to all main centres,
- a tradition of building in 'green' timber in New Zealand. The additional cost associated with kiln-drying and the subsequent storage and protection requirements would increase the cost of timber framing and close the competitive gap between timber and steel systems.

Until recently the initial set-up cost associated with the pre-fabrication of LSF building elements and the requirement for supporting services such as material supply, design, and construction, has been prohibitive when off-set against the expected returns in a small and competitive New Zealand market.

1.2 The Future for LSF Drywall Systems in New Zealand

During the early 1990s a timber shortage internationally led to an increase in timber prices and export opportunities for premium timber grades. This also resulted in a decrease in timber quality on the local market, hence a stronger competitive positioning for steel framing and the establishment of prefabricated LSF systems in New Zealand as a viable alternative to timber framing.

The position of LSF has also strengthened due to increased use of thin wallpapers and paint finishes, and rising customer expectations with regard to the quality of interior finishes. Quality problems associated with shrinkage of green timber are currently forcing the timber industry to supply kiln-dried framing to the high-cost end of the New Zealand residential construction market.

Additional market opportunity for framed systems (both timber and steel) in low-rise industrial and commercial construction has also been created by the introduction of a performance based New Zealand Building Code administered by the Building Industry Authority (BIA, 1992). In the area of fire safety this performance base has caused the removal of long-standing prescriptive requirements for concrete construction.

Although timber prices have stabilised, they are not expected to return to historical low levels as international demand for framing timber is expected to remain high. Steel framing companies are now established in most main centres in New Zealand and LSF is currently estimated to hold between 1-2% of the total framing market. An illustration of typical LSF house construction is given in Figure 1.1.

Growth is expected to follow overseas experience and will be influenced by aggressive marketing initiatives in Australia. The competitive positioning of LSF systems will further improve as prefabrication and construction techniques become more streamlined and sophisticated. This growth of LSF systems is expected to increase the demand for economical solutions where specific performance is required, such as in the area of fire resistance.

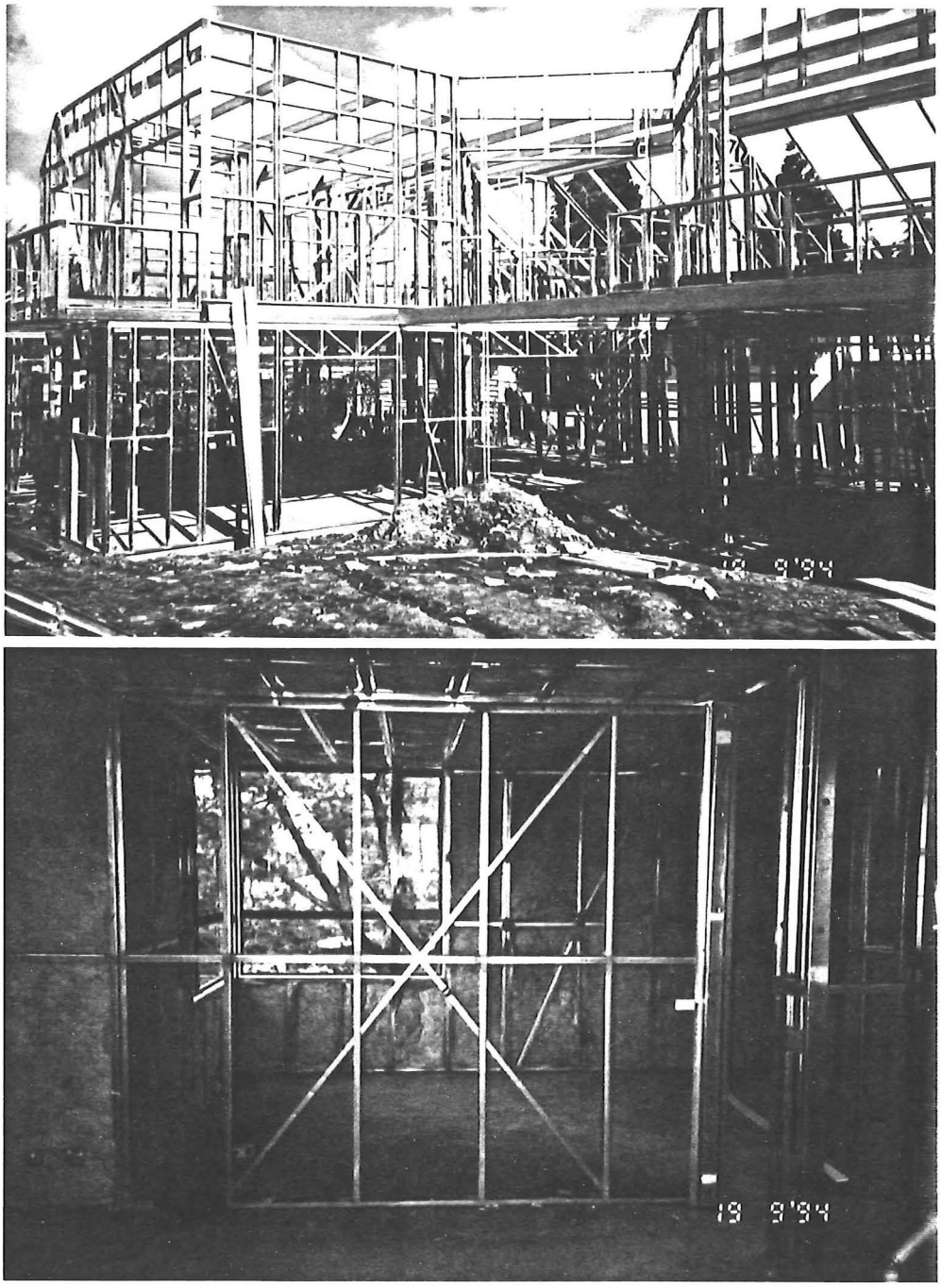

Figure 1.1 : Example of residential LSF in New Zealand
(Steel Technology Ltd., Auckland)

1.3 Fire Resistance of Non-Loadbearing LSF Drywall Systems

Non-loadbearing LSF drywall systems have an established history of use, mainly in light industrial and commercial partitioning. Advantages over timber framing include;

- light-weight nature of framing components (high strength-to-weight ratio),
- dimensional stability of the frame,
- speed and ease of frame erection (often friction fit connections of studs to top and bottom channels),
- no lining delays due to high framing moisture content,
- aesthetic quality of finished wall,
- demountability.

These advantages have resulted in a ready acceptance of non-loadbearing LSF drywall systems as 'infill' partitioning in buildings which have a conventional structural shell, such as reinforced concrete or masonry construction. In response to a market demand for fire separations in this area of light industrial and commercial partitioning, lining manufacturers have developed, tested and published a range of fire resistance ratings. In New Zealand tested non-loadbearing LSF drywall systems are published by Winstone Wallboards (1992a) and achieve fire resistance ratings ranging from 30 to 120 minutes. These systems are based on full-scale fire resistance tests against the standard ISO fire curve in accordance with AS 1530 : Part 4 (SAA, 1990).

1.4 Fire Resistance of Loadbearing LSF Drywall Systems

Loadbearing LSF drywall systems are less likely to be used as 'infill' commercial partitioning, and will more likely form part of a total LSF construction system.

With the developing use of LSF in loadbearing applications, the demand for fire resistance ratings has increased. Winstone Wallboards (1992a) has published a range of loadbearing LSF systems to meet this market demand. The approved fire resistance ratings for these systems are based on conservative opinions and the concept of limiting steel temperature. No fire tested loadbearing LSF drywall systems exist in New Zealand.

1.5 Fire Engineering Design

In parallel with the growing interest in LSF drywall systems, the understanding and application of specific Fire Engineering Design is used increasingly for the fire safety design of buildings and building elements in New Zealand.

Fire testing against standard time-temperature furnace conditions will give good comparative data for systems tested under identical conditions. However, standard fire resistance tests do not accurately model the performance of a building element when exposed to a 'real' fire.

In 'real' fires the fire growth phase, steady state and decay will depend on aspects such as the total fuel load in the fire compartment, fuel type, fuel configuration, compartment size and ventilation openings, and thermal properties of building materials. A comparison of 'real' fire curves against the standard ISO834 test curve is given in Figure 1.2. Examples are included for a hydro-carbon pool fire with a rapid growth, short duration and a rapid decay phase, and the scenario of a wood crib fire with a slow temperature rise, long duration and a slow decay .

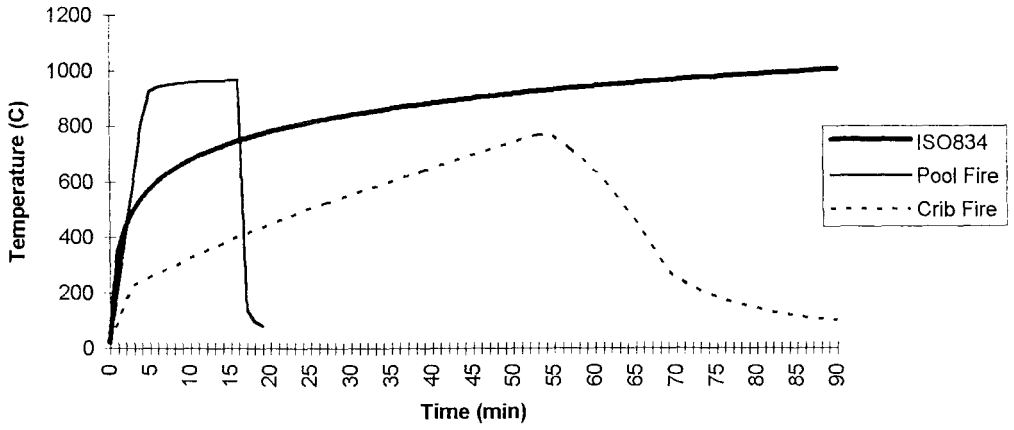

Figure 1.2 : Comparison of 'real' fires with the standard ISO834 curve

The standard ISO834 test fire curve is defined by the relationship,

$$T_t = T_0 + 345\log(8\tau+1) \qquad \text{(Eq.1.1)}$$

where,

T_0 is the ambient temperature (°C) at the start of the test

T_t is the furnace temperature (°C) at time t

τ is the elapsed time (minutes)

To more accurately apply Fire Engineering Design, a better understanding of the performance of building elements in 'real' fires is required. Considering the cost and physical resources required to carry out full-scale fire testing, it is not practical to test building elements against a range of time-temperature curves.

In New Zealand work is currently being carried out by Thomas et al (1994) and Collier (1994a) on the computer modelling of the thermal response of light timber frame drywall systems against standard ISO834 and 'real' compartment fires. Similar work is being carried out by Clancy et al (1994) in Australia.

1.6 Aim of this Study

The aim of this study is to develop an understanding of the performance of loadbearing LSF drywall systems and to model the performance against standard ISO834 and 'real' compartment fires by;

- carrying out a survey of existing literature,
- comparing and verifying existing structural design approaches at room temperature,
- determining the effects of elevated temperature on the structural performance using existing test data to verify theoretical predictions,
- predicting steel temperatures by extending previous work on LTF systems and the thermal response of cavity walls,
- verifying the model with full-scale loadbearing LSF fire resistance tests.

CHAPTER 2

LITERATURE REVIEW

2.1 General

Literature searches were carried out using the Canterbury University library database, the building industry library database at the Building Research Association of NZ, the ICONDA CD-ROM international database, and the international on-line engineering database. The main keywords used; steel, fire, (fram* or stud*), (wall* or partition*).

2.2 Fire Resistance of Hot-Rolled Structural Steel

A large pool of data exists on the fire protection of hot-rolled structural steel members. This data includes design information for insulated and un-insulated steelwork and is mainly based on the concepts of *limiting temperature rise* and *thermal response factor*. Steel sections with a large ratio of heated perimeter (H_p) over cross-sectional area (A) have a large surface area to collect heat and a small mass to absorb it. These sections will take a shorter time to reach a critical temperature than sections with a small H_p/A ratio.

In the UK this concept has been systematically developed for a large range of steel sections and protection systems. Recommendations have been published by ECCS (1983) and were adopted by the fire rating committee of Standards NZ (SNZ, 1989) for use in New Zealand. Similar concepts have been developed and are in use in other countries. Although terminology may differ from country to country, the principles and end-results of calculations are similar according to Bastings (1986).

Good overviews of reference material available for steel protection from fire have been presented in New Zealand by Bastings (1986) and HERA (1990). More recently a European working group of fire engineering experts, chaired by Schleich (1993), has published a 'State of the Art' report which provides excellent international reference material for the fire engineering design of steel structures.

2.3 Fire Resistance of Cold-Formed LSF

In comparison with the wealth of information available for hot-rolled structural steel, the information for fire resistance of cold-formed LSF drywall systems is sparse.

The most relevant work was carried out by Klippstein (1978,1980a,1980b) sponsored by the American Iron and Steel Institute (AISI). The work aims to predict the structural behaviour of cold-formed studs in loadbearing walls lined with gypsum-based plasterboard when exposed to the conditions specified in ASTM E119-79 ' *Standard Methods of Fire Tests of Building Construction and Materials* ' (ASTM, 1979).

Klippstein (1978) reports on generic ratings for wall systems with cold-formed steel studs. As part of this study, tension and stub-column (compression) specimens were tested at room and elevated temperatures up to 650 °C. This paper outlines the parameters and assumptions necessary for the proposed analytical method for predicting performance against ASTM E119-79. Predictions against non-standard ('real') fires do not form part of this study.

Klippstein (1980a,b) reports the major findings of the study and presents a detailed discussion of two fire tested wall assemblies. The work is summarised by AISI (1981) and concludes that the failure time of cold-formed steel stud walls is a function of the thickness of gypsum-based plasterboard linings and the load-ratio $LR=P_a/P$, where P_a is the applied load (or stud failure load at elevated temperature) and P is the stud failure load at room temperature. The load-time relationship as presented by the AISI report is reproduced in Figure 2.1.

Figure 2.2 shows a comparison between the ASTM E119-79 time-temperature curve used for the AISI tests and the AS 1530 : Part 4 curve commonly used for fire resistance testing in New Zealand (SAA, 1990). The AS 1530 curve is the same as the standard ISO834 curve. From this comparison it is clear that the time-temperature differences are relatively insignificant and that the AISI results can be used to calibrate the findings of this study with respect to the standard ISO834 test fire.

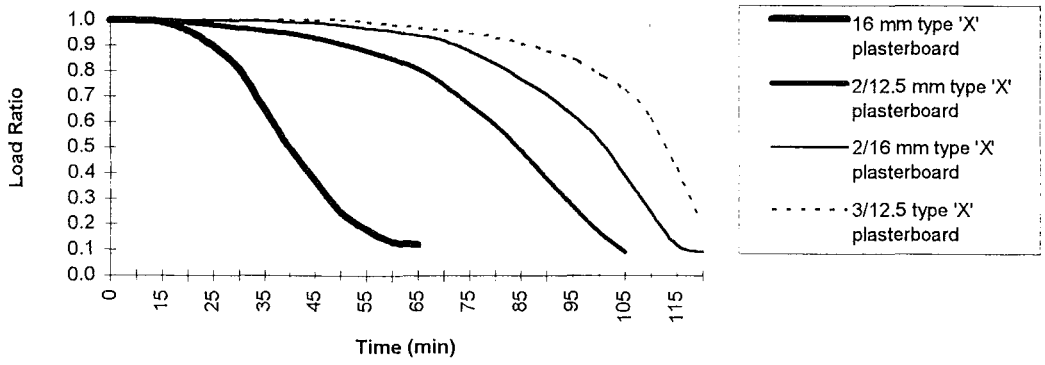

Figure 2.1: Load versus time relationship for walls with steel studs

(reproduced from AISI (1981))

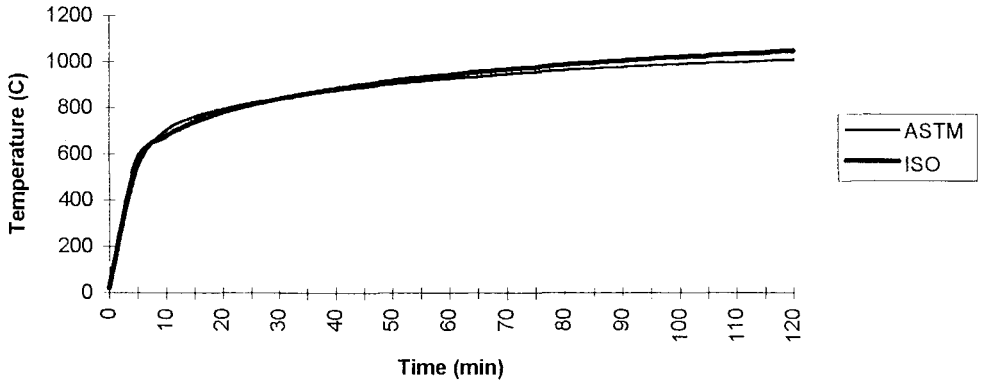

Figure 2.2: Comparison of ASTM E119 and AS 1530 fire test curves

Cooke (1987) describes the structural response of hot-rolled structural steel beams and columns heated along one flange. The report includes data on steel properties at elevated temperatures. Cooke derives useful theories for the thermal bowing displacements of members having temperature gradients across the section. These correlations are equally applicable to temperature gradients in steel studs of cold-formed LSF drywall systems exposed to fire on one side and are further discussed in Chapter 4 of this report.

In the UK the Steel Construction Institute, SCI (1993), describes the properties of cold-formed steel at elevated temperatures and outlines the general requirements for the construction of fire resistant cold-formed steel wall assemblies lined with gypsum-based plasterboard linings. The report does not offer detailed analysis but refers to and tabulates generic and proprietary fire test data. To estimate the average steel stud temperature of loadbearing studs in relatively thin (undefined) walls a simple (and conservative) method is suggested. An estimate of the temperature of the steel is determined from the average temperature on the exposed and unexposed faces of the wall assembly. Stud designs may then be carried out by using the reduced steel capacity which corresponds to this calculated average temperature.

CHAPTER 3
STRUCTURAL MODEL

3.1 General

In order to be able to predict the structural behaviour of loadbearing LSF drywall systems exposed to elevated temperatures experienced in fires, it is first necessary to develop an understanding of the performance at room temperature.

Of particular interest is the ultimate limit state condition as the fire resistance rating of a loadbearing LSF drywall system is expected to be governed by structural collapse due to degrading material properties with increasing temperature. Temperature effects are described in detail in Chapter 4. This Chapter outlines structural considerations at room temperature and considers the following essential design input parameters;

- material properties
- construction details
- restraint conditions
- structural design codes
- structural testing

The Chapter will conclude with a brief summary of findings.

3.2 Material Properties

Cold-formed steel framing members are normally manufactured by roll-forming galvanised sheet steel coil. The process involves progressive plastic deformation of the sheet steel to form the desired shape.

The galvanised sheet coil feed material has a minimum specified yield strength which usually falls within the range from 250-550 MPa with a designation in the form G250-G550, where G denotes 'galvanised'. Steel sheet for cold-forming is commonly

specified in thicknesses of 0.3 - 2.0 mm in accordance with NZS3441:1978 in New Zealand (SNZ, 1978) and AS1397:1984 in Australia (SAA, 1984). There is no restriction on the maximum yield strength and often material is supplied at a significantly higher yield strength than the specified minimum.

The mechanical properties of the sheet steel are also affected by the cold work of forming which takes place mainly in the regions of the bends. Ultimate tensile strength and yield strength in these regions are enhanced and ductility is reduced.

Therefore, although the minimum yield strength of cold-formed steel members is specified, the actual yield strength is relatively unknown but would be higher and therefore conservative from a general design perspective. However, to be able to carry out an accurate analysis of fire test results with the aim to model the performance of cold-formed steel members, it is necessary to more reliably establish the actual yield strength and influence of variations in yield strength.

The elastic modulus E (Young's modulus) is the ratio of stress to the strain (ε) it produces. In the linear elastic range up to the proportional limit (typically $\varepsilon = 0.15$ %), E is given as 200,000 MPa for most structural steels and is considered similar for cold-formed steel (SCI, 1993). Hancock (1988) gives experimental values of between 188,000 Mpa (near corner folds) and 202,000 MPa (in flat regions). Structural design codes AS1538 (SAA, 1988) and BS5950 (BSI, 1987) adopt values of 200,000 and 205,000 MPa respectively. Manufacturer's data (Rondo, 1993) gives 200,000 MPa. For the purposes of this study a room temperature value for the Young's modulus of E = 200,000 MPa will be adopted.

Similarly a shear modulus (G) of 80,000 MPa, typically used for structural steel, will be used for the analysis of cold-formed steel members at room temperature.

3.3 Construction Details

One of the main advantages of cold-formed light steel framing is the ability to form stud and channel sections from galvanised steel coil into any shape, tailored to meet particular requirements. Common shapes for non-loadbearing framing applications are C-section top and bottom channels and lipped C-section studs. Studs of 65 x 30 mm with a base metal thickness (prior to galvanising) of 0.55 mm have been in common use in commercial partitioning in New Zealand for walls up to 3.0 metres in height.

For loadbearing applications simple C-section bottom channels and studs are most commonly used. Top channels can be C-sections or special sections formed to provide additional span capability, as shown in Figure 3.1. The steel base metal thickness is commonly in the range from 0.7-1.6 mm depending on the application.

In non-loadbearing applications connections between studs and channels are often by 'friction-fit'. Sometimes nominal connections such as single screws or rivets are provided to stop studs being accidentally knocked out of alignment during construction and installation of services. In fire rated systems the lack of a requirement for positive fixing has the advantage that joints can be designed to allow for movement due to thermal expansion.

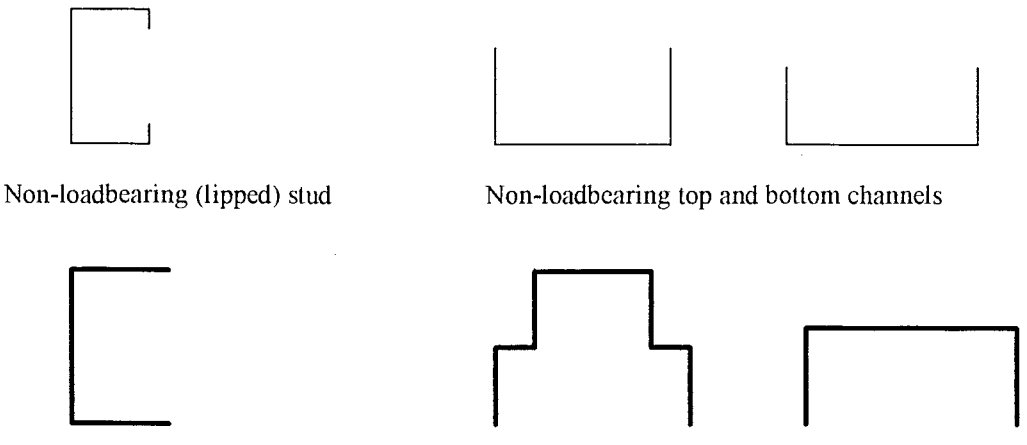

Figure 3.1: Common steel framing sections

In loadbearing applications a positive stud to channel fixing is required to transfer the applied axial loads. The steel framing industry has typically used screws or welded connections. More recently tab-in-slot and clinching methods have been used. Typical connections are illustrated in Figure 3.2.

Design codes and manufacturer's data, as described in Section 3.5, allow for reliance on wall linings to provide lateral restraint when studs are lined on both sides. For stud walls without linings or with sheet material linings on one side only, a minimum of one central row of nogging is recommended. Further rows may be required depending on the slenderness ratio of the wall.

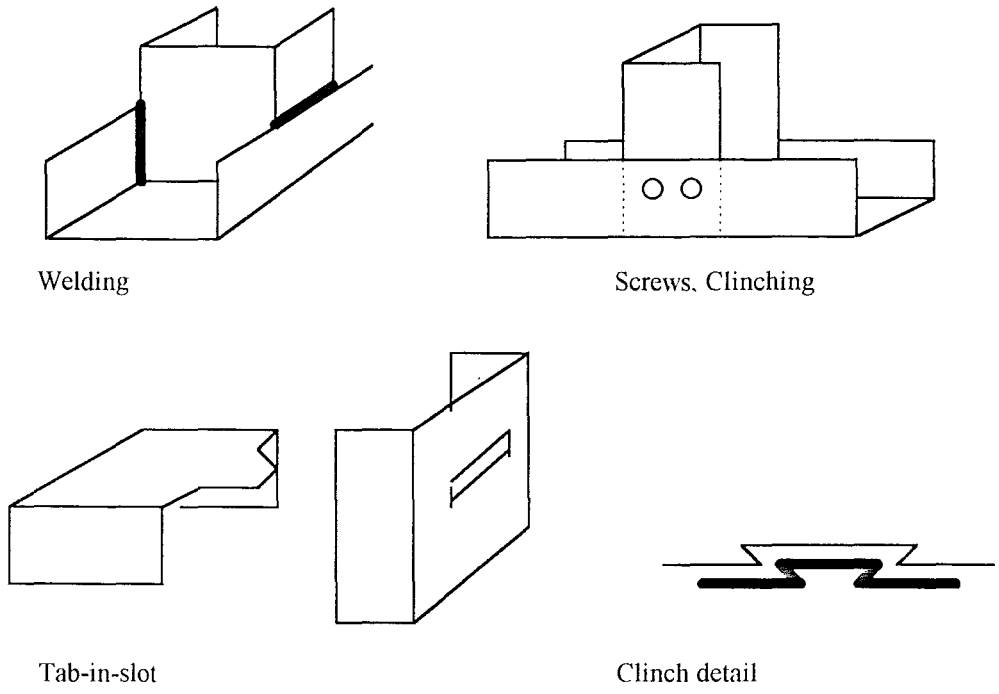

Figure 3.2: Typical stud to channel connections

3.4 Restraint Conditions

Under room temperature conditions lateral restraint against torsional buckling and buckling about the minor axis is effectively provided by sheet lining materials such as gypsum based plasterboard. However, as discussed in Chapter 4 of this study, the

properties of lining materials change significantly when exposed to fire temperatures. The ability of the exposed linings to prevent buckling is expected to be negligible when steel temperatures reach critical levels (>300-400°C). In the design of fire rated steel framed systems the lateral restraint provided by exposed linings must be ignored when assessing fire induced ultimate limit state conditions. Design codes typically do not make allowance for linings on one side only to provide lateral restraint. In the absence of such information it is therefore current practice to design loadbearing fire-rated steel framed systems in accordance with the provisions for unlined walls.

Typical fixings of studs to top and bottom channels, and the fixings of channels to floor and ceiling provide minimal restraint against out-of-plane rotation of the wall. However, under axial loading the re-location of load application due to rotation at stud-to-channel fixings is expected to result in a restraining moment (M_r) as shown in Figure 3.3). The maximum possible value of M_r is given by,

$$M_{r(max)} = P_a \times D/2 \qquad \text{(Eq. 3.1)}$$

where,

P_a	is the applied axial load	(kN)
D	is the channel depth	(mm)

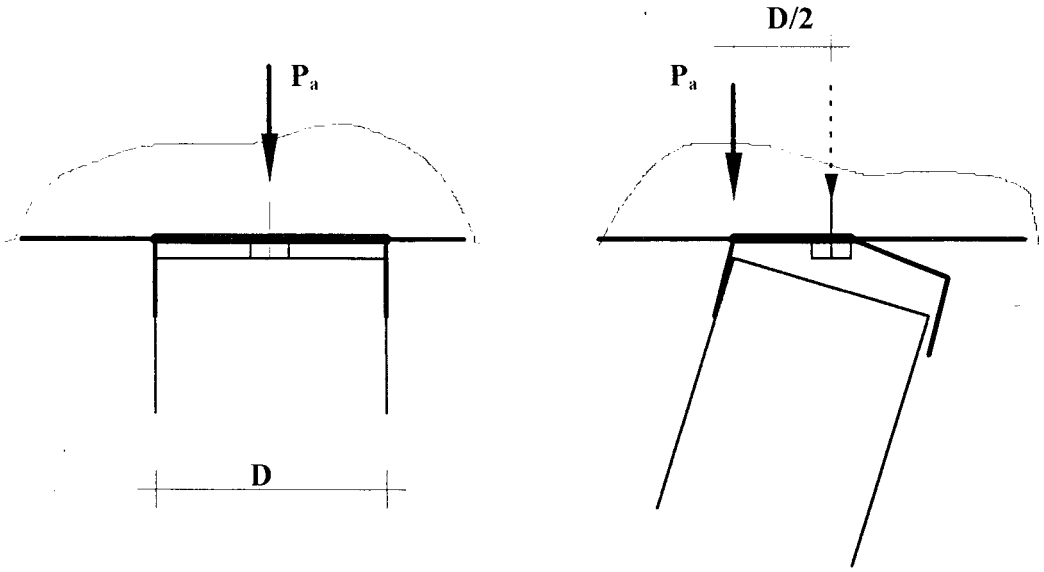

Figure 3.3: Restraining moment at stud to channel fixings due to stud rotation

3.5 Structural Design Codes

Cold-formed steel structural members can be used very efficiently in many applications where hot-rolled steel members or other materials are more expensive. Typical applications are in framed walls and floor/ceiling systems. However the behaviour of thin cold-formed sections is significantly different from that of hot-rolled structural steel and special design specifications are required. Typical problems encountered in the structural design of cold-formed steel compression members are illustrated in Figure 3.4 and include local buckling of thin plate elements and the susceptibility to torsional flexural buckling due to a low torsional stiffness.

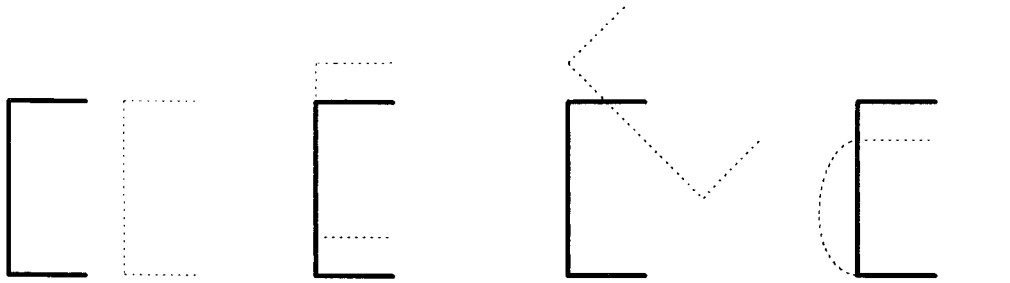

Figure 3.4: Buckling modes of cold-formed steel studs

Design of structural steel in New Zealand is carried out in accordance with NZS3404:1992 *'Steel Structures Standard'* (SNZ, 1992). This standard specifically excludes the design of steel members with a thickness less than 3.0 mm. No standard exists in New Zealand for the design of thin cold-formed steel structures. Reference to overseas standards is therefore required.

Australian Standard AS1538:1988 *'Cold-Formed Steel Structures Code'* (SAA, 1988) is most commonly used but is written in working stress design format and therefore incompatible with the current New Zealand loadings code NZS4203:1992 *'General Structural Design and Design Loadings for Buildings'* (SNZ, 1992) which is written in limit state design format. The modelling of loadbearing LSF walls exposed to fire is

concerned with predicting the failure condition at ultimate limit state. Therefore the 'permissible design loads' derived in accordance with the working stress design format of AS1538 are of limited value for the purposes of this study. However many existing designs have been carried out in accordance with AS1538 and design output has been included in this report to provide a base for comparison.

A combined committee of Standards Australia and Standards New Zealand (SAA/SNZ, 1994) is currently assessing the adoption of a cold-formed steel design code in limit state design format based on the *'LRFD Cold-Formed Steel Design Manual'* developed by the American Iron and Steel Institute (AISI, 1991).

Two limit state design methods for the design of cold-formed steel structures have been applied to predict the room temperature ultimate limit state condition of loadbearing LSF walls in this study. The first method (in anticipation of the SAA/SNZ committee initiatives) is in accordance with the AISI (1991) design manual. Although in imperial units, the correlations for members in compressions and combined bending and compression lend themselves to ready conversion to metric units. For comparison a second limit state design method was included in accordance with BS5950 *'Structural Use of Steelwork in Building. Part 5. Code of Practice for Design of Cold-Formed Sections'* (BSI, 1987).

The equations in AS1538, BS5950 and the AISI design manual are cumbersome and lend themselves to solution by spreadsheet. Appendix A describes the governing equations in detail and presents the spreadsheet analysis.

3.5.1 Examples

Figures 3.5 and 3.6 give a comparison of the predicted axial load at failure for a given uniformly distributed lateral load (without application of load reduction factors). The wall assemblies are those used for the structural and fire testing described in this study. Figure 3.5 illustrates the predicted structural performance of a 2850 mm high wall with 76 x 32 x 1.15 mm cold-formed steel C-section studs at 600 mm centres. Figure 3.6 is

for a 3600 mm high wall with 102 x 52 x 1.0 mm lipped C-section studs. Data points for the test results are included in the graphs and further discussed in Section 3.6.

Reasonable agreement is found between the two limit state design methods of BS5950 and the AISI design manual. The BS5950 predictions are generally higher than the AISI design manual, particularly for low stud loads. As expected the working stress design values from AS1538 are significantly lower.

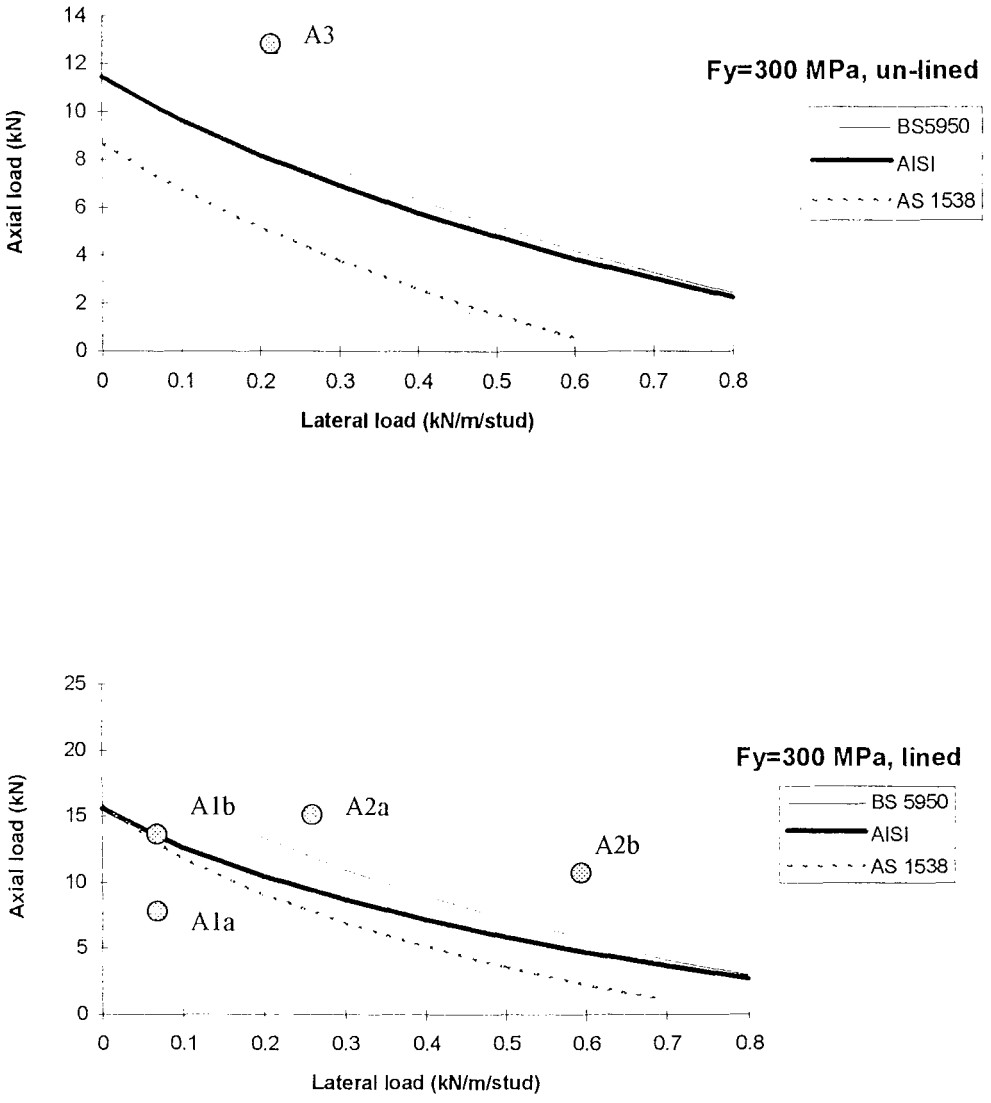

Figure 3.5: Comparison of cold-formed steel design codes (76 x 32 x 1.15 mm C-section studs)

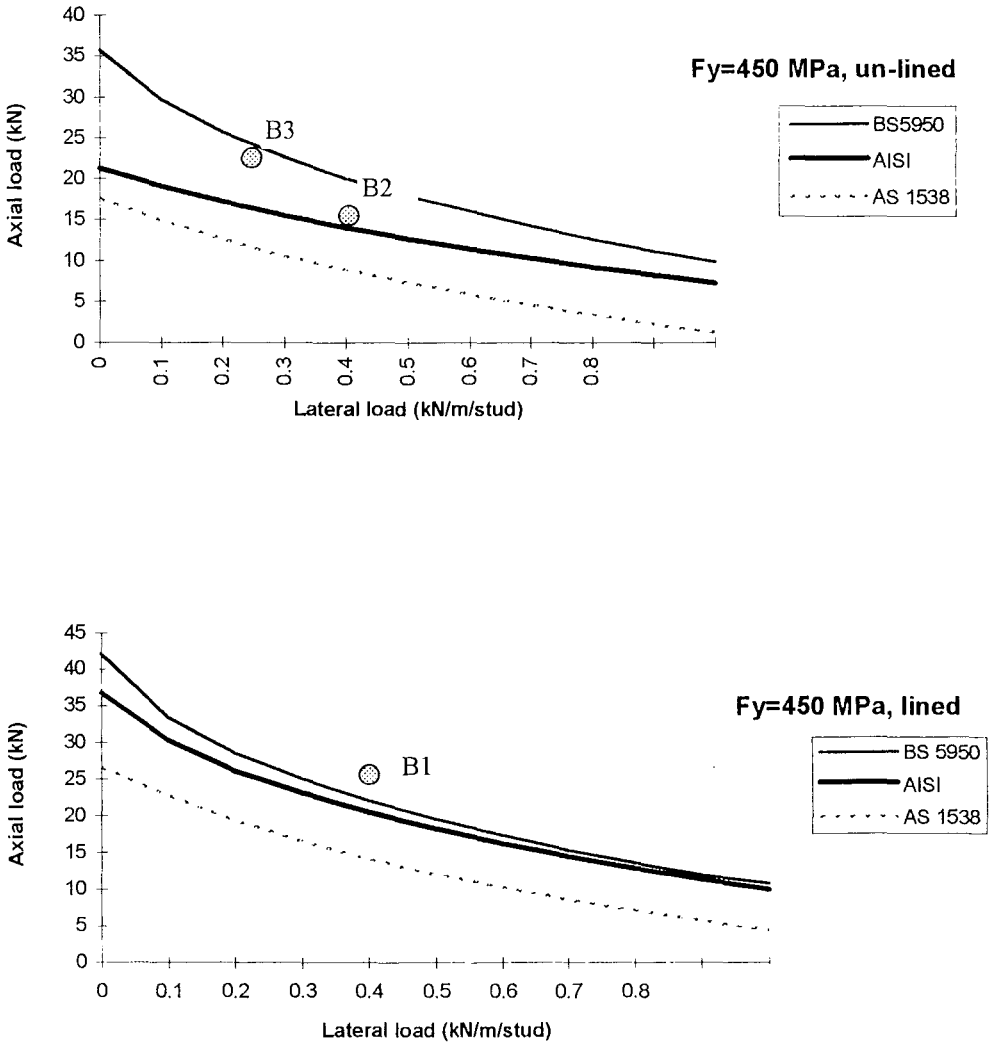

Figure 3.6: Comparison of cold-formed steel design codes (102 x 52 x 1.0 mm lipped C-section studs)

3.6 Structural Testing

In order to calibrate the analytical design methods, structural testing for material yield strength and combined axial loading and bending was carried out at room temperature.

This testing also served to more accurately determine the cold capacity and failure mode of specimens prior to full scale fire testing.

3.6.1 Material yield strength testing

To establish the yield strength of the steel framing material supplied, tensile and compressive stub-column testing in accordance with AS1538 was carried out. The test set-up for tensile testing for yield strength is illustrated in Figure 3.7 and the set-up for stub-column testing in Figure 3.8.

The tensile test specimens were fitted with strain gauges. Continuous load-deformation plots were obtained. The short stub-column specimens were placed between the test machine rigid platens and loaded in compression. A continuous plot of load versus cross head displacement was obtained. The results of the yield strength testing are presented in Table 3.2.

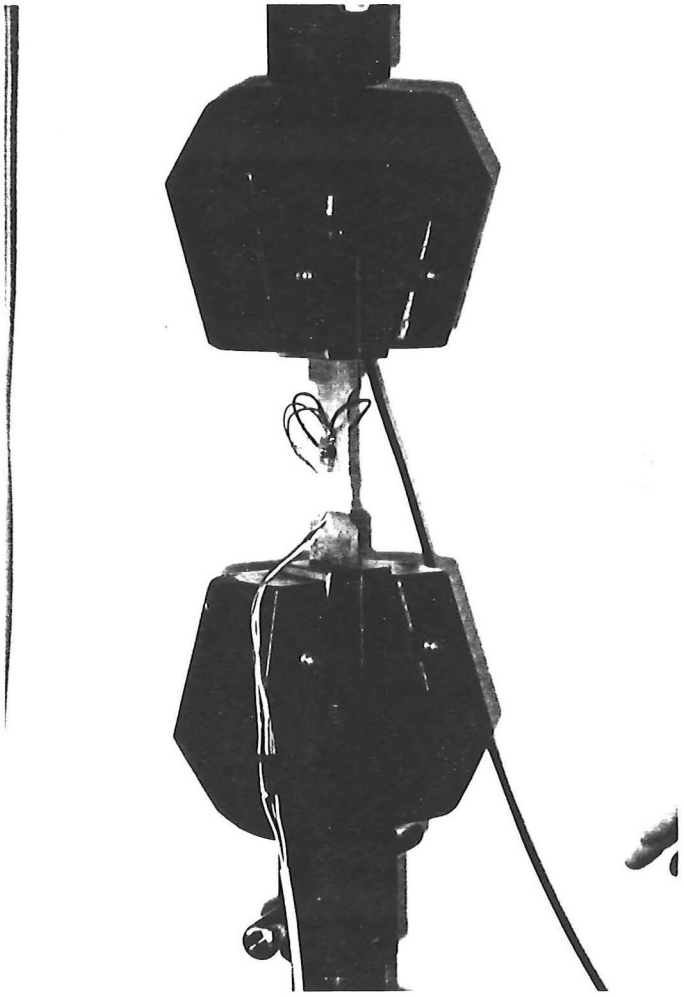

Figure 3.7: Tensile testing for yield strength

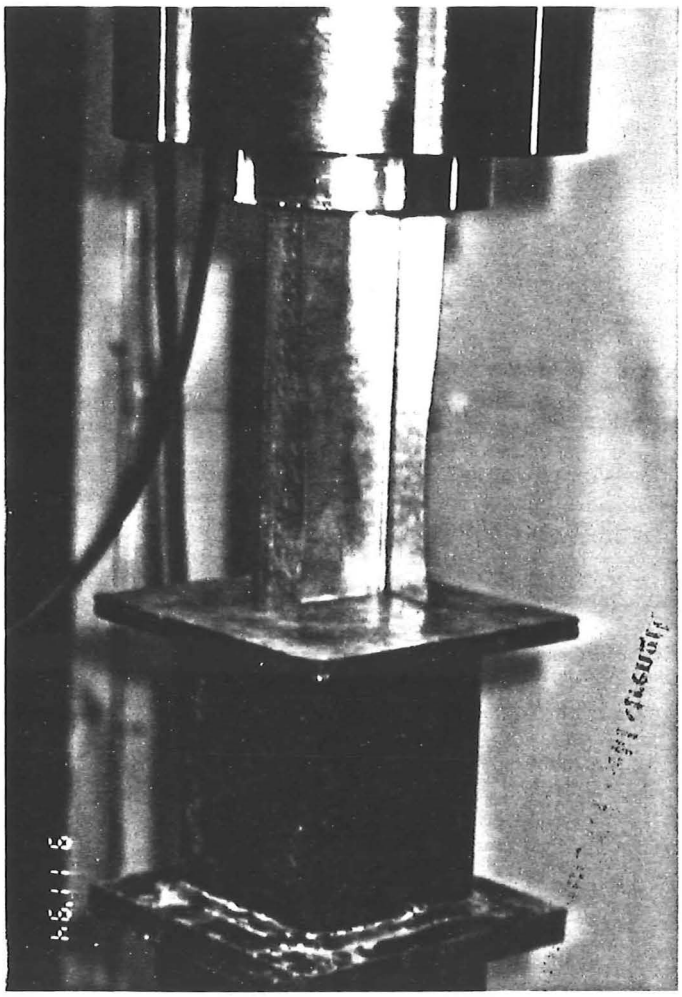

Figure 3.8: **Stub-column testing for yield strength**

3.6.2 Test set-up and specimens for combined axial loading and bending

Specimens for structural testing were identical to those used in the full scale fire tests except that the specimen width was reduced to two studs spaced at 600 mm centres. As shown in Figure 3.9, specimens were mounted horizontally and axial load was applied by a manually operated hydraulic jack at the top channel level through a heavy structural steel spreader beam supported on rollers. At the bottom channel level the reaction was provided by a rigid continuous support which was securely bolted to the reaction floor. Loads were recorded by means of a 44 kN capacity load-cell placed at the top of the specimen between the jack and spreader beam.

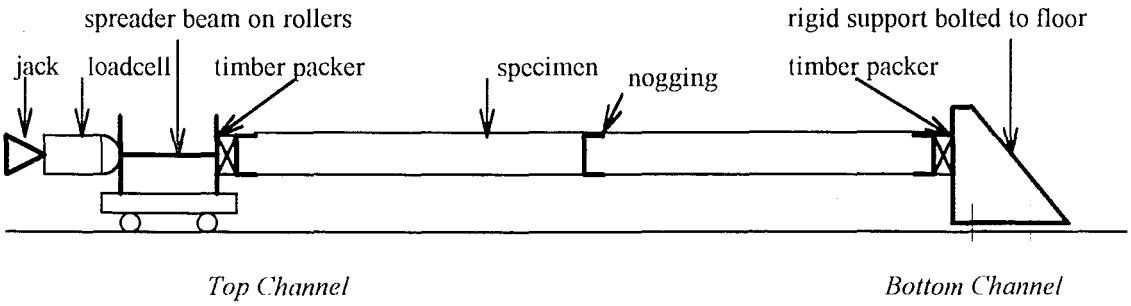

Figure 3.9: Test set-up for combined axial loading and bending

Specimens were tested both lined (on the top face) and unlined. The bottom face was unlined in all cases. Simulated uniformly distributed loads were applied by means of concrete blocks placed on the top surface of the specimens as shown in Figure 3.10.

The first series (A) of tests had 2850 mm long 76 x 32 x 1.15 mm C-section studs with one central row of nogging and a 1.6 mm top-hat section for the top channel.

The second series (B) of tests had 3600 mm long 102 x 51 x 1.0 mm lipped C-section studs with one central row of nogging and 1.6 mm C-section top and bottom channels.

The relevant section properties for the studs are given in Table 3.1.

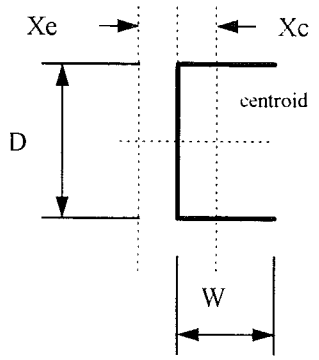

76 x 32 x 1.15
C-section

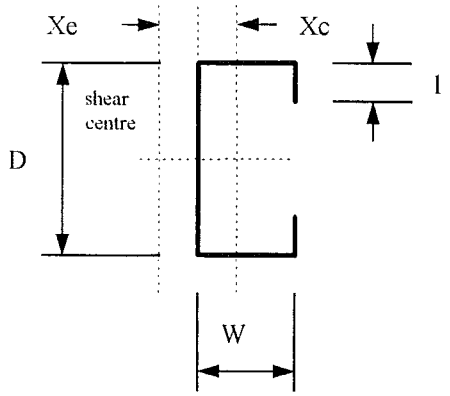

102 x 51 x 1.0
lipped C-section

Property	Symbol and Units	76 x 32 x 1.15 mm C-section	102 x 51 x 1.0 mm lipped C-section
Stud depth	D (mm)	76.2	102.0
Stud Width	W (mm)	32.0	51.0
Lip Width	l (mm)	N/A	12.5
Thickness	t (mm)	1.15	1.0
Centroid	Xc (mm)	7.81	16.1
Shear Centre	Xe (mm)	10.81	23.9
Gross Area	A (mm)	157.0	215
Mass	M (kg/m)	1.27	1.75
Moment of Area (x)	Ix (10^3 mm^4)	140.4	364.0
Moment of Area (y)	Iy (10^3 mm^4)	15.6	75.0
Section Modulus (x)	Zx (mm^3)	3687	7130
Section Modulus (y)	Zy (mm^3)	644	2190
Radius of Gyration (x)	Rx (mm)	29.9	41.1
Radius of Gyration (y)	Ry (mm)	10.0	18.7
Form Factor	Q (dimensionless)	0.661	0.680
Torsion Constant	J (mm^4)	69.3	72
Warping Constant	Iw (10^6 mm^6)	15.53	163

Table 3.1: Steel stud section properties

3.6.2 Test Results

A summary of test results is presented in Table 3.2. Testing confirmed the specified values for yield strength. The results from axial load testing are compared with ultimate limit state values calculated in accordance with BS5950 and the AISI design manual.

Individual tests results are also presented in Figure 3.5 and Figure 3.6. Failure modes are discussed in more detail below. The AISI design manual generally gives conservative predictions of maximum axial loads. BS 5950 is non-conservative in some instances.

Test Series	Test No.	Framing	Lining (top face)	Lateral load kN/m/stud	Specified Yield Strength MPa	Tested Yield Strength MPa	BS5950 Axial Load kN/stud	AISI Axial Load kN/stud	Tested Axial Load kN/stud
A	1a	75 x 32 x 1.15 mm C-section	16 mm gypsum plasterboard	0.07	300	300	17.9	13.4	7.6
A	1b	75 x 32 x 1.15 mm C-section	16 mm gypsum plasterboard	0.07	300	300	17.9	13.4	14.1
A	2a	75 x 32 x 1.15 mm C-section	16 mm gypsum plasterboard	0.25	300	300	12.1	9.5	15.8
A	2b	75 x 32 x 1.15 mm C-section	16 mm gypsum plasterboard	0.60	300	300	5.4	4.7	10.8
A	3	75 x 32 x 1.15 mm C-section	unlined	0.20	300	300	4.2	3.8	12.7
B	1	100 x 50 x 1.0 mm lipped C-section	12.5 mm gypsum plasterboard	0.41	450	450	21.9	20.5	26.9
B	2	100 x 50 x 1.0 mm lipped C-section	unlined	0.40	450	450	20.3	13.4	15.5
B	3	100 x 50 x 1.0 mm lipped C-section	unlined	0.25	450	450	24.1	16.1	23.6

Table 3.2: Results of structural testing

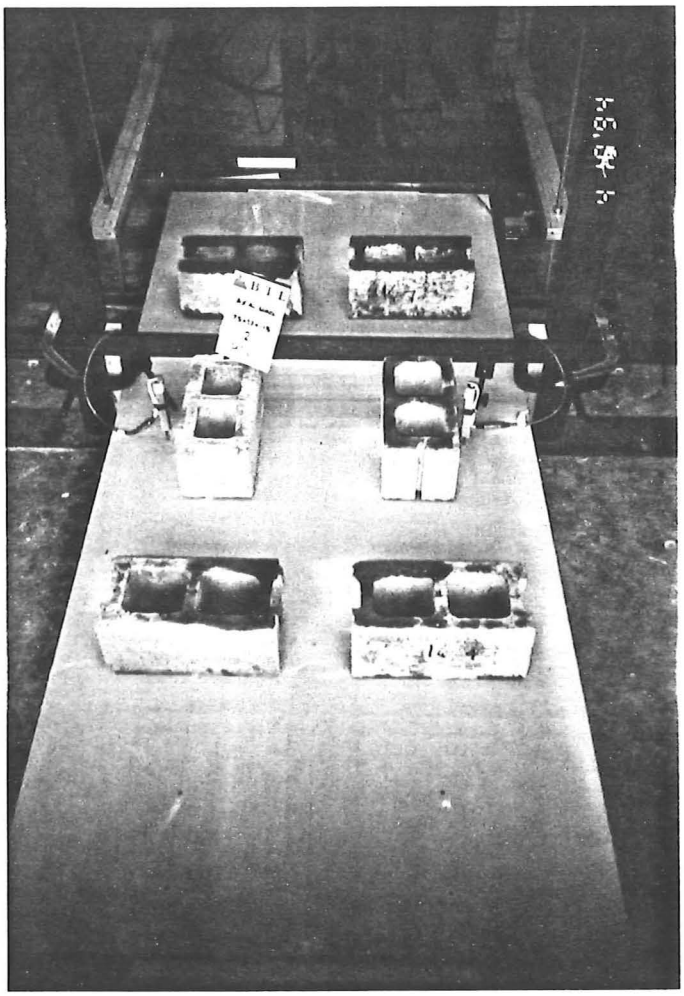

Figure 3.10: Combined axial loading and bending test set-up

The first test (series A, test 1a) was carried out with a lining of 16 mm glass-fibre reinforced gypsum-based plasterboard screw fixed at 300 mm centres to the top face of the studs. No additional lateral load was applied. Failure occurred first at an axial stud load of 7.6 kN due to local buckling of the top-hat top channel section. This section was then stiffened by means of a timber packer and the test was continued (series A, test 1b). Bearing failure then occurred at a load of 14.1 kN per stud between the timber packer and the stud webs. At no stage did the studs reach an ultimate limit state condition. Figure 3.11 illustrates the failure mode of these tests.

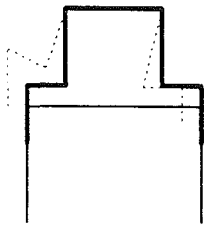

Test A1a: Buckling of the top-hat section

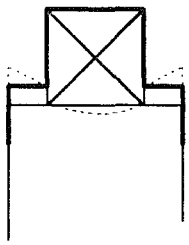

Test A1b: Top hat section stiffened bearing failure of stud web

Figure 3.11: Failure modes of tests A1a and A1b.

The next test (series A, test 2a) was similarly carried out with a 16 mm gypsum plasterboard lining. Concrete blocks were placed on top of the specimen so that the total lateral load was increased to 0.25 kN/m/stud. The axial load was increased to 15.8 kN per stud, a level above that predicted by the design codes. The load was then released. In the next sequence (series A, test 2b) the lateral load was increased to 0.60 kN/m/stud and the axial load was applied until failure occurred occurred at 10.8 kN per stud. The failure mode was by local buckling of the critical compression flange of one of the studs adjacent to a service penetration as illustrated in Figure 3.12.

The last test in the first series (series A, test 3) was carried out on an unlined specimen with a lateral loading of 0.20 kN/m/stud. Failure occurred at an axial load per stud of 12.7 kN due to flexural torsional buckling of one of the studs (initiated near a service penetration) as illustrated in Figure 3.13.

All specimens in the second test series (series B, tests 1,2,3) failed by flexural or flexural torsional buckling of the critical compression flange. The failure loads were 26.9, 15.5 and 23.6 kN per stud respectively. A typical failure is shown in Figure 3.14.

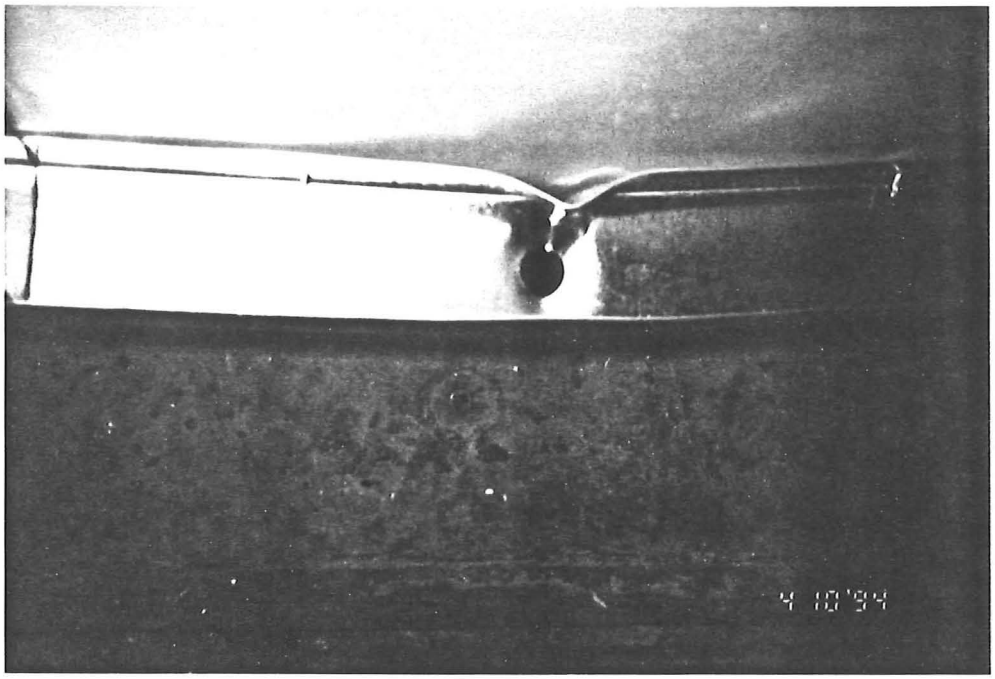

Figure 3.12: Failure mode of series A, test 2b

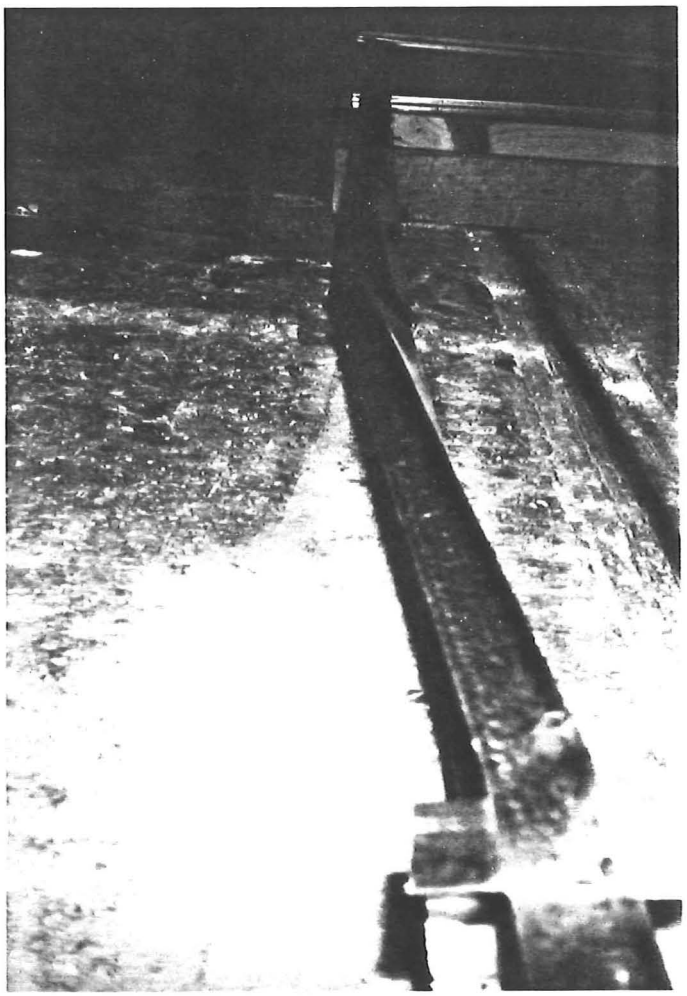

Figure 3.13: Failure mode of series A, test 3

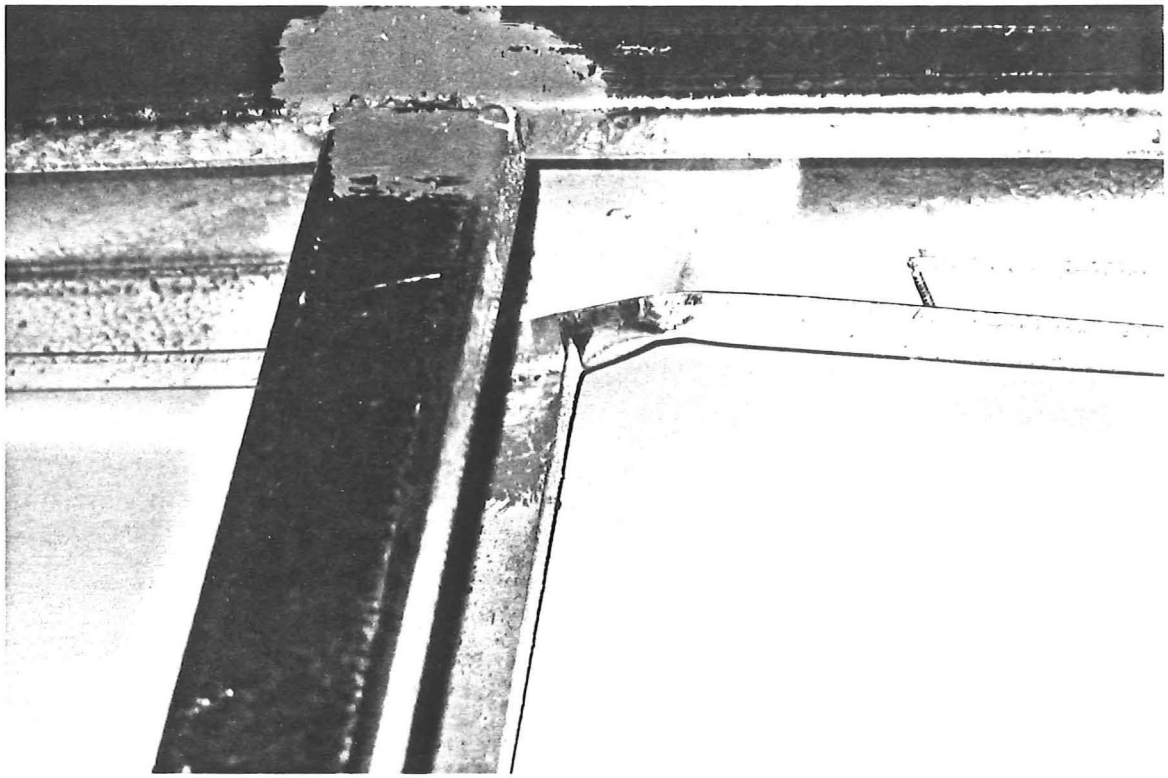

Figure 3.14: Failure mode of series B, test 1

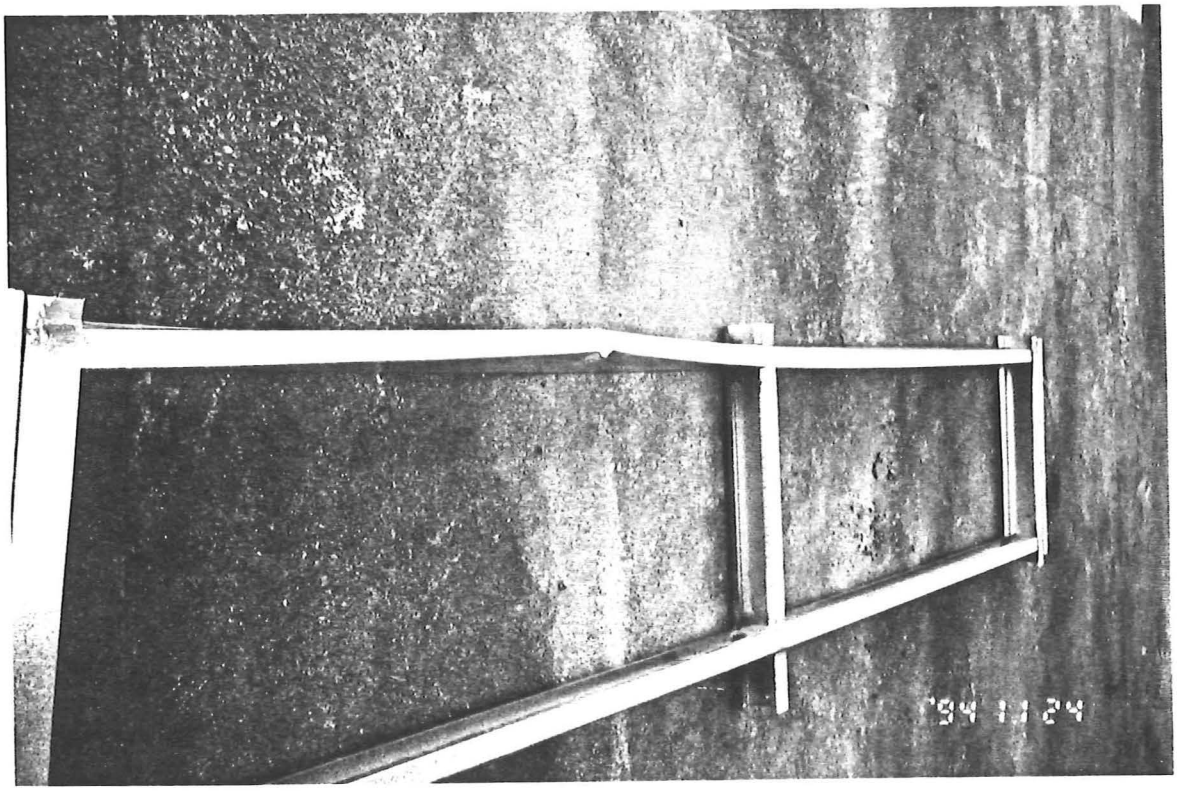

Figure 3.15: Failure mode of series B, test 2

3.7 Findings

Predicted failure conditions in accordance with limit state design code BS5950 : Part 5 (BSI, 1987) and the design manual by AISI (1991) were compared with actual test results for cold-formed steel stud wall assemblies subjected to combined axial loading and bending.

Reasonable agreement was established between the limit state design methods of BS5950 and the AISI design manual.

The AISI design manual gave reasonably conservative predictions in all cases. However, in some instances the predictions in accordance with BS5950 were non-conservative.

The AISI manual is currently being considered for adoption as a limit state design code for New Zealand and Australia and will be used for the structural analysis and modelling of loadbearing LSF drywall systems in this study.

The equations governing the design of cold-formed steel structures in all codes are cumbersome and a frequent comment by structural engineers is that the correlations are too difficult to use for day-to-day designs (Hancock, 1988). However, the design process can be streamlined by the application of spreadsheets such as those described in Appendix A.

The perceived complexity of design codes is mainly caused by the use of thin members in cold-formed steel structural systems and the associated potential for local buckling failures. This was confirmed by the observed failure of the top-hat section in the first test series. Careful load-path analysis is required. This characteristic is recognised by most literature on the design of cold-formed steel structures, as well as by the cold-formed steel design codes.

A further detailed analysis of the performance of cold-formed steel systems at room temperature is considered outside the scope of this study.

CHAPTER 4

TEMPERATURE EFFECTS

4.1 General

The dominant consideration when assessing the performance of loadbearing LSF drywall systems against fire is the effect of elevated temperature on the behaviour and material properties of the steel stud wall assembly. This chapter describes the performance of gypsum plasterboard linings, the cold-formed steel properties at elevated temperatures and considerations such as increased P-Δ effects due to thermally induced deformations.

4.2 Properties of Gypsum Plasterboard Linings at Elevated Temperatures

Gypsum plasterboard linings are commonly used to provide fire resistance in framed construction. Pure gypsum consists of calcium sulphate with free water at equilibrium moisture content (approximately 3%), and chemically combined water of crystallisation (approximately 20%). Its chemical formula is $CaSO_4.2H_2O$ (calcium sulphate di-hydrate). When exposed to fire the free water and chemically combined water is gradually driven off at temperatures above approximately 100°C. This causes a temperature 'plateau' on the unexposed face of the lining. The length of this plateau is a function of the lining thickness, density and composition, and is commonly referred to as the 'time delay'.

The process of removal of chemically combined water is called 'calcination' and results in a loss of strength and shrinkage of the sheet material. The chemical formula for the resultant product is $CaSO_4.{}^1/_2H_2O$ (calcium sulphate semi-hydrate) known commercially as plaster of Paris, a powder which has much less strength than the original gypsum. Further gradual product disassociation occurs at temperatures exceeding 200°C.

The paper facings which contain the core material and provide tensile strength to the plasterboard linings, will be burned away after temperatures reach about 300 °C.

The fire resistance of gypsum plasterboard may be enhanced by the additives such as vermiculite and glass-fibre reinforcing. Vermiculite expands when exposed to heat, which will partly off-set the shrinkage of the gypsum core. Glass-fibre reinforcing will bridge any cracks that occur as a result of shrinkage and will enhance the integrity of the board during the calcination process and after the loss of paper facings. Glass fibre reinforcing also delays ablation and thus slows down the calcination process as the calcined board is forming a protective insulating layer.

4.2.1 Mechanical Properties

At room temperature gypsum plasterboard wall linings, screw-fixed at close centres (commonly 300 mm), provide adequate restraint against lateral buckling of the steel studs about the minor axis. However, during and after exposure to fire this ability to provide lateral restraint will be significantly diminished.

When steel temperatures on the hot side of the wall assembly reach critical levels the exposed plasterboard lining have completely calcined and will no longer provide lateral restraint.

In comparison the lining on the cold side of the assembly will degrade to a lesser degree. Its ability to provide lateral restraint will depend on the calcination depth and the remaining thickness of sound lining. This aspect is discussed further in Chapter 6 following the full scale furnace tests.

4.2.2 Thermal Properties

Thomas et al (1994) summarises data measured by Mehaffey (1991) for the thermal conductivity and enthalpy of glass-fibre reinforced gypsum plasterboard as a function of temperature. Thomas' values for the thermal conductivity of gypsum plasterboard are presented in Figure 4.1. Enthalpy values are presented in Figure 4.2 and represent the summation of the product of specific heat and temperature, expressed per unit of volume. Enthalpy values are used in modelling to avoid numerical instabilities resulting from the sharp peaks that may occur in the specific heat of materials containing water, due to evaporation of moisture.

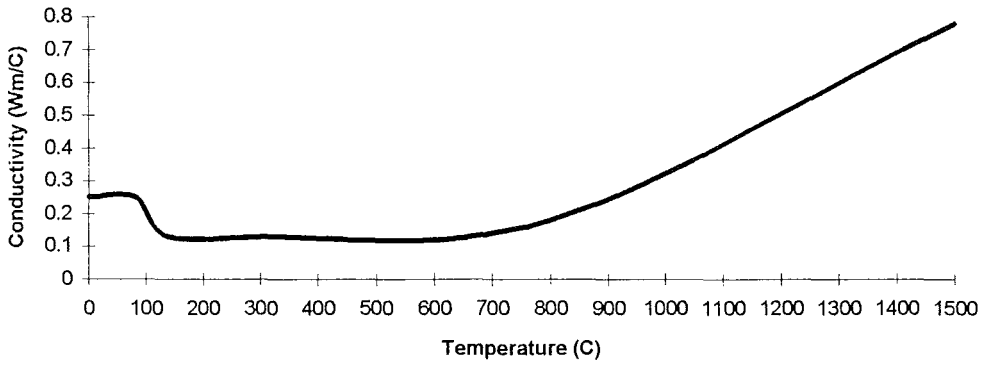

Figure 4.1 : Thermal conductivity of gypsum plasterboard

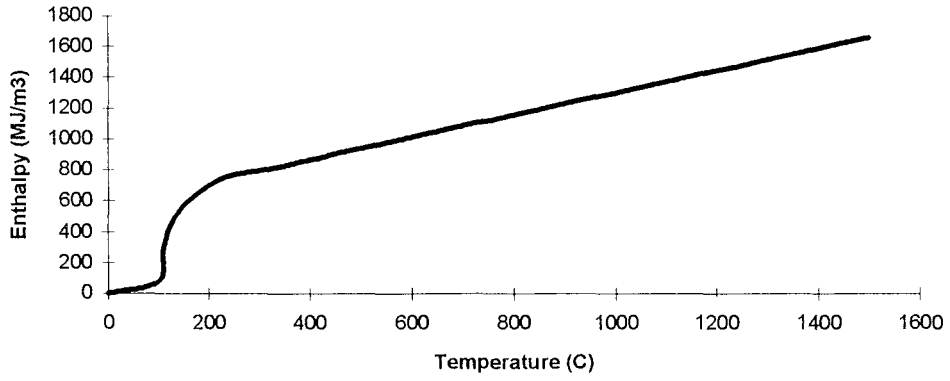

Figure 4.2 : Specific volumetric enthalpy of gypsum plasterboard

4.3 Properties of Cold-Formed Steel at Elevated Temperatures

The mechanical and thermal properties of steel are of interest when considering the behaviour at elevated temperatures. Significant mechanical properties are the density, yield strength, modulus of elasticity and coefficient of thermal expansion. Relevant thermal properties are the specific heat and thermal conductivity. With the exception of density, all these parameters are strongly influenced by temperature. In addition the crystalline structure of carbon steels typically used in construction also changes at temperatures above approximately 650 °C (Milke, 1988). However, failure of

loadbearing LSF systems is expected before crystalline steel structure changes become a factor.

4.3.1 Mechanical Properties

Strength

Equations for the reduction of yield strength with temperature for hot-rolled structural steel have been published by Lie (1992) and Milke (1988),

$$F_{yT} = F_{y0} (1 - 0.78 \theta - 1.89 \theta^4), \text{ for } \theta < 0.63 \ (T < 650 \ ^\circ C) \qquad \text{(Eq. 4.1)}$$

or by the European Convention for Constructional Steelwork (ECCS, 1983),

$$F_{yT} = F_{y0} \{1 + T / [767 \ln(T / 1750)]\}, \text{ for } T < 600 \ ^\circ C \qquad \text{(Eq. 4.2)}$$

where,

F_{yT} is the yield stress (MPa) at elevated temperature T (°C)

F_{y0} is the yield stress (MPa) at room temperature (≈20°C)

θ = (T-20)/1000

T is the temperature of the steel (°C)

Lie (1992) compares these equations for hot-rolled steel with data for cold-drawn wire and concludes that cold-drawn steel loses its strength at relatively lower temperatures. The performance difference is illustrated graphically by Lie, but no equations for cold-drawn material are given. Lawson (1993) indicates that the strength of cold-formed steel is 10-20% less than that of hot-rolled steel at elevated temperatures.

Klippstein (1980b), on behalf of the AISI, carried out experimental work on the yield strength as a function of temperature for cold-formed steel framing members.

Figure 4.3 shows a comparison of yield strength correlations. The curve by Klippstein is most specific to the materials used in this study and for this study a polynomial was fitted to these data which gives,

$$F_{yT}/F_{y0} = 1\text{-}5.3T/10^4 + 4.0T^2/10^6 - 1.9T^3/10^8 + 1.7T^4/10^{11} \qquad \text{(Eq. 4.3)}$$

where the notation is as for Eq.s 4.1 and 4.2

Stiffness

Similarly the reduction of modulus of elasticity E (Youngs modulus) with temperature for hot-rolled structural steel is published by Lie (1992) as,

$$E_T = E_0 [1 + T / 2000\ln(T / 100)], \text{ for } T < 600°C \qquad \text{(Eq. 4.4)}$$

where,

E_T is the modulus of elasticity (MPa) at temperature T (°C)

E_0 is the modulus of elasticity (MPa) at room temperature(≈20°C)

T is the temperature of the steel(°C)

Lie does not give a correlation for the modulus of elasticity for cold-formed steel, but claims that values for 'cold-drawn wire' are 20% lower than those for hot-rolled steel.

Klippstein (1980b) presents experimentally derived data for the modulus of elasticity for cold-formed steel studs. For this study a polynomial was fitted to these data which gives,

$$E_T/ E_0 = 1 - 3.0T/10^4 + 3.7T^2/10^7 - 6.1T^3/10^9 + 5.4T^4/10^{12} \qquad \text{(Eq. 4.5)}$$

where the notation is as for Eq. 4.4

Figure 4.4 shows a comparison of expressions for modulus of elasticity as a function of temperature.

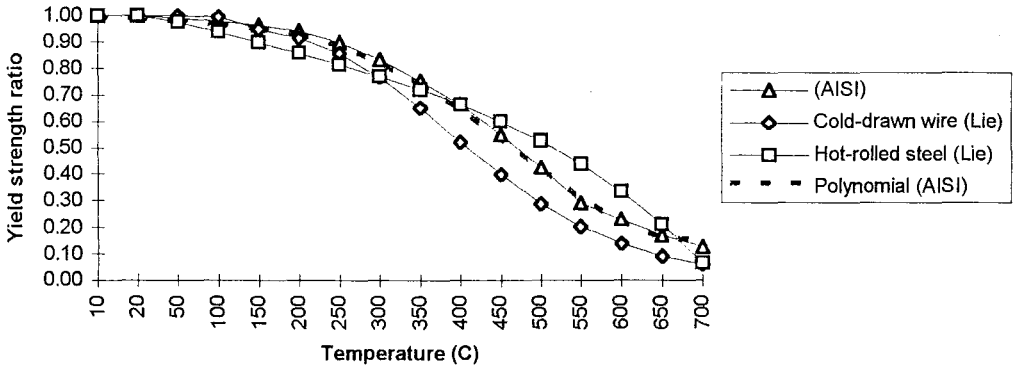

Figure 4.3 : Comparison of data for yield strength against temperature

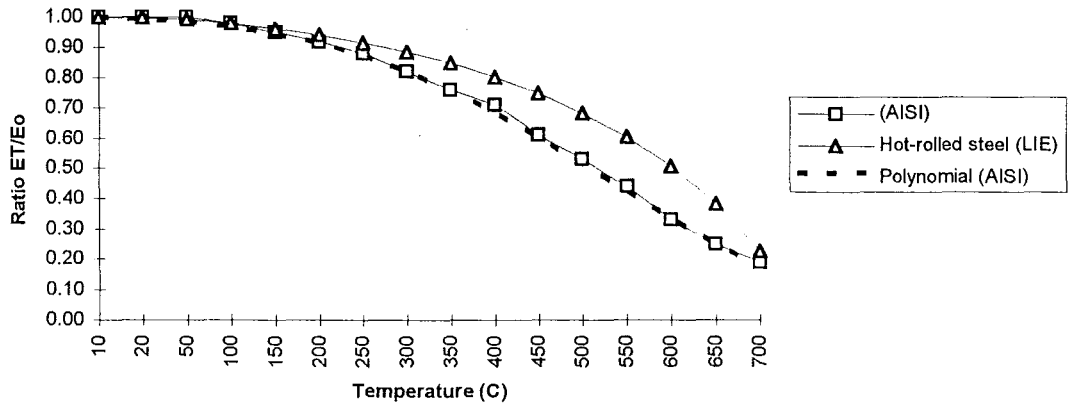

Figure 4.4 : Comparison of data for Youngs Modulus (E) against temperature

Thermal Expansion

The effect of temperature on the coefficient of thermal expansion is published by Lie (1992) as,

$$\alpha_T = (0.004T + 12) \times 10^{-6} \text{ , for } T < 1000 \text{ °C} \qquad \text{(Eq. 4.6)}$$

where,

α_T is the coefficient of thermal expansion ($°C^{-1}$) at temperature T (°C)

T is the temperature of the steel (°C)

4.3.2 Thermal Properties

The temperature rise of a steel member as a result of heat flow is a function of the thermal conductivity and specific heat of the material.

Thermal Conductivity

The thermal conductivity varies somewhat with chemical composition at room temperature, but at elevated temperatures it may be considered identical for most structural steels. The approximation for the thermal conductivity as a function of temperature used for this study is given by the following equation (Lie, 1992),

$$k = - 0.022T + 48, \text{ for } 0 < T < 900 \text{ °C} \qquad \text{(Eq. 4.7)}$$

where,

k is the thermal conductivity (W/m°C)

T is the steel temperature (°C)

In Figure 5 Lie's equation is compared with data presented by Anderberg (1983) and Sterner and Wickstrom (1990) for the thermal conductivity of steel.

Specific Heat

The specific heat (c) describes the heat input required to raise a unit mass of material a unit of temperature. For most structural steels its value increases gradually with temperature. Between 600°C and 800°C there is a steep increase over a narrow temperature range. There is a wide scatter in reported data, but considering the minor

overall influence on the behaviour in fire a constant value of 600 J/kg°C is suggested for temperatures below 600°C (Lie, 1992 and Anderberg, 1983). For this study data for higher temperatures is not required as stud failure is expected to occur at temperatures below 600°C.

The specific volumetric enthalpy of steel is the product of specific heat and temperature, expressed per unit volume. The values presented by Anderberg (1983) and Sterner and Wickstrom (1990) in Figure 4.6 are the same as those used for the heat transfer modelling described in Chapter 5.

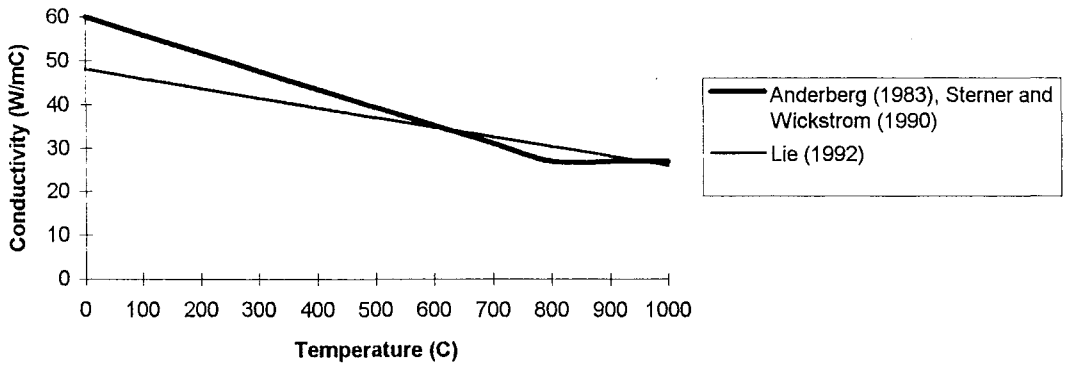

Figure 4.5: Thermal conductivity of steel

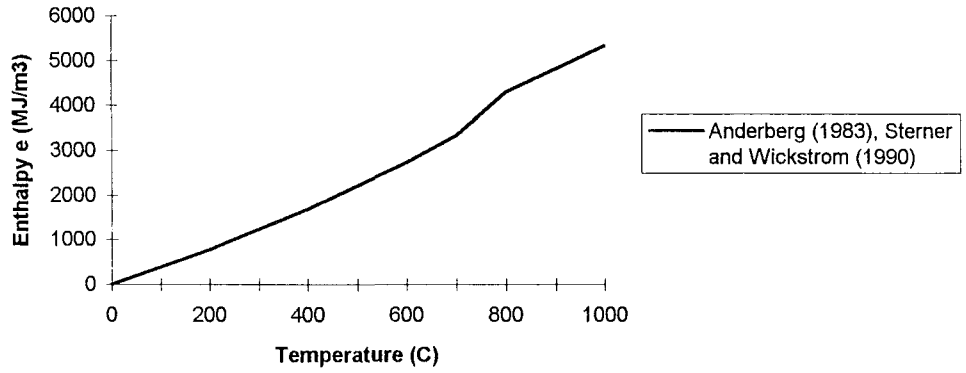

Figure 4.6: Specific volumetric enthalpy of steel

4.4 Thermal Deformations

Cooke (1987) considers the thermal bowing of simply supported steel members due to a temperature gradient across the section and derives the following expression for mid-span deflection,

$$\Delta_1 = \frac{\alpha L^2 \delta T}{8D} \qquad \text{(Eq. 4.8)}$$

where,

Δ_1	is the mid-span deformation due to thermal bowing	(mm)
α	is the expansion coefficient for steel	($°C^{-1}$)
L	is the member length (wall height)	(mm)
δT	is the temperature difference across the member	(°C)
D	is the member depth	(mm)

BRANZ reports FR 1579 (BRANZ, 1990) and FR 1722 (BRANZ, 1992) describe the testing of two full-scale non-loadbearing LSF drywall systems. In both tests the studs were held in top and bottom channels by 'friction-fit' and 15 mm clearance was used to allow for free expansion at both ends. The framing comprised 64 x 30 x 0.55 mm thick lipped C-section studs. FR 1579 was lined with one layer of 12.5 mm glass-fibre reinforced plasterboard on each side of the frame and FR 1722 was lined with two layers of 12.5 mm glass-fibre reinforced plasterboard.

Figures 4.7a and 4.8a show the measured steel stud flange temperatures. Figures 4.7b and 4.8b show the measured deformations and those calculated using Eq. 4.8.

At relatively moderate temperatures (< 400 °C) Eq. 4.8 reasonably predicts the mid-span deformation, provided that the steel studs are free to rotate and expand at both ends. At higher temperatures the correlation between measured and calculated deformations is less accurate. At high steel temperatures the temperature difference across the steel member reduces. Actual deflections do not return to the calculated levels due to plastic deformations of the steel. This is simulated by the heavy lines for the calculated deflections in Figures 4.7b and 4.8b.

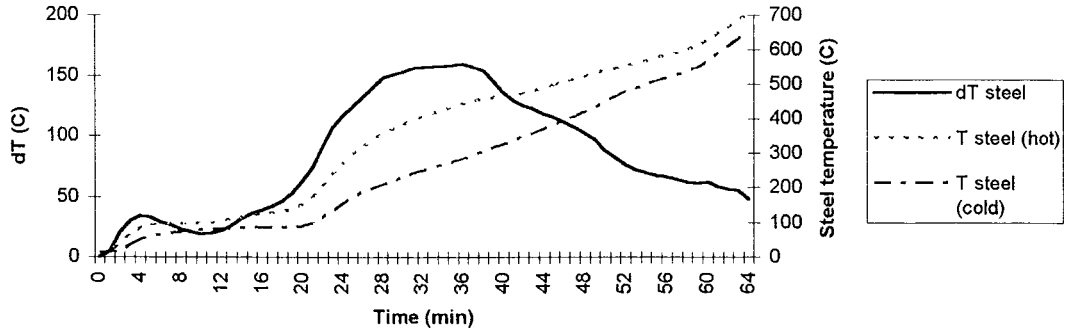

Figure 4.7a: FR 1579 Steel temperatures

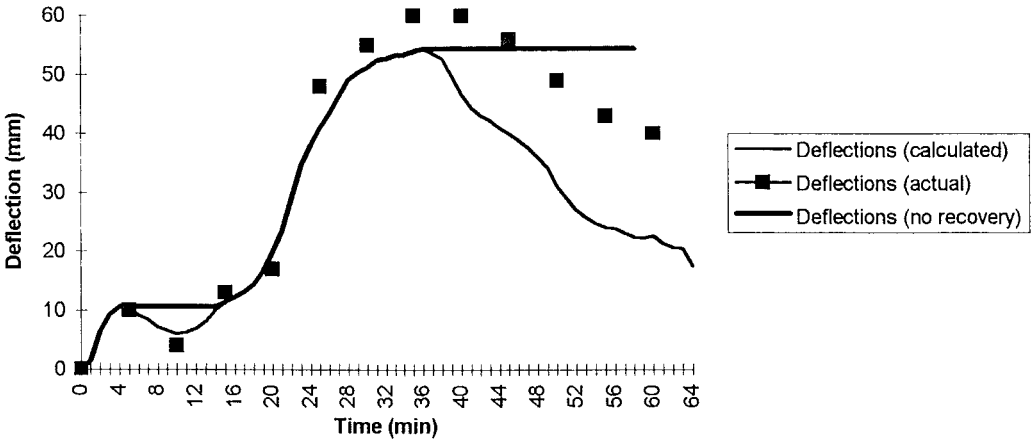

Figure 4.7b: FR 1579 Thermal deformations

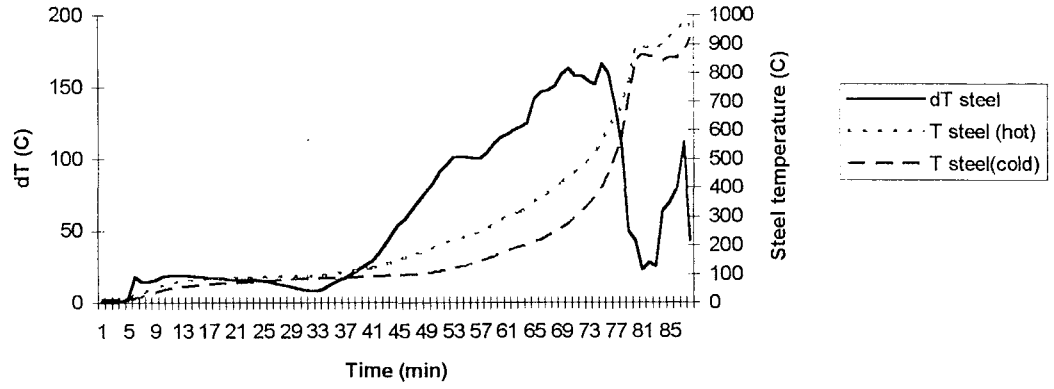

Figure 4.8a: FR 1722 Steel temperatures

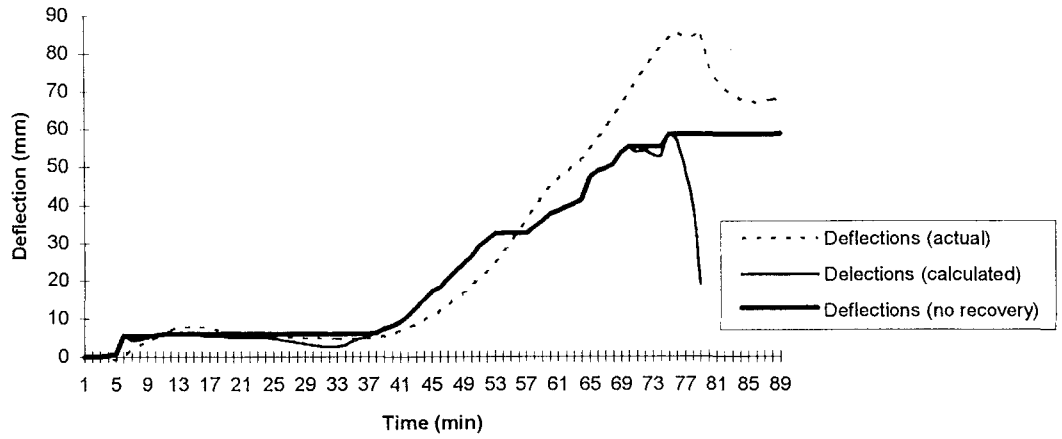

Figure 4.8b: FR 1722 Thermal deformations

4.5 P-Δ Effects

With loadbearing systems additional horizontal deformations will occur as a result of P-Δ effects. The stress-free thermal deformation as described under 4.4 above can be treated as an initial eccentricity (Δ_1) when considering the bending moment at mid-span. The initial bending moment P-Δ_1 will result in an additional horizontal deflection Δ_2 as illustrated in Figure 4.9.

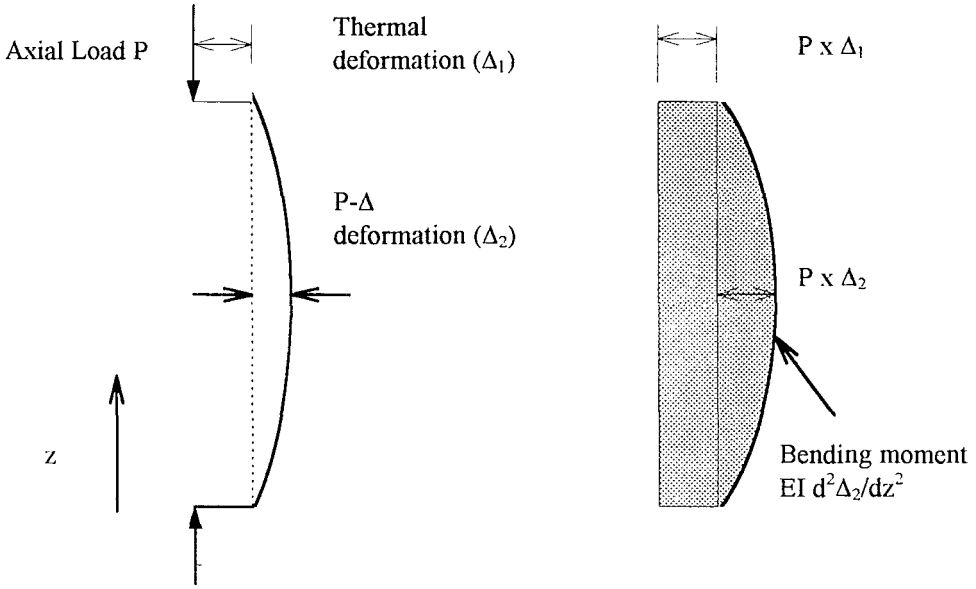

Figure 4.9: Total horizontal deflection for loadbearing systems.

The total horizontal displacement of the member will be the sum of the thermal deformation and the deformation due to P-Δ effects. The P-Δ component may be predicted analytically by solving the following moment equilibrium equation,

$$E_T I_x \frac{d^2\Delta_2}{dz^2} = P_a(\Delta_1 + \Delta_2) \qquad \text{(Eq. 4.9)}$$

where,

E_T	is the elastic modulus of steel as a function of temperature	(MPa)
I_x	is the second moment of area of the cross section	(mm^3)
P_a	is the applied axial load	(N)
Δ_1	is the initial eccentricity (thermal deformation)	(mm)
Δ_2	is the P-Δ deformation	(mm)
z	is the height	(mm)

The solution to this equation for Δ_2 at mid height is obtained as (Deam, 1993),

$$\Delta_2 = \Delta_1 \left[\cos\frac{\mu L}{2} + \left(\frac{1}{\sin \mu L} - \frac{1}{\tan \mu L} \right) \sin\frac{\mu L}{2} - 1 \right] \qquad \text{(Eq. 4.10)}$$

where,

μ is $\sqrt{\frac{P}{E_T I_x}}$ (mm^{-1})

L is the wall height (mm)

The total mid-span wall deflection thus becomes $\Delta_1 + \Delta_2$.

In Chapter 6 the measured curvature of the steel studs at various time intervals during full-scale furnace tests is discussed. The conclusion is that, for the details used in this study, any restraining moments at the stud end-fixings are insufficient to significantly restrain thermal deformations.

In the absence of evidence of restraining moments the thermal deflections are calculated using Eq. 4.8 assuming pinned joints. These deflections are entered as the initial eccentricity to calculate the P-Δ deflection in accordance with Eq. 4.10.

Figures 4.10, 4.11 and 4.12 compare the deflections measured in furnace tests FR2020, FR2028 and FR2031 with the total horizontal deflection calculated as described above assuming free rotation at the stud ends.

Some of the differences can be attributed to friction due to the test boundary conditions but generally good agreement between calculated and measured values is achieved. This further supports the assumption that any rotational end-restraints are insufficient to restrain thermal deformations.

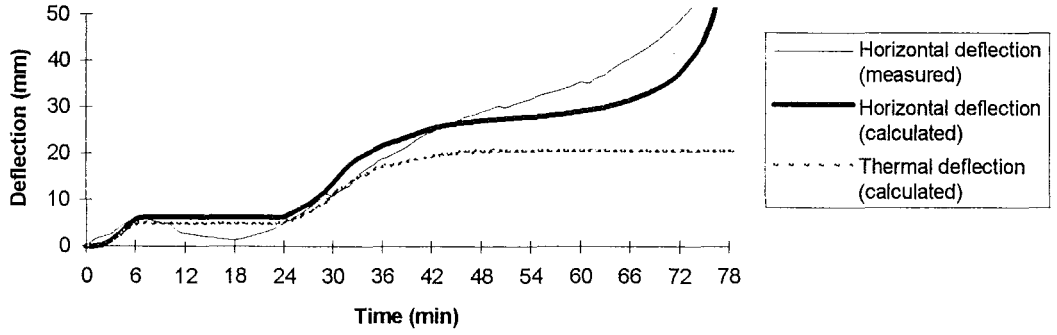

Figure 4.10: Measured horizontal deflection compared with predictions

(Loadbearing test FR2020)

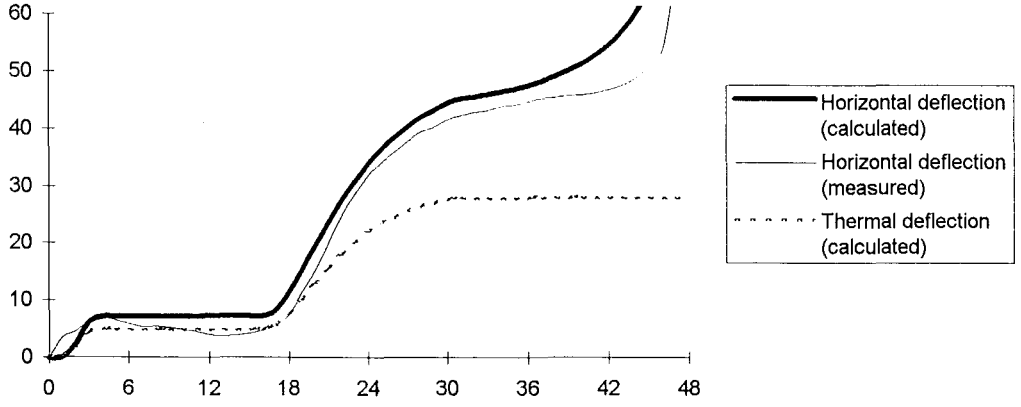

Figure 4.11: Measured horizontal deflection compared with predictions

(Loadbearing test FR2028)

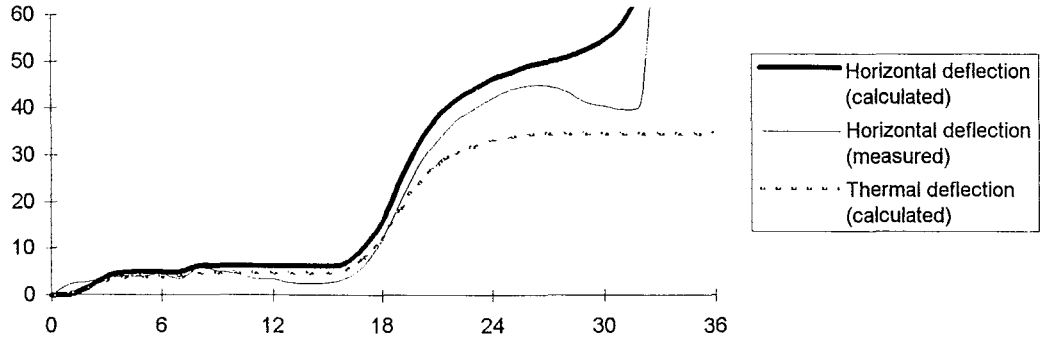

Figure 4.12: Measured horizontal deflection compared with predictions

(Loadbearing test FR2031)

4.6 Findings

The temperature effects on material properties and thermal deformations are discussed in this Chapter and summarised below.

Gypsum Plasterboard

The mechanical properties of gypsum plasterboard at elevated temperatures are relatively unknown. The ability of thermally degraded linings to prevent lateral buckling of the compression flange of steel studs is further discussed in Chapter 6. Further research is suggested.

Reliable data exists for the thermal properties of gypsum plasterboard. These data were obtained from Thomas (1994) who used values measured by Mehaffey (1991). TASEF modelling of timber framed cavity walls by Thomas achieved good agreement with measured temperatures.

Cold-Formed Steel

Reasonable agreement exists in the literature with respect to temperature effects on the mechanical properties of cold-formed steel. Experimental data by Klippstein (1980) was found to be most specific to the materials considered in this study. Polynomials were fitted to these data to obtain analytical expressions for the yield strength and modulus of elasticity of cold-formed steel as a function of temperature.

Good agreement was also found for the thermal conductivity and specific heat of steel as a function of temperature.

Thermal Deformations

Expressions for the thermal deformation of steel studs as derived by Cooke (1987) are compared with non-loadbearing test results. An analytical method is proposed for estimating super-imposed deflections due to P-Δ effects. Good agreement is achieved with measured deformations.

CHAPTER 5
THERMAL MODEL

5.1 General

Chapter 3 presents a model for predicting the structural performance of loadbearing cold-formed steel frames at room temperature. Chapter 4 outlines the effects of high temperatures on material properties and also presents a method for predicting the thermal deformation of steel framing members for a given history of steel temperature and temperature gradient across the section (and thus the expected increased stresses due to P-Δ effects). To complete a model which will predict the structural performance of LSF drywall systems exposed to fire it is therefore necessary to predict the time-temperature history of the steel framing.

Proprietary heat transfer models for timber framed cavity drywall systems are currently being developed in New Zealand by Collier (1994a) and in Australia by Clancy et al (1994). These models show promising correlation when compared with lining and framing temperatures recorded in actual fire test. It is anticipated that these proprietary models can be modified to yield useful results for steel framed systems by adjusting the thermal properties of the framing members from timber to steel.

Thomas et al (1994) describe the development of a model to predict the performance of light timber framed walls exposed to standard ISO834 test fires and 'real' compartment fires, using the commercially available heat transfer model TASEF (Sterner and Wickstrom 1990). The model was calibrated using four full scale furnace test results and good correlation was achieved.

The TASEF model was used to predict the heat transfer and steel framing temperatures in this study.

5.2 Description of the TASEF Heat Transfer Model

TASEF (Temperature Analysis of Structures Exposed to Fire) is a two dimensional finite element heat transfer program developed by the Swedish National Testing Institute. It is specifically designed to model heat transfer through materials and composite construction elements exposed to fire. The program uses a forward difference time integration scheme. The program can model voids and cavities within an assembly and the heat transfer (by radiation and convection) across these.

TASEF does not model mass transfer or ablation of materials. Mass transfer, particularly of water, does occur in LSF drywall systems due to the evaporation of water from the exposed lining material and subsequent deposit on the unexposed and cooler lining. This is expected to result in inaccuracies in predicted results for cavity temperatures up to about 120°C. However, mass transfer influences are expected to have little effect at higher temperatures when the steel framing reaches its limit state condition (> 400°C). Ablation (erosion due to heating) of gypsum plasterboard has been ignored as it occurs at high temperatures (> 800°C) and is not expected to be significant prior to structural failure of the steel framing.

The TASEF model is suitable for simulating 'real' fires as it allows for the input of any time-temperature curve. The ISO834 fire curve is a standard pre-programmed option.

5.3 TASEF Input Data

The required input data for TASEF is discussed below. Appendix B gives a typical TASEF result file which includes the input data (in units required by the model).

5.3.1 Finite Element Mesh

TASEF solves the matrices of the heat transfer equations by using a forward difference finite element method. A fine mesh will produce more accurate results, but at the expense of more computing time. Figure 5.1 shows the typical finite element mesh which was found to give reasonably accurate results at realistic program run times (approximately 40 minutes on a IBM-compatible 486PC).

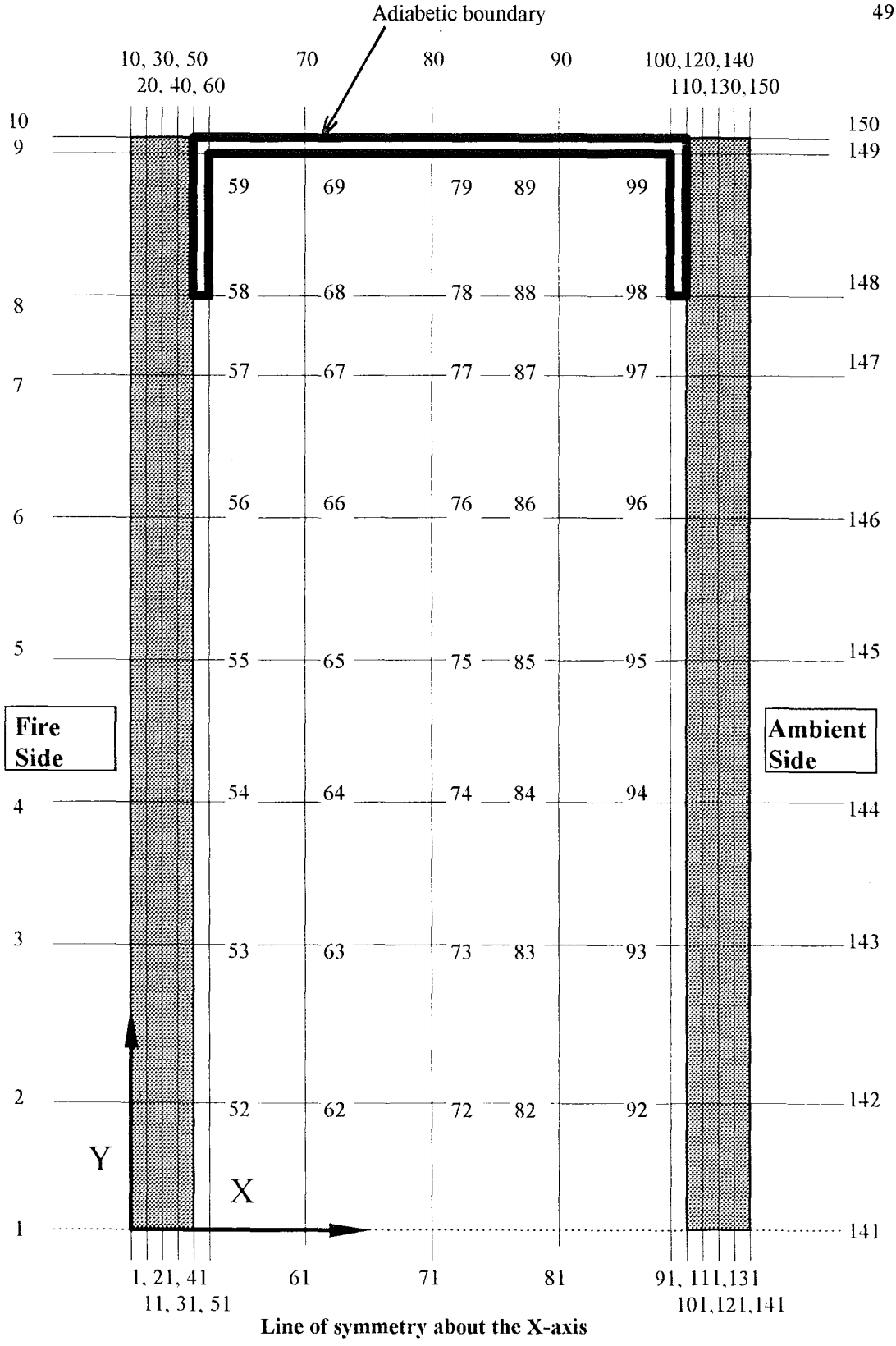

Figure 5.1: Typical finite element mesh for modelling LSF drywall systems using TASEF

5.3.2 Material Properties

TASEF requires material input data for each region except for voids. Conductivity and specific volumetric enthalpy need to be supplied as a function of temperature. The program holds a data-base for standard thermal properties of common construction materials such as steel and concrete.

For the gypsum lining material the thermal properties were generally as outlined in Chapter 4. Adjustments were made to account for the variations in density and formulation between the different thicknesses of gypsum plasterboard. These data were obtained from Thomas (1994). For reasons of confidentiality the detailed product information is not published in this report.

The standard material properties from the TASEF data-base were assigned to the steel framing members and are outlined in Chapter 4.

TASEF does not permit the angles between enclosing surfaces of voids to be greater than 180°. In the wall cavity shown in Figure 5.1, angles greater than 180° occur at node points 58 and 98. In order to enable TASEF modelling, the area of the cavity void was assumed to be contained within the rectangle defined by node points 51,59,91,98. The two areas between this void and the linings (defined by node groups 41,48,51,58 and 91,98,101,108) were given fictitious material properties. A high conductivity and low volumetric enthalpy were chosen in order to minimise the effect on the overall heat transfer of the model. The effective reduction of the cavity width by twice the steel flange thickness (approximately 2-3 mm) was considered negligible.

5.3.2 Heat Transfer Coefficients

The model was designed to be symmetrical about the X-axis with the following five boundaries between solid material and gases,

- the boundary on the Y-axis between the lining and the fire (node group 1 to 10),
- the boundary between the fictitious material adjacent to the 'hot' lining and the cavity void (node group 51 to 58),

- the boundary between the steel stud and the cavity void (node group 58,59,69,79,89,99,98)
- the boundary between the fictitious material adjacent to the 'cold' lining and the cavity void (node group 91 to 98),
- the boundary on the ambient side of the assembly (node group 141 to 150)

The heat transfer at these boundaries is governed by the correlation,

$$q = \varepsilon\sigma\left(T_g^4 - T_s^4\right) + \beta(T_g - T_s)^\gamma \qquad \text{(Eq. 5.1)}$$

where,

q is the rate of heat transfer (kW/m^2)

ε is the resultant emissivity of the gas and the boundary (dimensionless)

σ is the Stefan-Boltzmann constant ($5.67*10^{-8}$ W/m^2K^4)

β is the convection coefficient ($W/m^2K^{4/3}$)

γ is the convection power, usually 1.33

T_g is the gas temperature (K)

T_s is the surface temperature (K)

The values which were used for the boundaries in the finite element model are presented in Table 5.1 below.

Boundary Position	ε	β	γ
Fire side of the assembly	0.8	1.00	1.33
Lining, fire side of the cavity	0.6	1.00	1.33
Steel stud, in the cavity	0.8	1.00	1.33
Lining, ambient side of the cavity	0.6	1.00	1.33
Ambient side of the assembly	0.6	2.20	1.33

Table 5.1: Heat transfer coefficients for the TASEF model

5.4 Comparison of TASEF and Test Results

The output from TASEF runs was compared with actual test data. A detailed description of the furnace tests is given in Chapter 6. The furnace time-temperature conditions for tests FR2020 and test FR2028 was in accordance with the standard ISO834 fire curve. Time-temperature input for test FR2031 was a simulated 'real' fire with a relatively slow start and a rapid acceleration to temperatures significantly hotter than the ISO834 conditions after about 8 minutes.

The comparison between predicted and measured temperatures is illustrated in Figures 5.3a and 5.3b (furnace test FR2020), 5.4a and 5.4b (furnace test FR2028) and 5.5a and 5.5b (furnace test FR2031). An 'a' denotes lining temperatures at positions 2,5 and 6, and a 'b' denotes steel framing temperatures at positions 3 and 4. The positions are as illustrated in Figure 5.2. Heavy lines indicate the results from the furnace tests and the lighter lines indicate the predictions using the TASEF model.

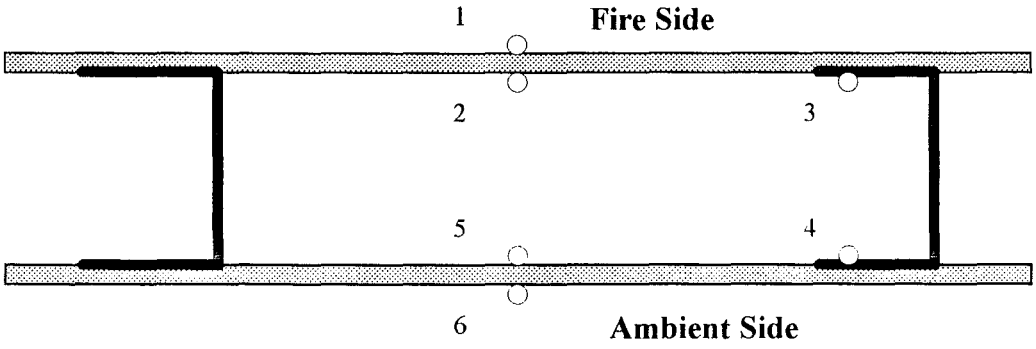

Figure 5.2: Temperature positions

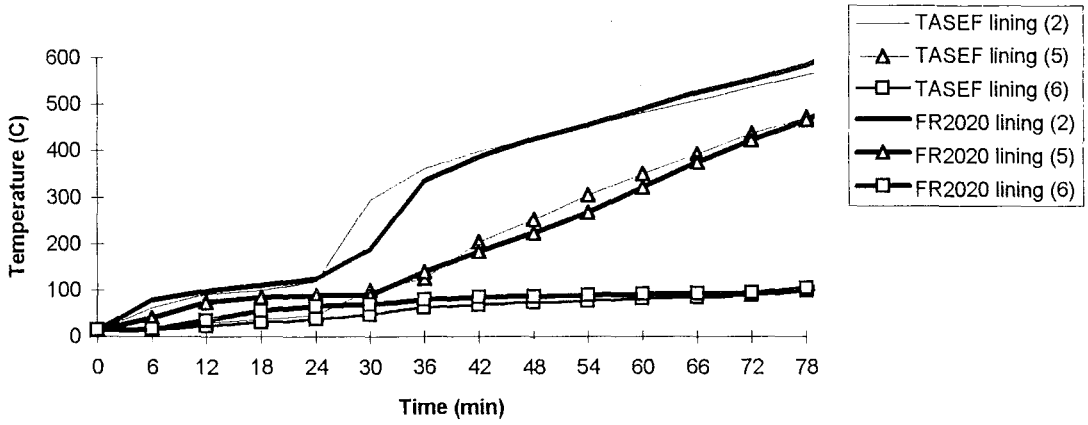

Figure 5.3a: FR2020 Lining temperatures

(Comparison of TASEF and furnace test results)

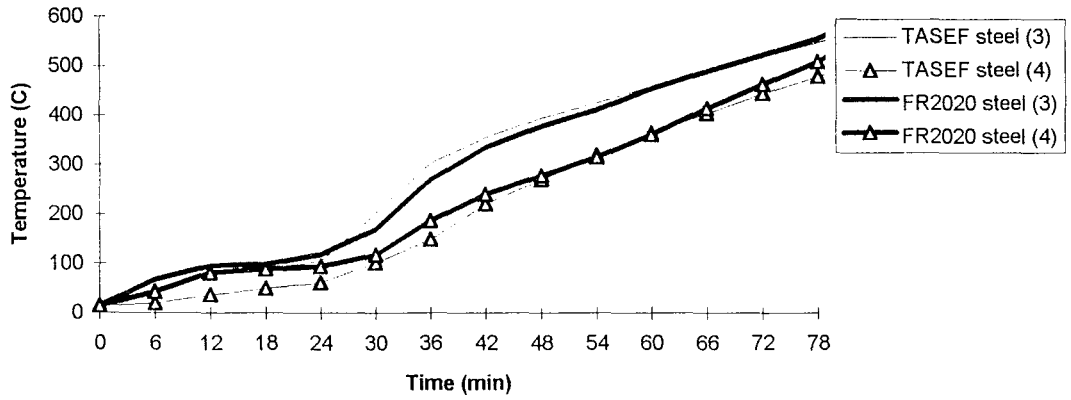

Figure 5.3b: FR2020 Steel framing temperatures

(Comparison of TASEF and furnace test results)

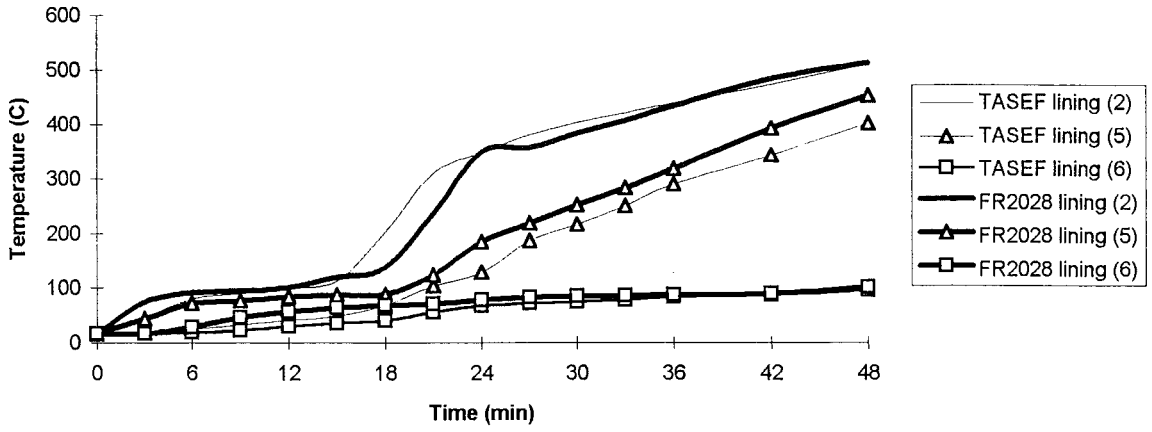

Figure 5.4a: FR2028 Lining temperatures

(Comparison of TASEF and furnace test results)

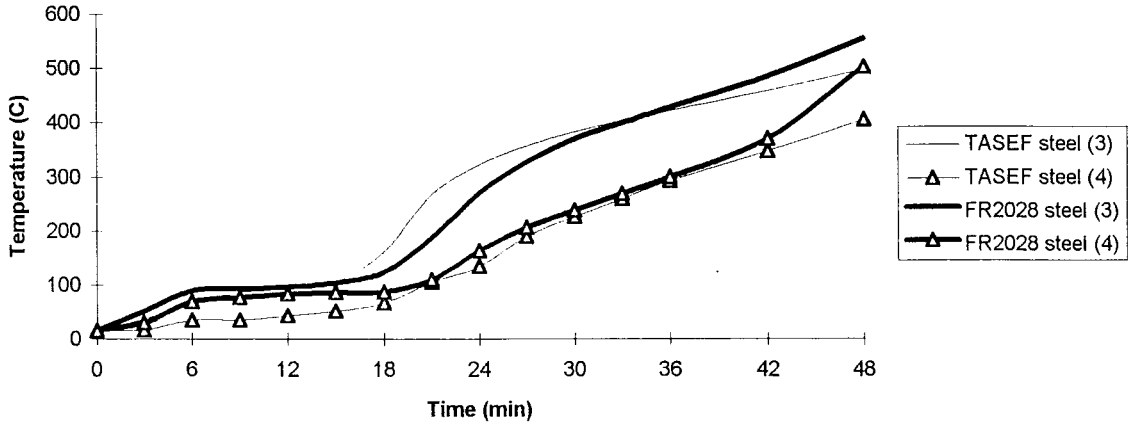

Figure 5.4b: FR2028 Steel framing temperatures

(Comparison of TASEF and furnace test results)

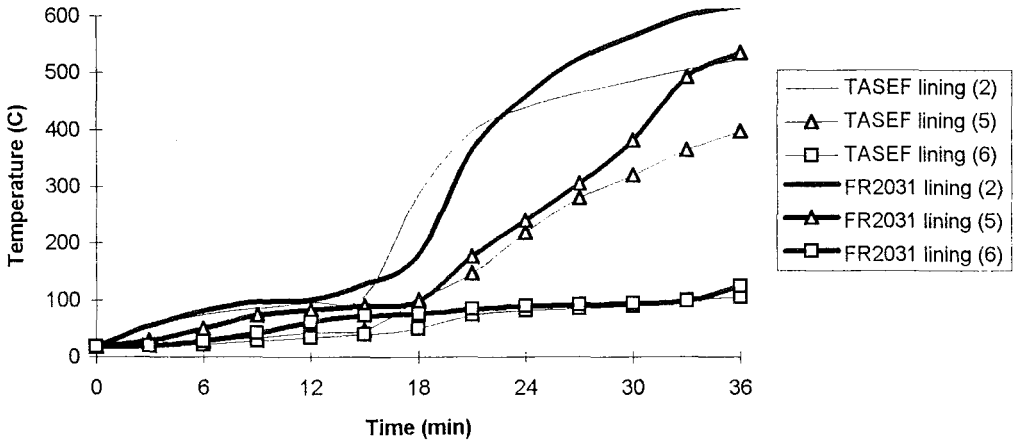

Figure 5.5a: FR2031 Lining temperatures

(Comparison of TASEF and furnace test results)

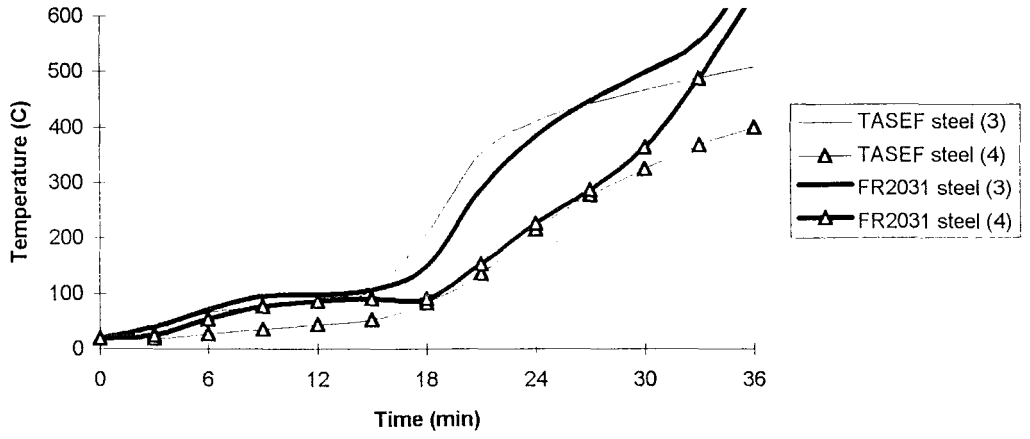

Figure 5.5b: FR2031 Steel framing temperatures

(Comparison of TASEF and furnace test results)

5.5 Findings

TASEF does not model mass transfer. As a result a discrepancy occurs at the ambient side of the wall assembly at positions 4, 5 and 6 at temperatures below 100 °C. The lining on the fire side of the cavity is losing water due to evaporation. The ambient side of the cavity is heated by moisture condensing on it. The energy input from condensation is equal to the energy required to evaporate it again later. The overall effect has been found to be negligible (Thomas, 1994).

At high temperatures, opening of the exposed sheet joints due to deformation of the framing members and cracking and ablation of the exposed linings will allow the passage of hot gases into the cavity. This is reflected by an accelerated rise in measured temperatures towards the end of the tests. TASEF does not model for ablation or degradation of linings. As a result inaccuracies between predicted and measured temperatures occur at high temperatures.

It is believed that a rapid rate of temperature rise and an early exposure to high temperatures, such as in test FR2031, results in an earlier and more severe lining degradation due to increased 'thermal shock'. This is confirmed by Collier (1994b) following work on timber framed cavity walls exposed to realistic fires. As a result TASEF temperature predictions for fires which are significantly hotter than the ISO834 conditions are non-conservative (ie, too low), as can be seen in Figure 5.5.

For wall assemblies exposed to cooler fires the effect of ablation is not expected to be greater than for exposure to ISO834 conditions and agreement between heat transfer model predictions and measured temperatures is expected to be similar. This is also confirmed by Collier (1994b).

To more accurately predict the performance of cavity wall systems against real fires further research is recommended into the behaviour of gypsum plasterboard linings when exposed to different time- temperature conditions.

The TASEF heat transfer model can be used to predict the temperature distribution of LSF drywall systems exposed to fire with reasonable accuracy. The results are within limits expected from a commercially available multi-purpose computer program. However, TASEF temperature predictions may be too low (non-conservative) for fires which are significantly hotter than the ISO834 time-temperature curve. Further accuracy may be achieved by modelling for ablation as is being done in the proprietary heat transfer models for cavity wall construction that are currently being developed (Collier 1994a, and Clancy 1994).

CHAPTER 6

FULL-SCALE FIRE TESTING

6.1 General

To evaluate the performance of loadbearing LSF drywall systems exposed to fire, three full scale furnace tests were carried out at the fire testing laboratory of BTL (Building Technology Limited) a wholly owned subsidiary of BRANZ (Building Research Association of New Zealand) at Judgeford, near Wellington.

All tests were carried out generally in accordance with AS1530 : Part4 (SAA, 1990), except that the furnace time-temperature curve for the third test was modified to represent a 'real' fire. For the other two tests the furnace temperature followed the prescribed ISO834 standard fire.

The fire resistance rating of a loadbearing test specimen is defined by AS1530:Part 4 as the time to failure, expressed in minutes, under one or more of the following three criteria,

- *Structural failure* is deemed to have occurred when collapse occurs,

- *Integrity failure* is deemed to have occurred upon collapse or the development of cracks, fissures, or other openings through which flames or hot gases can pass,

- *Insulation failure* is deemed to have occurred when either the average temperature of relevant thermocouples on the unexposed face of the specimen rises by more than 140°C, or when any one of these relevant thermocouples rises by more than 180°C above the initial temperature.

6.2 Description of the Test Specimens

The specimens were all constructed in a concrete lined specimen holder nominally 3 metres wide by 4 metres high. A 1 metre high concrete infill panel was used for testing the wall less than 3 metres in height. Solid timber infill plinths lined with double layers of gypsum plasterboard were bolted to the specimen holder at the top and bottom of the walls. The bottom platen of the specimen holder was free to move up and down. During construction of the specimens the platen was held in position, but during the fire tests load was applied to the wall assembly by means of hydraulic jacks placed between the platen and the frame as illustrated in Figure 6.1. Table 6.1 gives an overview of the specimens and tests carried out as part of this study.

Fire Test Number	FR2020	FR2028	FR2031
Wall height (mm)	2850	3600	3600
Steel Grade (MPa)	300	450	450
Framing type	C-section	lipped C-section	lipped C-section
Framing (mm)	76 x 32 x 1.15	102 x 51 x 1.0	102 x 51 x 1.0
Stud spacing (mm)	600	600	600
Nog spacing (mm)	one row central	one row central	one row central
Frame connections	welded	welded	welded
No. loadbearing studs	4	4	4
Load (kN/stud)	6	16	12
Lining exposed (mm)	16.0	12.5	12.5
Lining unexposed (mm)	16.0	12.5	9.5
Fire curve	ISO834	ISO834	'real'

Table 6.1: Full scale fire test specimens

6.2.1 Steel Frames

The test specimens for all three tests consisted of welded loadbearing steel framed walls. The studs were placed at 600 mm centres and all frames had a central row of nogs. A timber loading block was nailed to the timer infill and located on the top channel section to ensure loading of the central four studs only. Top and bottom channels were screw fixed to the loading block and timber infill with 50 mm wood screws at each stud location. The flanges of the top channel were cut in the end bays to minimise any load transfer to the cooler edge studs and to the specimen holder by means of friction. Figure 6.1 shows the outline of the steel frame in the specimen holder in broken lines. Figure 6.2 gives a typical detail at the edge stud.

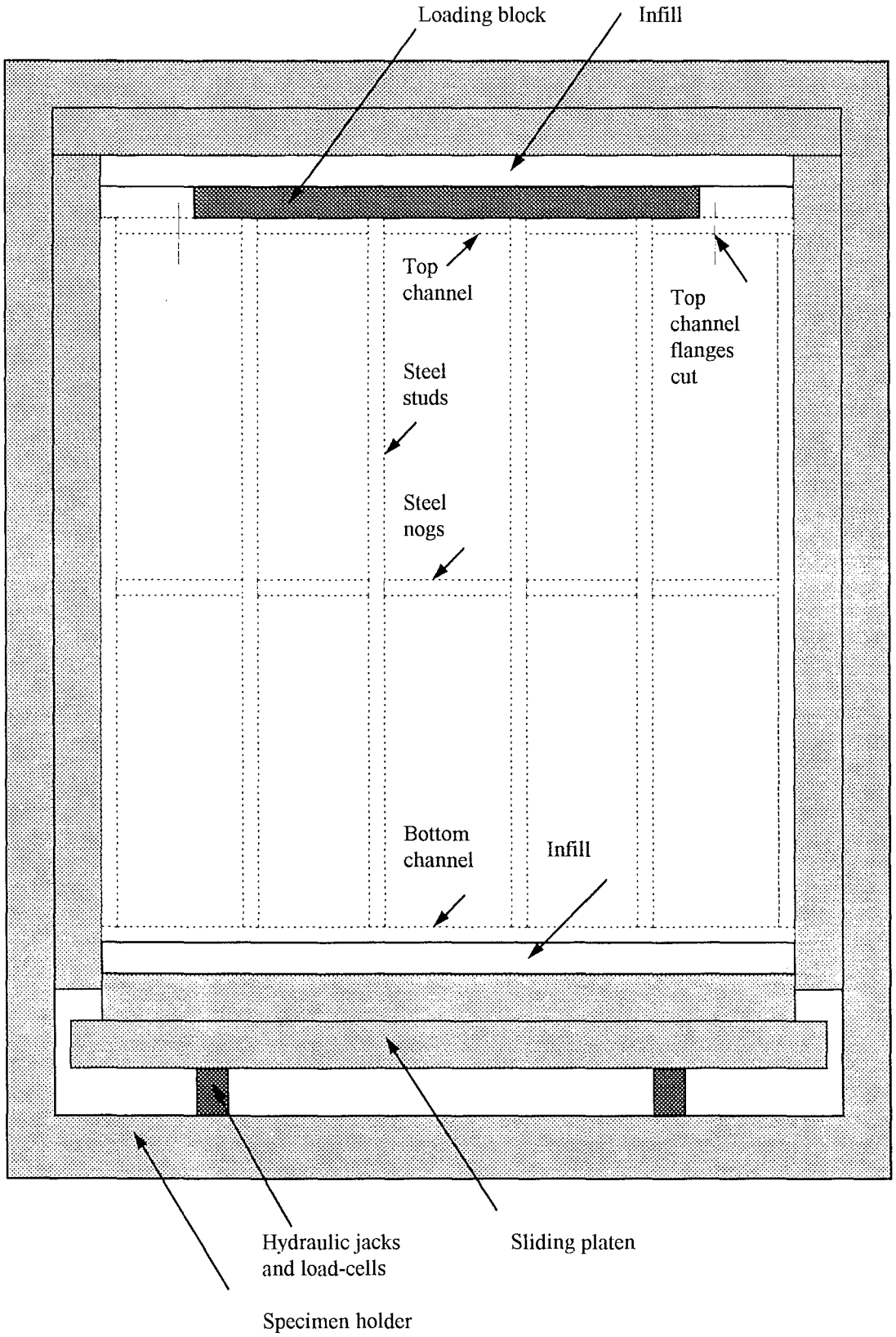

Figure 6.1: Test arrangement for loadbearing wall assemblies

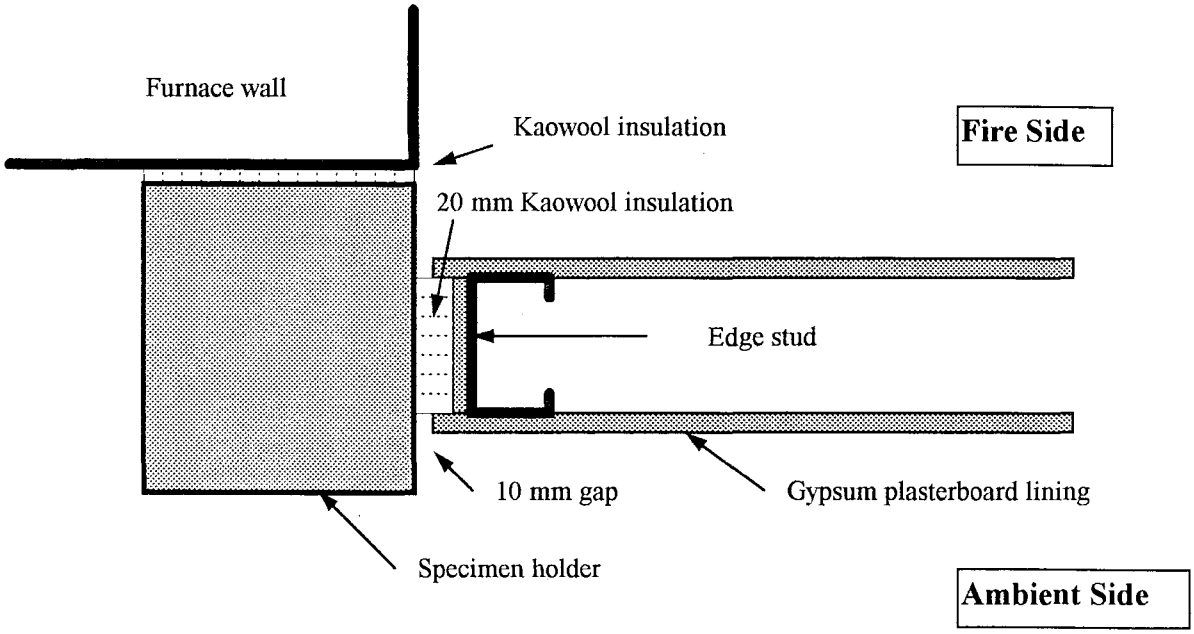

Figure 6.2: Typical edge detail

6.2.2 Gypsum Plasterboard linings

The steel frames were lined on both the exposed and unexposed face with a single layer of glass-fibre reinforced gypsum plasterboard. The sheets were fixed vertically to all studs with 6 gauge 32 mm long self drilling drywall screws spaced at 300 mm centres. The vertical sheet joints were formed over studs and tape reinforced and plaster stopped in accordance with recommended trade practice (Winstone Wallboards, 1992b) using paper tape and two coats of bedding compound. The sheet lenght covered the full frame height and no horizontal joints were needed.

6.3 Furnace Time-Temperature Input

The furnace time-temperature input for tests FR2020 and FR2028 was in accordance with the standard ISO834 fire curve as defined by equation 1.1 (Chapter 1). The curve is shown in Figure 6.3 and compared with the proposed temperature input for test FR2031. The FR2031 input fire curve was chosen to represent a fast 'pre-flashover' ignition stage, a relatively fast growth stage, and a ventilation controlled steady state. Testing a significant deviation from the standard ISO834 curve will allow the calibration of the theoretical model for predicting the performance of LSF drywall systems against 'real' fires.

In the actual fire test, the furnace temperatures were considerably different from those shown in Figure 6.3 because of difficulties in driving the furnace.

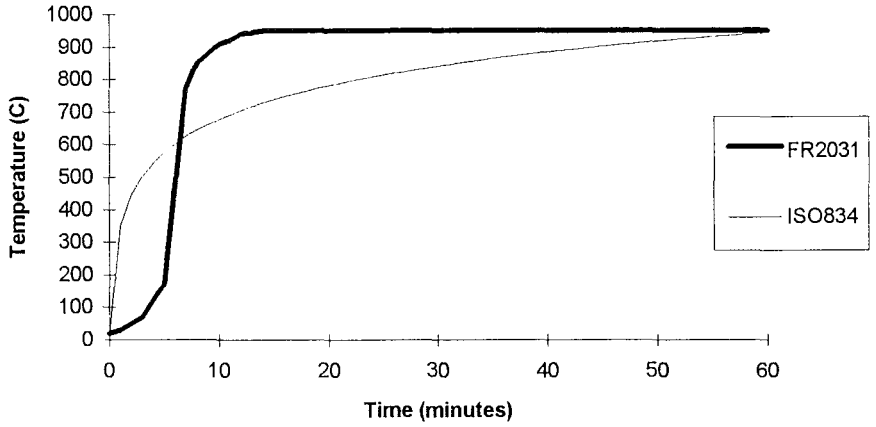

Figure 6.3: Furnace test input fire curves

6.4 Measurements

The specimen holder containing the wall assembly was sealed against the furnace and the furnace pressure was maintained at least 8 Pa greater than the laboratory pressure over the top two thirds of the specimen as outlined in AS1530:Part 4. In addition the following continuous measurements were made.

6.4.1 Load

The specimens were pre-loaded 30 minutes prior to the start of the fire test as required by the test standard. Load was recorded by means of load-cells placed between the jacks and the moving bottom platen. The load was kept constant for the duration of the test and vertical thermal expansion of the steel framing members was allowed to occur freely. In contrast, testing described by Klippstein (1980 a,b) in accordance with the requirements of the ASTM (1979) did not allow for this vertical expansion to occur and as a result the applied loads during the fire tests increased to almost twice the initial (design) load. Klippstein was critical of the test method and recommended a hydraulic response of the loading equipment to the change in stud length.

6.4.2 Temperatures

Furnace temperatures were measured using twelve thermocouples distributed evenly on a vertical plane approximately 100 mm from the exposed face of the specimen.

As required by the test standard the temperature on the unexposed face of the specimens was measured using five 'key' thermocouples, one at mid-point of the specimen and one at the centre of each of the four quarters of the specimen. In addition lining temperatures were recorded within the cavity on both the exposed and unexposed linings between framing members.

Steel temperatures were recorded at 1/4 points on the four central studs. At each location thermocouples were attached to the inside of the steel flange adjacent to the exposed lining, the inside of the steel flange adjacent to the unexposed lining, and the steel web.

6.4.3 Heat Flux

A heat flux meter was installed flush with the exposed side of the exposed lining at mid height of the specimen in all tests to provide information on the actual heat flow into the specimen compared with the heat flow predicted from furnace temperature. This data may be used to confirm a value for emissivity in the development of proprietary heat transfer models. Heat flux readings are not reported in this study.

6.4.4 Horizontal Deflections

Horizontal deflections of the specimen were recorded manually at 10 or 15 minute intervals by means of theodolite readings of points located on all loadbearing studs. For test FR2020 manual readings were taken at the ends and at 1/4 points along the studs. For tests FR2028 and FR2031 manual readings were taken at the ends and at 400 mm centres (1/9 points) along the studs. Linear potentiometers located at mid-height on the unexposed lining provided continuous electronic readings of horizontal mid-span deflection of all four loadbearing studs.

6.4.5 Vertical Displacements

A continuous record of the vertical displacement of the loading platen was obtained by using two linear potentiometers, one placed at each end of the platen.

6.5 Results

The test results and main observations are presented below. Formal test reports for each individual test have also been prepared by BTL (1995 a,b,c).

6.5.1 Temperatures

The 'severity' of a fire resistance test is established by comparison of the area under the curve of the mean measured furnace temperature with the area under the standard ISO834 curve for the same period. The severity for tests FR2020 and FR2028 was 100% in both cases which indicates a close agreement with the standard curve.

The severity measure was not applied to the FR 2031 'real' fire curve. The curve actually achieved is shown in Figure 6.4 and is considerably different from the proposed curve. The measured time-temperature curve was used as input for modelling purposes.

Measured lining and steel temperatures for the three tests are presented in Figures 6.4, 6.5, and 6.6. Numbers in brackets indicate the temperature position as illustrated in Figure 5.2. The temperatures represent the average of thermocouple readings within a specimen measuring the same location on the framing or linings (eg, the average of all exposed steel flange temperatures is presented). Individual temperatures were compared for consistency before averaging and spurious results were eliminated if required.

The lining and steel framing temperatures for all three furnace tests are also separately presented in Chapter 5 and compared with computer model predictions.

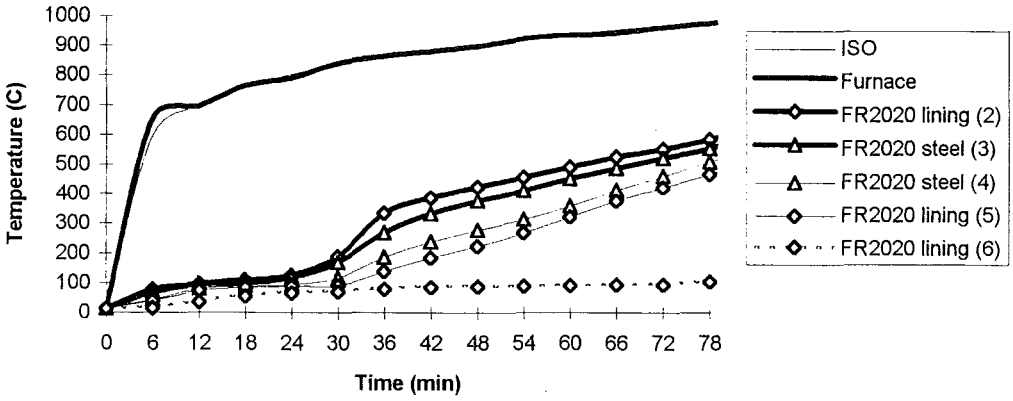

Figure 6.4: Recorded Temperatures - FR2020

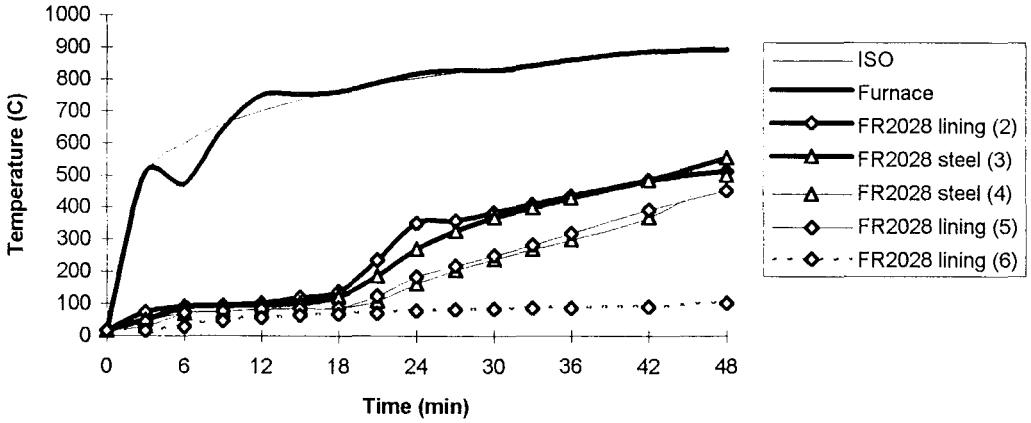

Figure 6.5: Recorded Temperatures - FR2028

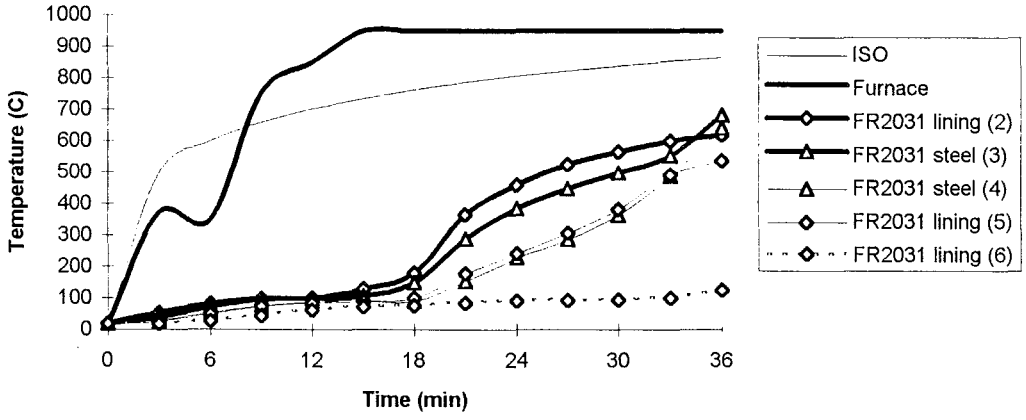

Figure 6.6: Recorded Temperatures - FR2031

6.5.2 Heat Flux

The measured heat flux was used to calculate a resultant furnace emissivity (presented in Table 6.2) using the expression,

$$q = \varepsilon_f \sigma (T_f^4 - T_a^4) \qquad \text{(Eq. 6.1)}$$

where,

q is the measured heat flux (kW/m^2)

ε_f is the resultant furnace emissivity (dimensionless)

σ is the Stefan Boltzmann constant (5.67×10^{-11} kW/m^2K^4)

T_f is the furnace temperature (K)

T_a is the ambient temperature (K)

Test Number	Resultant furnace emissivity (ε_f)
FR2020	0.92
FR2028	0.82
FR2031	0.87

Table 6.2 Resultant furnace emissivity (ε_f)

Differences may be related to the calibration and cleanliness of the measuring equipment and 'smokiness' in the furnace. Further analysis of the resultant furnace emissivity is considered outside the scope of this study.

6.5.3 Horizontal Deflections

In all cases horizontal deflections were towards the fire. The mid-span horizontal deflections for all three tests are presented in Chapter 4 and compared with predictions by calculation. The measured deflections at points along the length of the two central studs are presented in Figures 6.7, 6.8 and 6.9. Polynomial curves have been fitted to the data points to illustrate the curvature at two different time intervals.

6.5.4 Vertical Displacements

The vertical movement of the bottom platen due to thermal expansion of the studs is shown for the three tests in Figures 6.10, 6.11 and 6.12.

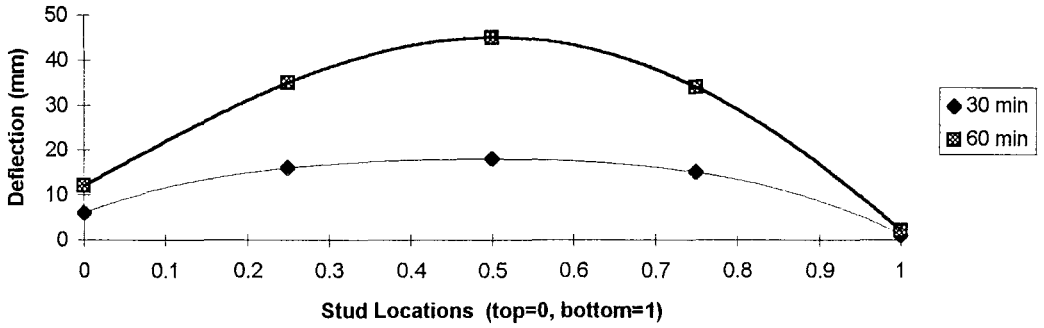

Figure 6.7: Measured stud curvature - FR2020

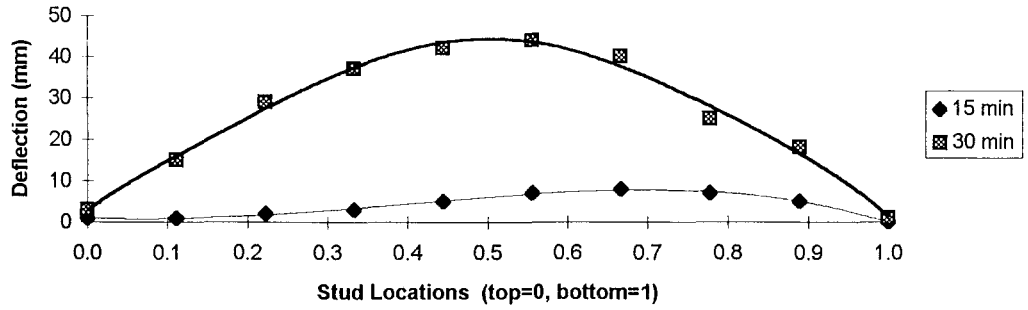

Figure 6.8: Measured stud curvature - FR2028

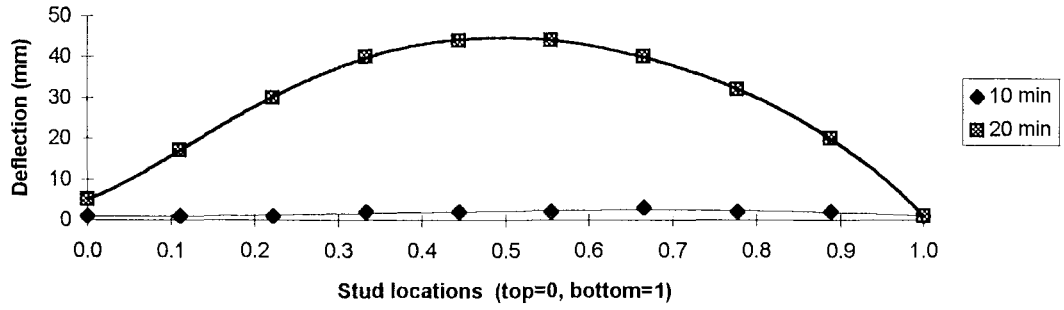

Figure 6.9: Measured stud curvature - FR2031

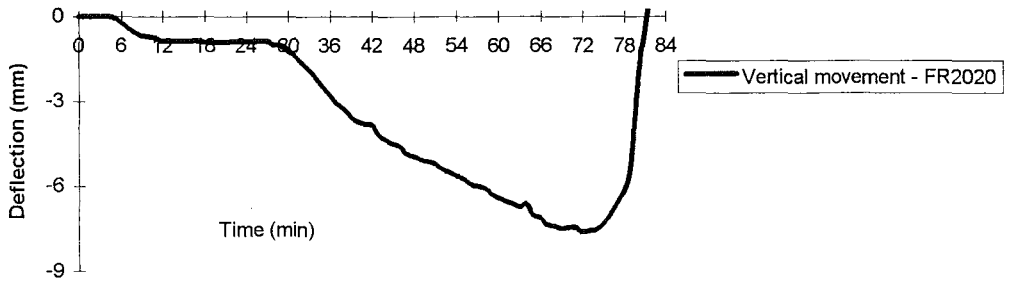

Figure 6.10: Measured vertical movement - FR2020

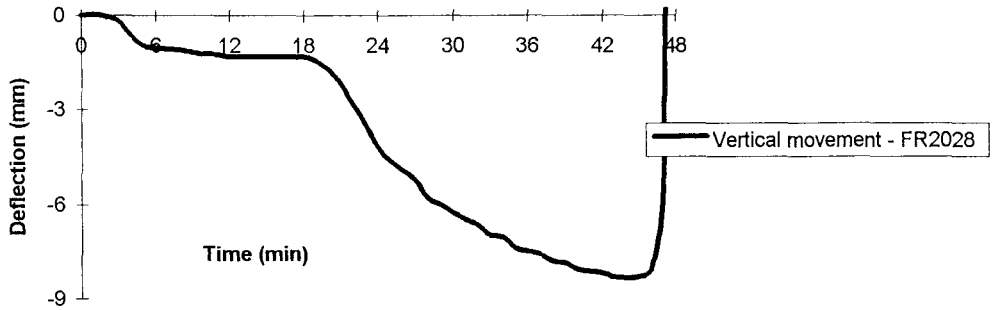

Figure 6.11: Measured vertical movement - FR2028

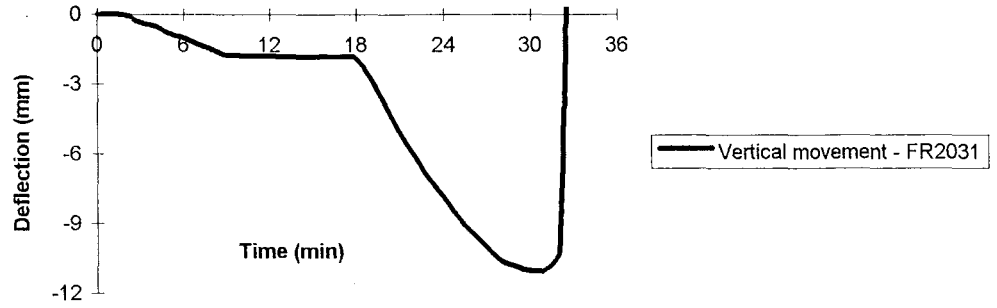

Figure 6.12: Measured vertical movement - FR2031

6.5.5 Failure Modes

In all three tests failure was initiated by structural collapse of the loadbearing studs. This was followed by integrity failure of the unexposed lining due to excessive deformations at the locations of stud buckling.

The failure mode for tests FR2020 and FR2028 was flexural buckling about the major axis initiated by local buckling of the compression flange between fasteners adjacent to the unexposed lining. The failure mode for test FR2031 was by torsional flexural buckling after the unexposed lining failed to provide lateral restraint to the compression flange. Failure modes for the three tests are shown in Figures 6.13, 6.14 and 6.15 and are further discussed under heading 6.6 below.

Structural failure was not clearly defined in test FR2020. At approximately 72 minutes a marked increase in horizontal deflections and a reversal in vertical movement was observed indicating failure of the loadbearing studs. However, load was redistributed through diaphragm action of the unexposed lining to the cooler edge studs which were supported by friction against the specimen holder. In tests FR2028 and FR2031 the applied stud load was significantly higher and thus the effect of any friction was minimised. The edge studs were also partly cut to eliminate significant loadbearing ability. As a result failure was much more sudden.

Table 6.3 gives the failure times for the three tests. Structural failure is defined by the reversal in vertical movement of the loading platen. Whilst the studs are supporting the applied load, the temperature induced expansion pushes the platen downwards. At failure the horizontal deflection of the frame will accelerate and the vertical movement will reverse.

Test Number	Structural Failure (min)	Integrity Failure (min)	Insulation Failure (min)
FR2020	72	78	not critical
FR2028	44	45	not critical
FR2031	32	32	not critical

Table 6.3: Summary of failure times for the full scale fire tests

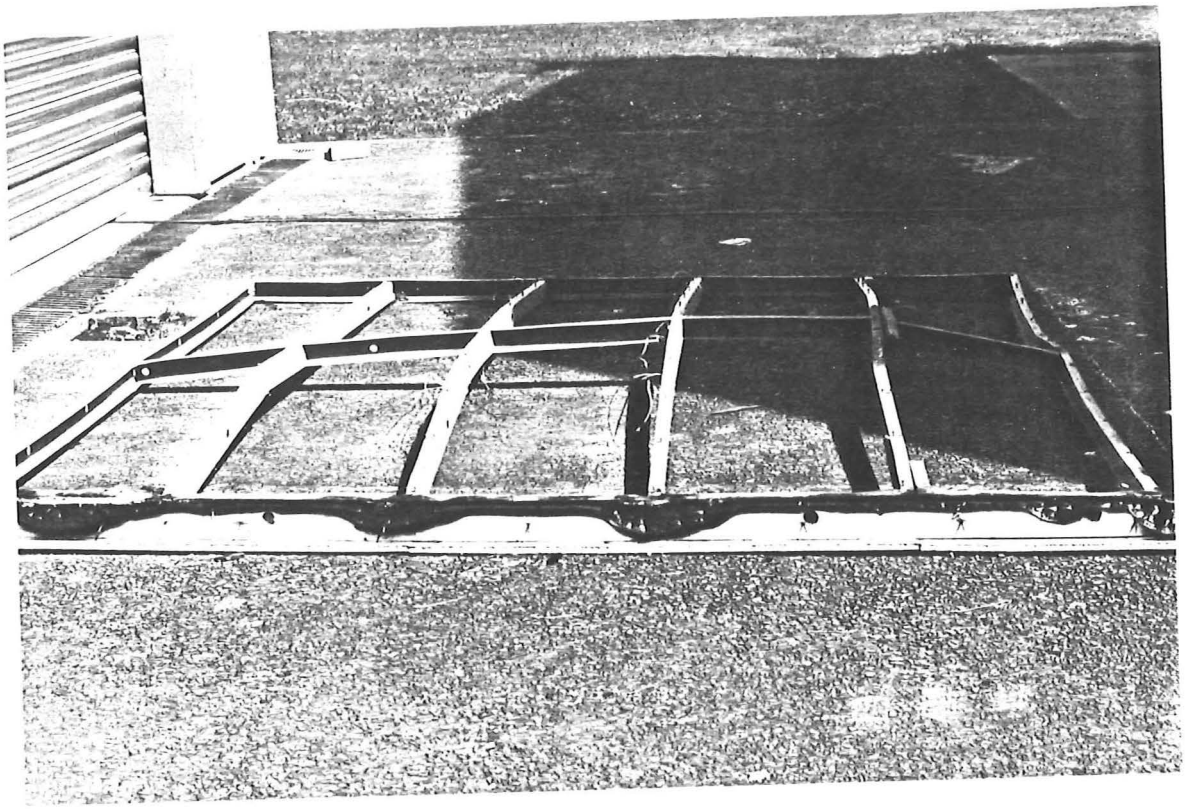

Figure 6.13: Failure mode - FR2020

(Flexural buckling about the major axis)

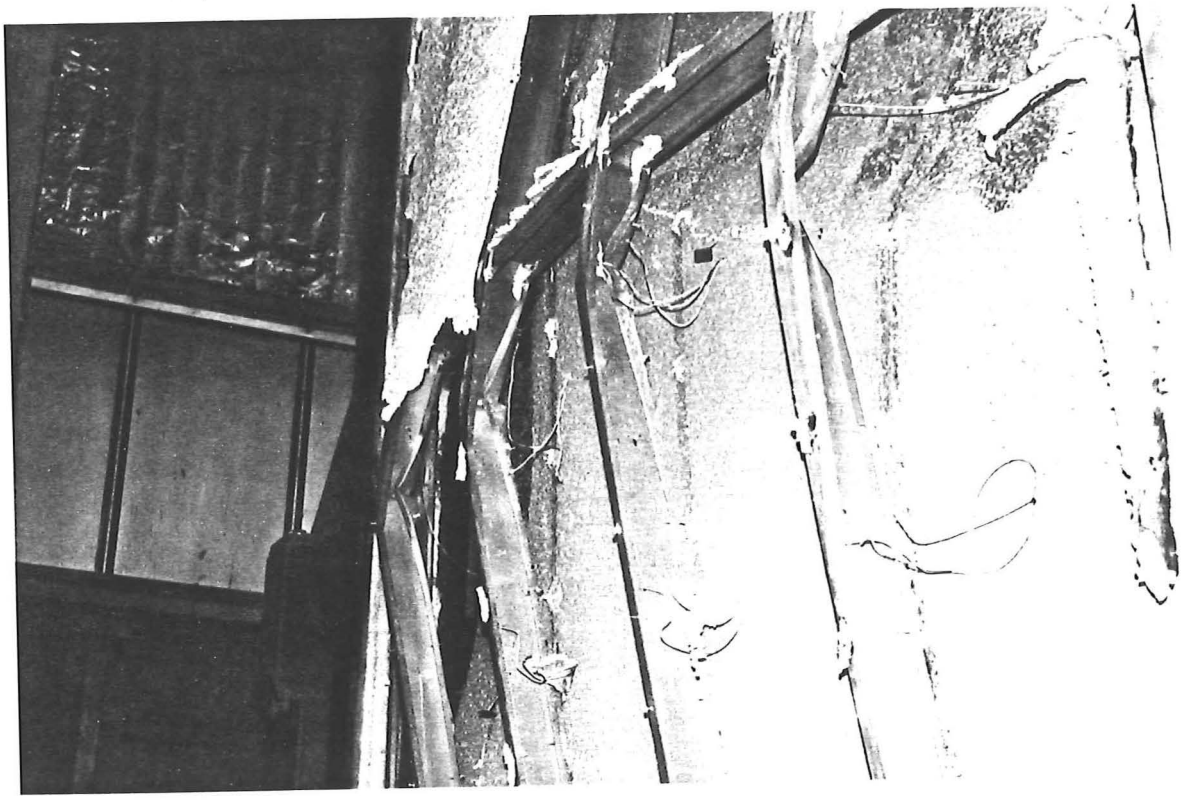

Figure 6.14: Failure mode - FR2028

(Flexural buckling about the major axis)

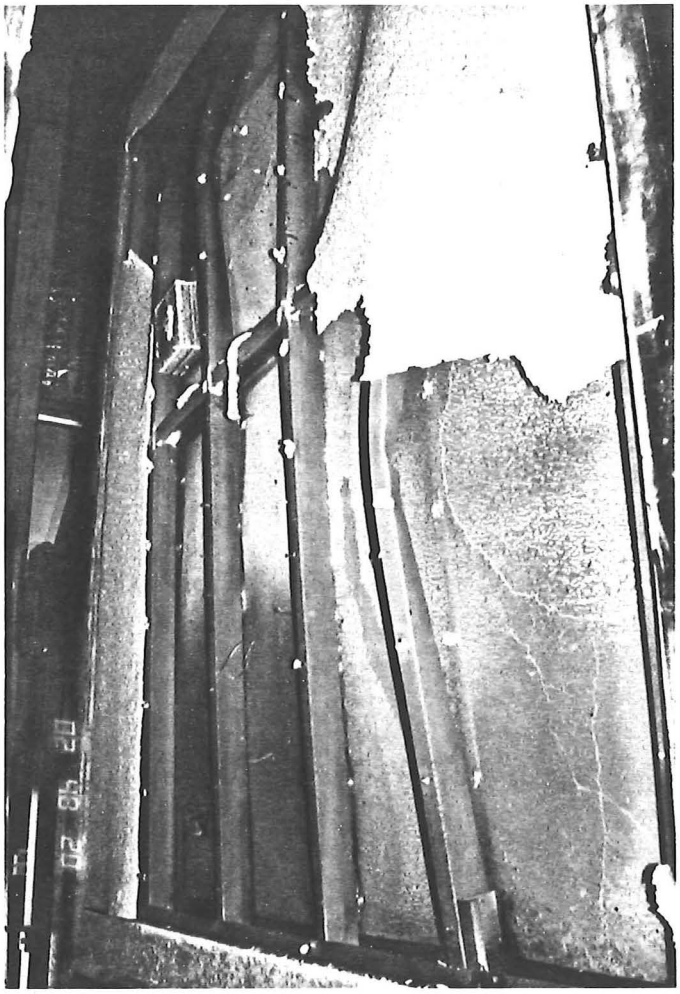

Figure 6.15: Failure mode - FR2031
(Torsional flexural buckling)

6.6 Discussion of Test Results

The test results presented under heading 6.5 above and the general observations during the tests are discussed below.

6.6.1 Temperatures

Tests FR2020 and FR2028 were carried out with the ISO834 fire curve as the furnace time-temperature input. Measured temperatures throughout the wall assembly were generally in accordance with TASEF heat transfer model predictions and consistent with expectations based on previous testing carried out for Winstone Wallboards on non-loadbearing steel framed drywall systems (BRANZ 1988, 1990, 1992).

After a short initial cooler phase the input fire for test FR2031 was significantly hotter than the ISO834 conditions. Measured temperatures were higher than heat transfer model predictions and expectations based on the higher furnace temperatures.

This is confirmed by Figure 6.16 which shows as an example the ratio of measured steel stud temperatures over the furnace temperature.

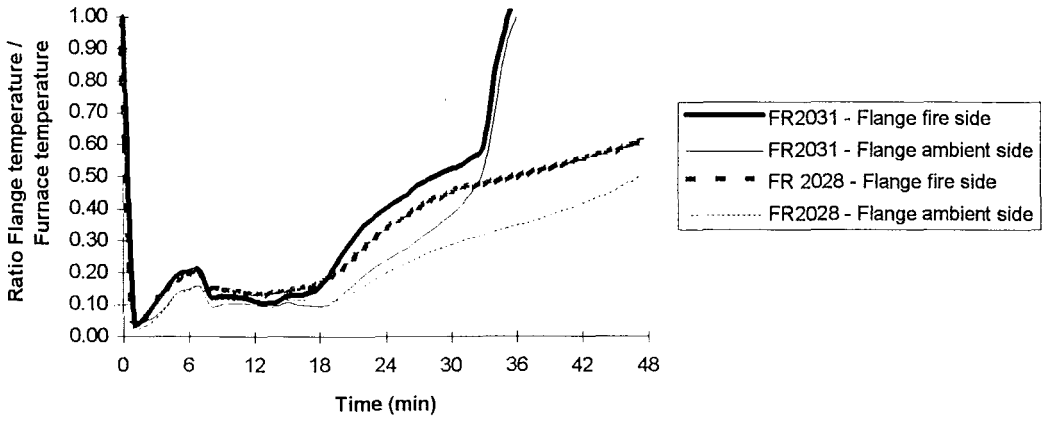

Figure 6.16: Ratio of measured stud temperatures over furnace temperatures for tests FR2028 and FR2031

Viewing holes in the test furnace allow parts of the exposed face of the specimen to be observed during a fire test. The cracking observed in the exposed lining of test FR2031 was more severe than that observed for test FR2028. It is believed that this is as a result of the higher early temperatures which result in a more severe 'thermal shock' and more sudden shrinkage of the exposed lining.

Further research into this phenomenon is recommended. Heat transfer computer models may require the input of a lining ablation or degradation factor for fires hotter than the ISO834 conditions.

6.6.2 Deflections

The measured mid-span horizontal deflections are presented and compared with analytical predictions for studs with pinned ends in Chapter 4. The stud curvatures for the three furnace tests are presented in Figures 6.7, 6.8 and 6.9. Although some indication of double curvature is suggested by Figure 6.8 for FR2028 at 15 minutes, no evidence of restraining moments is apparent for any of the tests near failure.

It is concluded that thermal deformations override any rotational restraint provided by stud-to-channel connections and any restraining moments due to load relocation. Further evidence of this was observed after inspection of the steel frame used in test FR2020. As illustrated in Figure 6.17 a 'waviness' occurred near the stud ends indicating a local buckling of the hot flange due to developing restraining moments.

The welded connections tested in this study are expected to provide the most rigid detail when compared with other typical stud-to-channel connections described in Chapter 3. It is unlikely that more restraint will be provided by alternative connections. A possible exception could be cantilever steel framing systems cast in concrete footings. However, such systems are considered outside the scope of this study.

There is no evidence to suggest that allowance can be made for rotational end-restraint in a structural model which predicts the fire performance of LSF drywall systems.

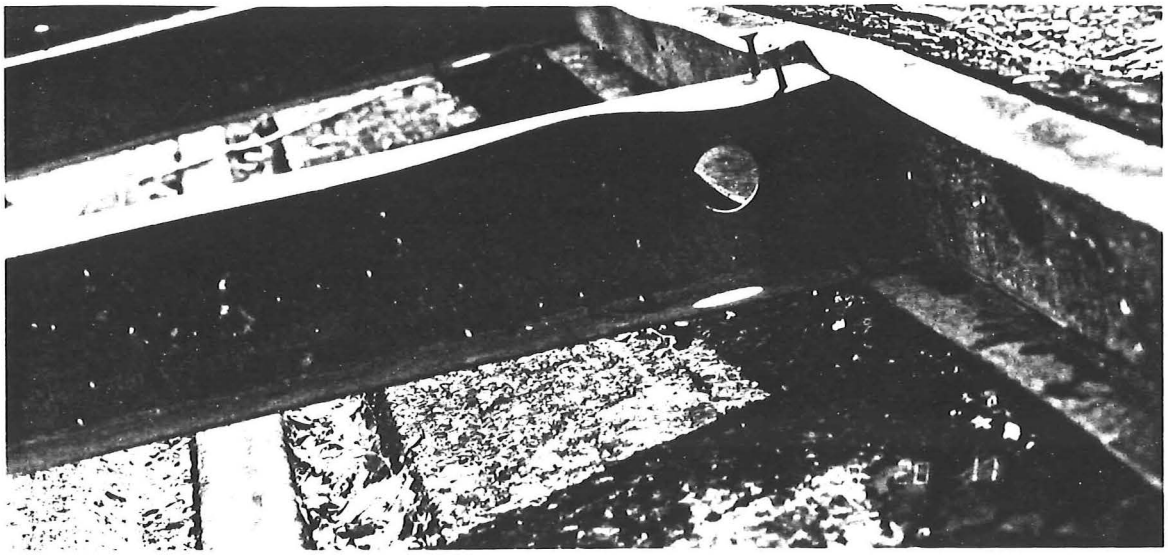

Figure 6.17: Local buckling observed near stud ends in test FR2020

6.6.2 Failure Modes

The failure mode for all three tests was by buckling of the cooler stud flange on the ambient side of the wall assembly near mid-span. This is the flange with the higher compressive stresses because deflection is towards the furnace. Lateral buckling about the minor axis and flexural torsional buckling was prevented by the unexposed linings in tests FR2020 and FR2028. In test FR2031 torsional buckling occurred as the thinner unexposed lining was unable to prevent this buckling mode. The reasons are discussed below.

Steel Stresses

Due to the temperature gradient in the steel section the curvature of the wall is always towards the fire. The steel stresses in the stud flanges can be calculated using the following expressions.

For the flange on the fire side,

$$\sigma = P/A - (P \times \Delta_z)/Z_x \qquad \text{Eq. 6.2}$$

For the flange on the ambient side,

$$\sigma_z = P/A + (P \times \Delta_z)/Z_x \qquad \text{Eq. 6.3}$$

where,

σ_z is the calculated steel stress (Mpa) at height z

P is the applied axial load (N)

A is the cross sectional area of the stud (mm^2)

Δ_z is the measured total horizontal deflection (mm) at height z

Z_x is the section modulus about the X-axis (mm^3)

The resulting stresses as a function of time are shown in Figures 6.18, 6.19 and 6.20 for mid-height (z=H/2) and at the stud ends (z=0 and z=H). Compressive stresses are shown positive.

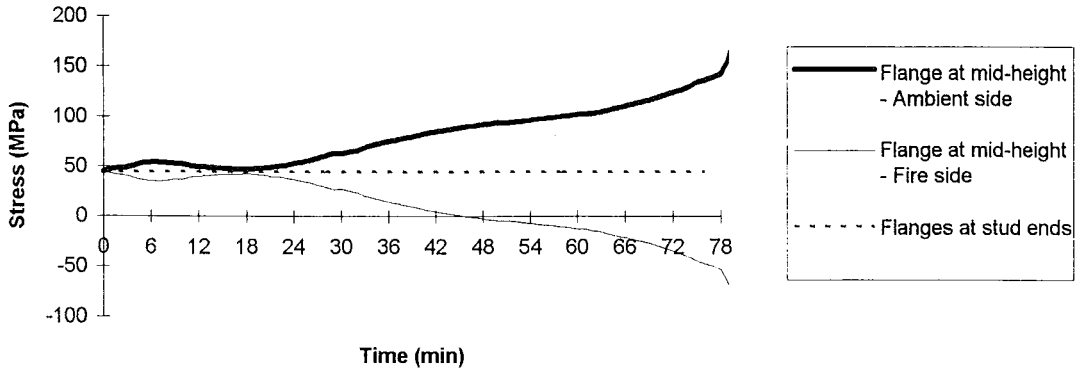

Figure 6.18: Steel stress distribution - FR2020

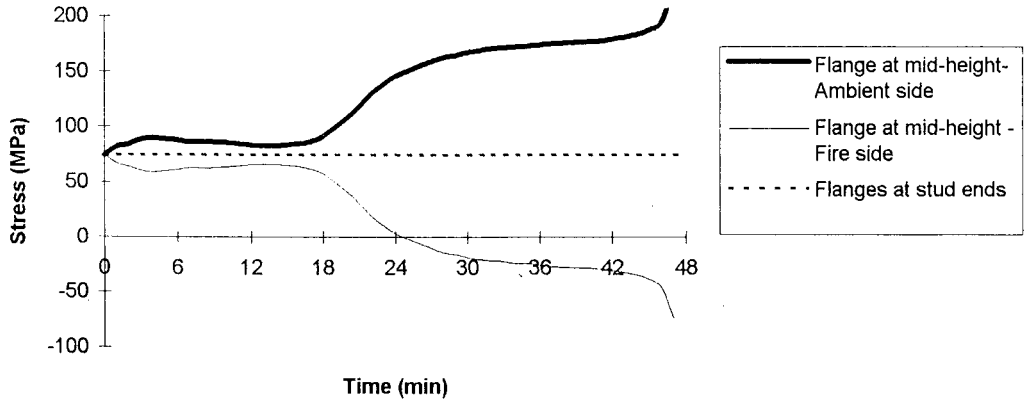

Figure 6.19: Steel stress distribution - FR2028

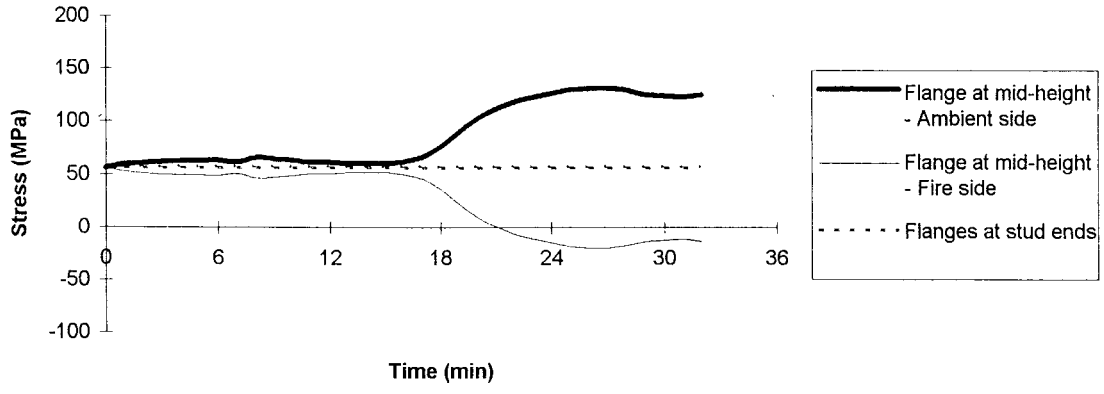

Figure 6.20: Steel stress distribution - FR2031

Lateral Restraint

The failure modes of tests FR2020 and FR2028 can be compared with the modes observed for the lined specimens in the structural testing at room temperature described in Chapter 3. The failure mode of test FR2031 can be compared with the unlined specimens tested at room temperature.

Test FR2031 was designed to achieve an insulation failure across the assembly near the point of structural failure of the framing. The unexposed lining was therefore selected to be thinner than the exposed lining. Once significantly degraded, the unexposed lining failed to provide lateral support to the screws restraining the compression flange of the steel studs. This resulted in pull-through of the fasteners and torsional flexural buckling of the studs. Examination of the unexposed lining after test FR2031 indicated a remaining non-calcined gypsum layer of approximately 2 mm.

A method is required to predict the minimum thickness of sound lining required to provide lateral restraint against buckling of the steel studs about the minor axis. Design codes provide no detailed information regarding the restraint required to prevent this buckling mode. Indicative minimum load resistance levels in BS5950 (BSI,1987) require a total lateral restraint of 3% of the compressive load in the critical flange, provided that the load resistance at each point of restraint is not less than 1%. Further research is recommended to establish minimum levels of restraint more accurately. Data is also required for the minimum restraint provided by gypsum plasterboard in various stages of degradation.

In the absence of detailed information it is proposed for this study that a minimum thickness of the unexposed lining remains uncalcined to prevent lateral buckling. This could be modelled by running TASEF with a finite element grid at this location and limiting the temperature within the thickness to 100 °C. From a comparison of TASEF runs and test results it was found that a 3 mm thickness gives reasonably (but not unduly) conservative predictions.

Figure 6.21, 6.22, and 6.23 show the agreement between the measured and predicted temperatures on the ambient side of the unexposed linings for the three tests. Discrepancies at low temperatures are due to the mass transfer not being modelled by TASEF. Agreement near failure is good. It is also noted that measured temperatures are expected to read somewhat higher than lining temperatures between points of measurement due to the test standard requirement for insulating pads on the back of the thermocouples. The line at 3 mm indicates the proposed minimum lining thickness required to prevent buckling about the minor axis. The effect of this provision on failure predictions using the proposed model is further illustrated in Chapter 7.

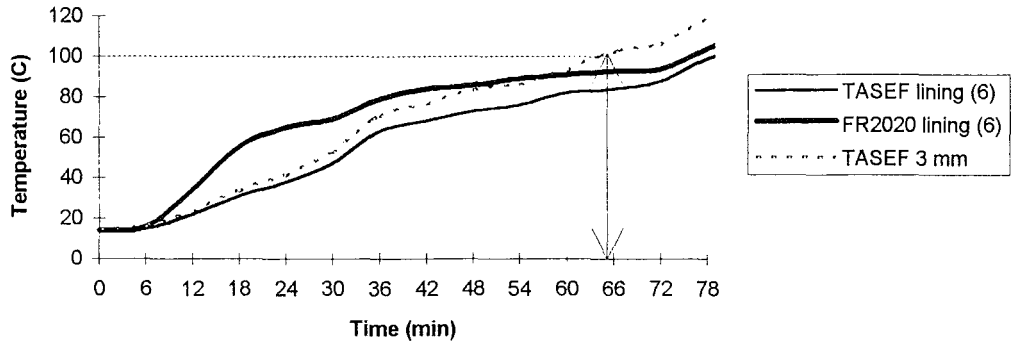

Figure 6.21: Temperatures on the unexposed lining/ ambient side - FR2020

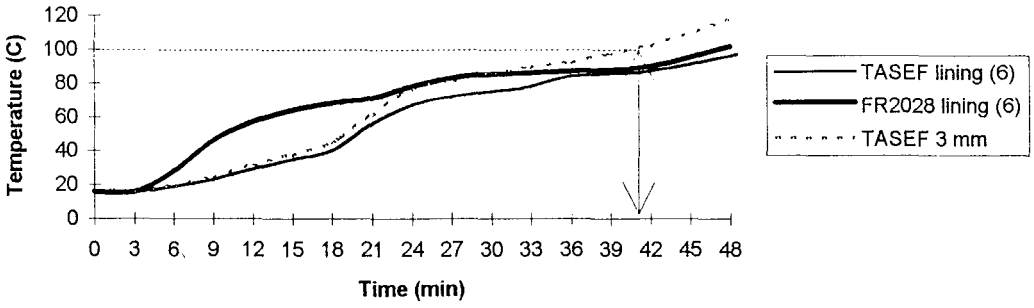

Figure 6.22: Temperatures on the unexposed lining/ ambient side - FR2028

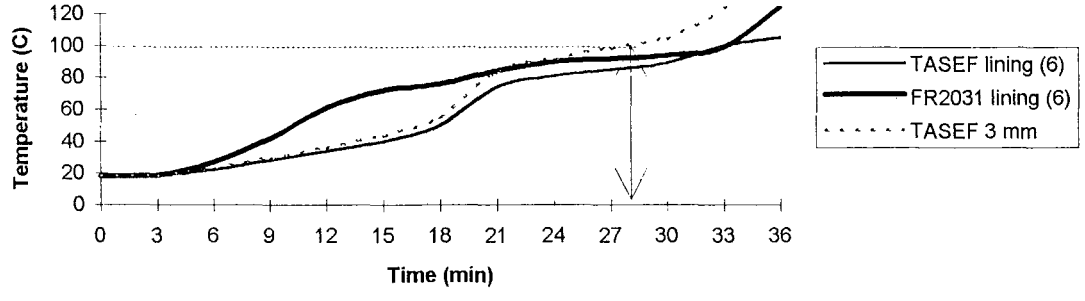

Figure 6.23: Temperatures on the unexposed lining/ ambient side - FR2031

6.7 Findings

Three full scale furnace tests were carried out on loadbearing LSF drywall systems at the BTL laboratories, Judgeford. The applied load was kept constant throughout the tests. Load was applied through a loading platen which was free to move vertically and follow the movement resulting from thermal expansion of the steel studs.

The main findings are summarised below.

6.7.1 Temperatures

The furnace time-temperature curve for the first two tests was in accordance with the standard ISO834 curve. A significantly hotter time-temperature curve was used in the third test representing a real fire. For the ISO834 time temperature curves reasonable agreement is achieved between TASEF heat transfer model predictions and measured temperatures. The agreement is less accurate for the real fire. This is believed to be as a result of a more rapid degradation and more severe cracking of the gypsum plasterboard linings due to increased thermal shock. Further research is recommended into the performance of linings in fires which significantly differ from the ISO834 conditions.

6.7.2 Deflections

Vertical displacements follow the thermal expansion of the steel frames. Reversal of vertical movement was found to be the most accurate means of defining the structural failure of the loadbearing studs.

Horizontal thermal deformations occur as a result of a temperature gradient across the steel studs. Super-imposed deflections result from P-Δ effects. Good agreement is achieved between the total measured horizontal deflections and analytical predictions assuming pinned stud ends.

No evidence was found of significant double curvature along the length of the studs in any of the test specimens. It is concluded that thermal deformations override any rotational end-restraint.

6.7.3 Failure Modes

The stress distribution in the steel studs results in buckling of the compression flange on the ambient side of the wall assembly. Failure was sudden in the two highly loaded tests. Due to load redistribution and frictional restraints provided by the specimen holding frame the relatively low loaded test continued significantly past the point of failure of the main loadbearing studs. This indicates possible non-conservative test results for low applied loads.

The lateral restraint provided by the unexposed lining is a function of the lining degradation. A method is proposed which limits the modelled temperature of the unexposed lining to 100 °C at a depth of 3 mm from the ambient face. Once this temperature has been exceeded, lining restraint can not be relied upon.

CHAPTER 7

THE PROPOSED MODEL

7.1 General

This chapter describes the proposed model for predicting the failure of loadbearing LSF drywall systems exposed to fire. The failure times predicted by the model are compared with the current practice of limiting temperature of the steel studs. Predictions are also compared with full scale furnace test results. A simple graphical method is proposed for quick reference by designers.

7.2 Limiting Temperature

The current practice of predicting the performance of LSF drywall systems is by limiting the temperature of the steel studs to 400 °C. This practice is based on ensuring that the steel yield strength is not reduced to less than about 60 % due to temperature effects (see Figure 4.3). This reduction is considered conservative for most applications when comparing the ratio of maximum fire design load to design stud capacity. Fire rated loadbearing LSF walls have been published by Winstone Wallboards (1992a) and are based on limiting steel temperature.

The practice of limiting steel temperature does not take into account thermal deformations and resulting P-Δ effects. Neither does it consider the effects of temperature on the modulus of elasticity of steel which is an important property in buckling analysis. Limiting temperature is believed to give conservative predictions, but the margin of 'comfort' is unknown. Results are compared with the proposed model and test results in Table 7.1.

7.3 The Proposed Model

The proposed model consists of two main components.

1. Heat transfer modelling is used to establish the temperature distribution and time-temperature history of the steel framing.

2. A spreadsheet is used for the structural analysis of steel studs subjected to a combination of axial loading and bending, whilst exposed to elevated temperatures.

7.3.1 Heat Transfer Modelling

The steel framing temperatures and time-temperature history may be determined by heat transfer modelling using computer programs. Heat transfer modelling is also used to determine the lateral restraint provided by the unexposed lining.

Temperatures

Chapter 5 describes the application of TASEF, a commercially available finite element package for the heat transfer modelling of building elements exposed to fire.

At high temperatures experienced near failure, TASEF gives good agreement when compared with measured temperatures from the tests described in Chapter 6. The agreement is best for ISO834 time-temperature curves and less accurate for significantly hotter fires. This is explained by the comparatively more severe degradation of the exposed lining and the inability of TASEF to model for ablation.

TASEF also does not model mass transfer which results in low predicted temperatures on the ambient side of the wall assembly during the early stages of exposure to fire. This results in an under-prediction of lining and framing temperatures on the ambient side and a greater temperature difference across the steel member. As is apparent from Eq. 4.8, a linear correlation exists between the temperature gradient and the thermal deformation. The predicted horizontal deflections using TASEF temperatures are therefore greater than the deflections calculated from measured temperatures. Greater deflections result in increased steel stresses due to P-Δ effects. Using TASEF temperatures will therefore result in conservative failure predictions. A comparison of deflections calculated from TASEF and measured temperatures is given in Figures 7.1, 7.2 and 7.3. The thermal deflections are calculated from the temperature gradient across the steel studs. The total deflection includes P-Δ effects.

Proprietary heat transfer models for cavity wall construction are currently being developed (Collier, 1994a and Clancy, 1994). Further accuracy in temperature predictions may be achieved, particularly if these models take account of mass transfer and allow for ablation of linings to be included.

Lateral Restraint

The unexposed lining on the ambient side of the wall assembly provides lateral restraint to the compression flange of the steel studs against buckling about the minor axis. During exposure to fire this lining will gradually degrade and may reach a condition at which it is no longer able to prevent lateral buckling. This was observed in full scale furnace test FR2031 as described in Chapter 6.

It is proposed that for heat transfer modelling a finite element grid is included within the unexposed lining at 3 mm from the unexposed face of the wall assembly. The temperature at this location must not exceed 100 °C. This aims to ensure that a minimum thickness of 3 mm of the unexposed lining retains its ability to provide lateral restraint to the stud compression flange.

As described in Chapter 6, this proposed measure was found to give reasonably conservative predictions when compared with full scale test results. Further research into the minimum requirements and the lateral restraint provided by degraded linings is recommended.

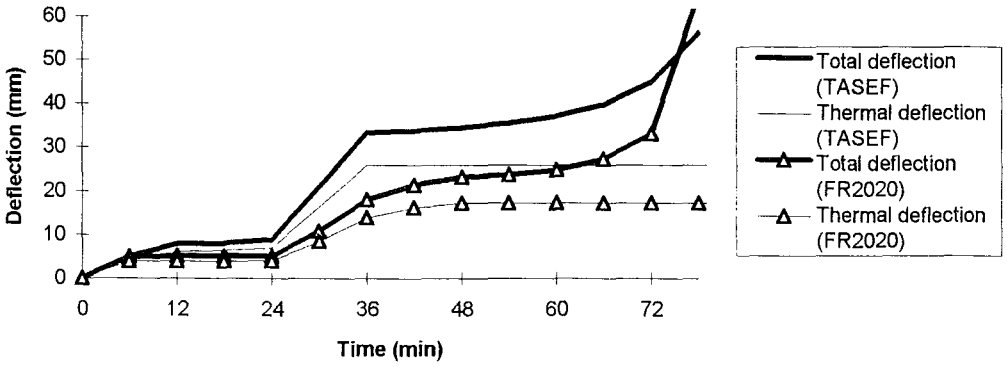

Figure 7.1: Comparison of calculated horizontal deflections based on TASEF and measured temperatures - FR2020

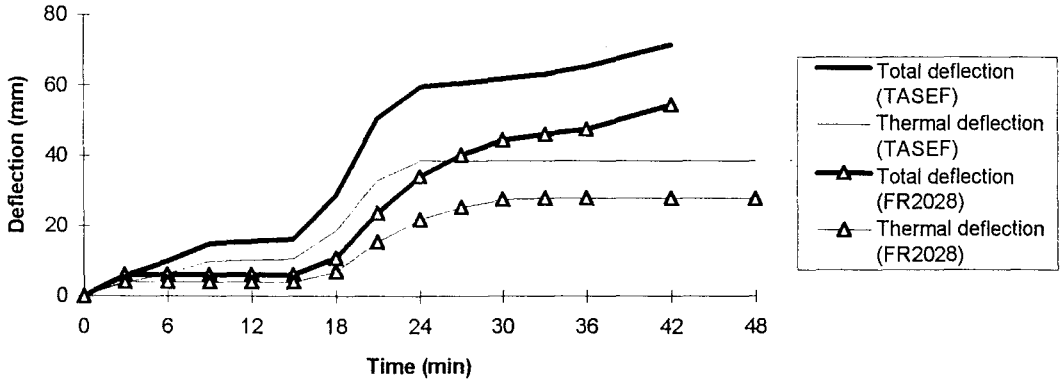

Figure 7.2: Comparison of calculated horizontal deflections based on TASEF and measured temperatures - FR2028

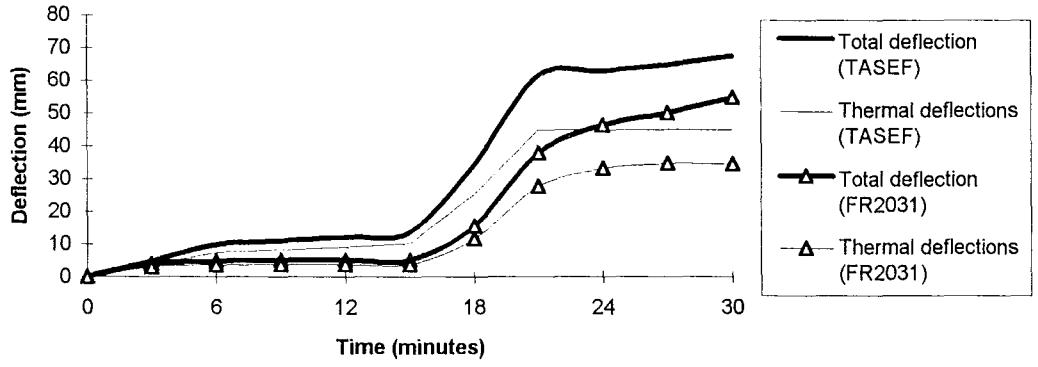

Figure 7.3: Comparison of calculated horizontal deflections based on TASEF and measured temperatures - FR2031

7.3.3 Structural Analysis

The spreadsheet analysis in accordance with the AISI design manual (AISI, 1991) as presented in Chapter 3 is modified to take into account the temperature effects discussed in Chapter 4. This is achieved by introducing a temperature input and by modifying the input values for yield strength and modulus of elasticity as a function of temperature in accordance with Eq. 4.3 and Eq. 4.5 respectively.

The thermal deformation as a result of the temperature gradient across the steel stud is calculated using Eq. 4.8, using the mean stud temperature to calculate the coefficient of thermal expansion in accordance with Eq. 4.6. As recommended in Chapter 4 the calculated deformations are conservatively assumed to remain constant when temperature gradients decrease. This is simply achieved by not allowing the calculated value for a given time step to be less than the calculation for the previous time step.

The total horizontal deflection of the system is calculated by adding the thermal deflection to the deflection due to P-Δ effects calculated in accordance with Eq. 4.10. The total deflection multiplied by the applied axial load gives the maximum stud bending moment. Any lateral loads may be entered if required.

A critical temperature is found at which the maximum permissible stud load is equal to the applied axial load. This temperature is then compared with the compression flange temperature on the ambient side of the wall assembly to find the time to failure.

An example of the spreadsheet analysis is shown in Figure 7.4.

DESIGN OF AXIALLY LOADED COMPRESSION MEMBERS (C-SECTION STUDS)						
IN ACCORDANCE WITH LRFD COLD-FORMED STEEL DESIGN MANUAL (AISI)						
INPUT DATA				ITERATION		
Section Properties:				Applied axial load	6.00	kN/stud
				Applied lateral load	0.00	kN/m/stud
Area (gross)	157	mm2		Critical steel temp.	378	C
Area (net)	157	mm2		Thermal deformation	26.00	mm
Section modulus Zx	3687	mm3				
Section modulus Zy	644	mm3		Yield strength Fyt	208	MPa
Moment of area Ix	140400	mm4		Youngs modulus Et	128942	MPa
Moment of area Iy	15600	mm4				
Warping constant Cw	1.55E+07	mm6		UDL deflection	0.00	mm
Radius of gyration Rx	29.9	mm		uL	1.61	
Radius of gyration Ry	10	mm		P-delta defl	11.55	mm
Shear centre Xo	10.81	mm		Total deflection	37.55	mm
Form factor Q	0.661			Deflection limit L/240	11.67	mm
Torsion constant J	69.3	mm4				
Effective length Lx (H	2800	mm		Iterate to get 1	1.00	
Effective length Ly	300	mm		Maximum stud load	6.02	kN
Effective length Lz	300	mm				
Flange thickness t	1.15	mm				
Flange width w	32	mm				
Material Properties:						
Yield stress Fy	300	MPa				
Youngs modulus E	200000	MPa				
Shear modulus G	80000	MPa				
Load Factors:						
Load factor P (0.85)	1.00					
Load factor M (0.9)	1.00					
Cmx (0.85)	1.00					
CALCULATIONS			X-axis	Y-axis		
Elastic buckling stress Fex			145.12		N	
Elastic buckling stress Fey				1414.02	N	
Polar radius of gyration Ro		33	mm			
Factor B		0.89				
Torsional buckling stress Ft		1291	MPa			
Tors./flex. buckling stress Fe		143	MPa			
Nominal buckling stress Fn		132	MPa			
Design axial strength Pn1		13739	N			
Design axial strength Pn2		10041	N			
Design axial strength Pn		10041	N			
Design strength		10041	N			
Pa/Pn + Ma/Mnx = 1		1				
Maximum stud load		6023	N			
Maximum stud load		6.02	kN			

Figure 7.4: Example of spreadsheet analysis

7.3.4 Design Example

This example follows the prediction of the failure time for the wall assembly tested in FR2020. The furnace input fire is in accordance with the ISO834 curve.

TASEF modelling, as described in Chapter 5, is used to predict the steel framing time temperature history as presented in Figure 7.5. Temperature is given on the left Y-axis.

Based on the temperature gradient across the steel studs the thermal deformation can be calculated as described in Chapter 4 using Eq. 4.8. The coefficient of thermal expansion is calculated in accordance with Eq. 4.6 using the mean stud temperature. The predicted thermal deformation is presented in Figure 7.5. Deflection is given on the right Y-axis.

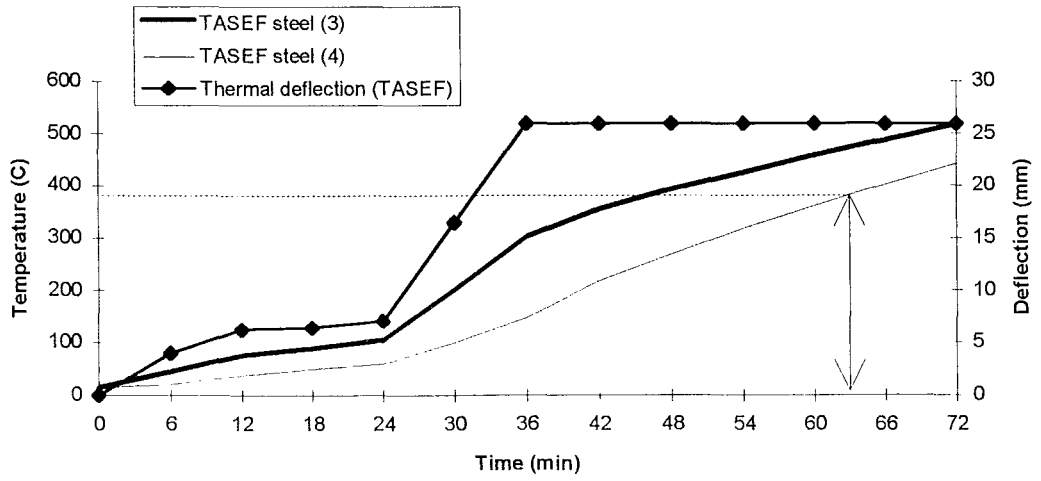

Figure 7.5: Predicted steel temperatures and thermal deformation (FR2020)

From the spreadsheet analysis presented for this example in Figure 7.4 it can be seen that for a calculated thermal deformation of 26 mm the critical compression flange temperature is 378 °C. At this temperature the maximum stud load is approximately equal to the applied axial load. A critical temperature of 378 °C gives a predicted failure time of approximately 63 minutes as illustrated in Figure 7.5.

Figure 6.21 (page 79) shows that the unexposed lining is expected to provide lateral restraint to the compression flange for about 65 minutes. The predicted failure time is therefore governed by flexural buckling about the major axis at 63 minutes.

7.4 Graphical Method

The proposed model has been used to generate data for loadbearing LSF drywall systems lined with 12.5 mm, 16 mm, and 19 mm glass-fibre reinforced gypsum plasterboard exposed to ISO834 fire conditions. Figure 7.6 shows the data points for the predicted failure times for various ratios of applied load to design stud capacity as determined using the AISI design manual.

It is suggested that a straight line drawn between a load ratio of unity and a published rating for a non-loadbearing system (Winstone Wallboards, 1992a) be adopted as a quick reference but conservative estimate of the fire resistance rating of loadbearing LSF drywall systems. It must be noted that true non-loadbearing systems sandwiched between semi-rigid structural members, such as concrete slabs, must be designed to allow for thermal expansion (Winstone Wallboards, 1992a).

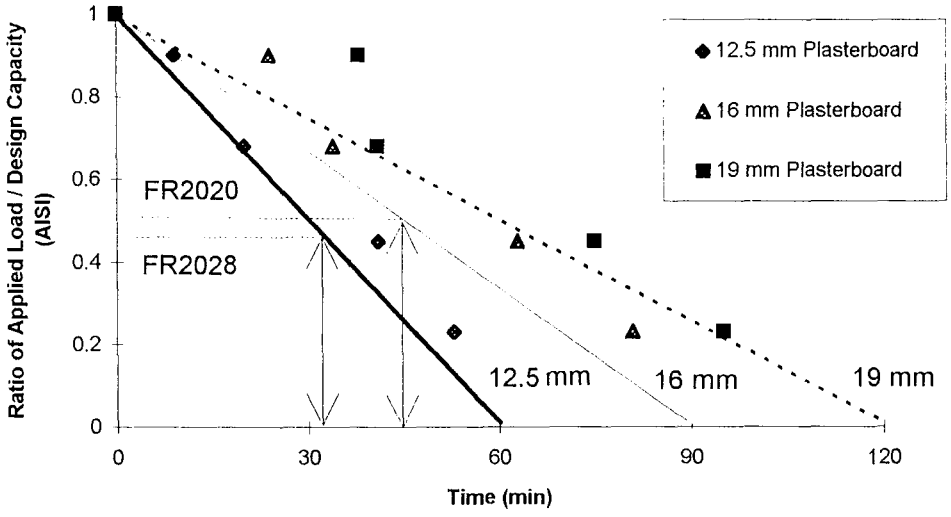

Figure 7.6: Proposed graphical method

7.5 Comparison with Full Scale Fire Tests

Table 7.1 gives a comparison of predicted times to failure in minutes. The percentage in brackets indicates the ratio of the prediction compared with the test result.

Method	Temperature data-base	FR2020	FR2028	FR2031
Published data	N/A	30 (42%)	15 (34%)	N/A
Limiting temperature	TASEF	49 (68%)	32 (72%)	23 (72%)
	Measured	51 (71%)	33 (75%)	24 (75%)
Graphical method	N/A	45 (62%)	32 (73%)	N/A
Proposed model	TASEF	63 (88%)	35 (80%)	28*(88%)
	Measured	66 (92%)	39 (89%)	31**(97%)
Test Result	N/A	72	44	32

Table 7.1: Comparison of failure predictions and test results (minutes)

* *controlled by unexposed lining failure*

** *unexposed lining not modelled*

7.6 Findings

A model is proposed for predicting the failure time of loadbearing LSF drywall systems exposed to fire. The model consist of a heat transfer module using TASEF, and a temperature sensitive structural spreadsheet analysis. The proposed model was used to generate a simple graphical method for predicting the performance of LSF drywall systems exposed to the standard ISO834 fire.

Failure predictions using the proposed model are compared with published data, the current practice of limiting the steel stud temperature, the graphical method, and actual test results.

The 'published data' is a general application of the method of limiting steel temperature. Predictions in accordance with this method are non-sensitive to the ratio of applied load to design capacity. For the load ratios tested predictions ranged from

68-75% of test results. Predictions are expected to be considerably more conservative for systems with a low load ratio.

The graphical method is derived from the proposed model. Predictions ranged from 62-73% of test results. The level of conservatism is expected to be similar for different load ratios. This offers designers the option of more economical systems for low ratios of applied axial load to design capacity, as is often the case in deflection controlled designs.

The proposed model gives the closest predictions ranging between 80-97% of test results. Accuracy is best when predictions are based on measured temperatures. This is as a result of conservative thermal deformation predictions using TASEF temperatures. The proposed model is sensitive to load ratios and lends itself to modelling against real fires.

CHAPTER 8

SUMMARY AND CONCLUSIONS

8.1 Summary

This study was carried out to develop an understanding of the performance of loadbearing light steel frame (LSF) drywall systems and to model the performance against the ISO834 time-temperature curve and real compartment fires.

Structural testing at room temperature was carried out to determine a reliable method for predicting the ultimate limit state conditions for cold-formed steel studs subjected to a combination of axial loading and bending. A comparison was carried out between relevant structural design codes.

The effect of temperature on the steel strength and stiffness has been investigated. In order to predict stud bending moments, analytical methods are proposed for calculating the thermal deformation arising from temperature gradients across the steel members and the super-imposed deformation due to P-Δ effects.

Heat transfer modelling using a commercially available computer package (TASEF) was carried out to predict the steel framing time-temperature history.

Full-scale furnace tests were carried out to evaluate the proposed model against the ISO834 time-temperature curve and a significantly hotter realistic fire.

8.2 General Conclusions

8.2.1 Conclusions from existing literature

1. The AISI (1991) design manual provides the most recent and reliable source for predicting the ultimate limit state conditions of cold-formed steel studs at room temperature when subjected to a combination of axial loading and bending.

Structural designs in accordance with the AISI manual were found to be reasonably conservative.

2. No reliable data exist on the performance of loadbearing LSF drywall systems exposed to fire. The most relevant information was produced by the AISI (1981), however testing did not allow for freedom of stud expansion and as a result fire test loads increased to twice the intended design loads. The results presented by the AISI are believed to be non-conservative for high load ratios.

3. Relationships for temperature effects on the strength and stiffness of cold-formed steel members have been derived from available data. The expressions adopted for this study give reasonably accurate failure predictions.

8.2.1 Conclusions from testing and modelling

4. Thermal deformations as a result of temperature gradients and deflections due to P-Δ effects can be predicted with good accuracy.

5. Finite element heat transfer modelling by computer (TASEF) predicts the time-temperature history of LSF drywall systems exposed to fire with reasonable accuracy. Refinement is needed for modelling against fires significantly hotter than ISO834 conditions.

6. The failure mode of steel studs in LSF drywall systems exposed to fire is governed by buckling of the compression flange on the ambient side of the wall assembly.

7. Thermal deformations override any rotational restraints provided by stud-to-channel fixings or the relocation of load.

8. Walls with low levels of axial load may perform better in fire tests than in actual fire situations because frictional restraints and re-distribution of load can enhance the test result.

9. The current practice of limiting the steel flange temperature on the fire side of the wall assembly is unduly conservative for low load ratios.

10. A simple graphical method is proposed for quick reference by designers.

11. A model is proposed which consists of finite element heat transfer modelling using TASEF to predict steel framing temperatures and a structural analysis using spreadsheets. The model gives predictions within 80-90% of measured failure times. This level of conservatism is considered satisfactory for design purposes.

8.3 Further Research

Further research is recommended to be carried out into the following topics,

I. Incorporation of the principles of mass transfer in heat transfer modelling during the early stages of exposure to fire is expected to result in better agreement with the measured temperature difference between the fire and ambient side of steel framing. As a result thermal deformations may be predicted more accurately.

II. The performance of gypsum plasterboard linings in fires significantly hotter than the ISO834 time-temperature conditions requires further investigation. Suitable ablation factors in proprietary heat transfer models may improve the accuracy of predictions.

III. Investigation is needed into the minimum requirement for lateral restraint to prevent lateral buckling of cold-formed steel stud compression flanges and the restraint provided by gypsum plasterboard linings at various stages of degradation after exposure to elevated temperatures.

NOTATION

A	section gross area	(mm^2)
c	specific heat	(J/kg°C)
D	section depth	(mm)
e	enthalpy	(MJ/m^3)
E_0	steel modulus of elasticity at ambient temperature	(Mpa)
E_T	steel modulus of elasticity at elevated temperature T	(Mpa)
F_{y0}	steel yield stress at ambient temperature	(Mpa)
F_{yT}	steel yield stress at elevated temperature T	(Mpa)
I_x	moment of area about the x-axis	(mm^4)
I_y	moment of area about the y-axis	(mm^4)
I_w	warping constant	(mm^6)
J	torsion constant	(mm^4)
k	thermal conductivity	(W/m°C)
l	section lip width	(mm)
L	member length	(mm)
M	section mass	(kg/m)
P_a	applied axial load	(kN)
q	rate of heat transfer (heat flux)	(kW/m^2)
Q	section form factor	(dimensionless)
R_x	radius of gyration about the x-axis	(mm)
R_y	radius of gyration about the y-axis	(mm)
t	steel thickness	(mm)
T	temperature	(°C)
T_o	initial temperature	(°C)
T_t	temperature at time t	(°C)
T_a	ambient temperature	(K)
T_f	furnace temperature	(K)
T_g	gas temperature	(K)
T_s	surface temperature	(K)
W	section width	(mm)
X_e	section shear centre	(mm)
X_c	section centroid	(mm)
Z_x	section modulus about the x-axis	(mm^3)
Z_y	section modulus about the y-axis	(mm^3)
α_T	coefficient of thermal expansion at temperature T	($°C^{-1}$)
β	convection coefficient	($W/m^2K^{3/4}$)
δT	temperature difference	(°C)
Δ_1	deformation due to thermal bowing	(mm)
Δ_2	deformation due to P-Δ effects	(mm)
ε	emissivity	(dimensionless)
γ	convection power	(dimensionless)
σ	Stefan Boltzmann constant	($5.67*10^{-8}$ W/m^2K^4)
τ	elapsed time	(min)

BIBLIOGRAPHY

Anderberg Y (1983). *'Properties of Materials at High Temperatures, Steel'.* Division of Building Fire Safety and Technology. Lund Institute of Technology. Lund, Sweden.

Andersson L, Jansson B (1987). *'Analytical Fire Design with Gypsum - a Theoretic and Experimental Study'.* FSD Report IFSD87-MG001. Institute of Fire Safety Design. Lund, Sweden.

AISI (1981). *'Fire Resistance Rating of Load-Bearing Steel Stud Walls with Gypsum Wallboard Protection with or without Cavity Insulation'.* American Iron and Steel Institute. Washington, USA.

AISI (1991). *'Load and Resistance Factor Design Specification for Cold-Formed Steel Structural Members'.* American Iron and Steel Institute. Washington, USA.

ASTM (1979). *'ASTM E119-79 : Standard Methods of Fire Tests of Building Construction and Materials'.* American Society for Testing and Materials. USA.

Bastings D (1986). *'Recent Developments in Techniques for Protecting Steel from Fire.'* BRANZ Reprint No 48. Building Research Association of NZ. Judgeford, New Zealand.

BIA (1992). *'New Zealand Building Code and Approved Documents'.* Building Industry Authority. Wellington, New Zealand.

BSI (1987). *'BS 5950 : Part 5 : Structural Use of Steelwork in Building. Part 5. Code of practice for Design of Cold-Formed Sections.'* British Standards Institution. London, UK.

Buchanan AH (1994). *'Fire Engineering Design Guide'.* Centre for Advanced Engineering. University of Canterbury. Christchurch, New Zealand.

BRANZ (1988). *'FR 1411 : Report on the Fire Resistance Properties of a Non-Loadbearing Steel Framed Wall Lined with One layer of 19 mm Fyreline Gibraltar Board.'* Confidential report for Winstone Wallboards Ltd. Auckland, New Zealand.

BRANZ (1990). *'FR 1579 : Report on the Fire Resistance Properties of a Non-Loadbearing Steel Framed Wall Lined with 12.5 mm Fyreline Gibraltar Board.'* Confidential report for Winstone Wallboards Ltd. Auckland, New Zealand.

BRANZ (1992). *'FR 1722 : Report on the Fire Resistance Properties of a Non-Loadbearing Steel Framed Wall Lined with Two layers of 12.5 mm Fyreline Gibraltar Board.'* Confidential report for Winstone Wallboards Ltd. Auckland, New Zealand.

BTL (1995a). *'FR 2020 : Report on the Fire Properties of a Loadbearing Steel Framed Wall.'* Confidential report for Winstone Wallboards Ltd. Auckland, New Zealand.

BTL (1995b). *'FR 2028 : Report on the Fire Properties of a Loadbearing Steel Framed Wall.'* Confidential report for Winstone Wallboards Ltd. Auckland, New Zealand.

BTL (1995c). *'FR 2031 : Report on the Fire Properties of a Loadbearing Steel Framed Wall.'* Confidential report for Winstone Wallboards Ltd. Auckland, New Zealand.

Clancy P, Young S, Beck V, Leicester R H (1994). *'Modelling of Timber-Framed Barriers in real Fires'.* Proceedings, Pacific Timber Engineering Conference, Volume 2, pages 273-282. Timber Research and Development Advisory Council. Queensland, Australia.

Collier P (1994a). *'Fire Resistant Light Timber Framed Walls'.* Proceedings, Pacific Timber Engineering Conference, Volume 2, pages 248-254. Timber Research and Development Advisory Council. Queensland, Australia.

Collier P (1994b). *'A Model for Predicting the Fire Resistance Performance of Cavity Walls in Realistic Fires'.* Draft Journal Paper. Building Technolgy Limited. Judgeford, New Zealand.

Cooke G M E (1987a). *'Thermal Bowing and how it Affects the Design of Fire Separating Construction'.* Fire Research Station. Building Research Establishment. Herts, UK.

Cooke G M E (1987b). *'The Structural Response of Steel I-Section Members Subjected to Elevated Temperature Gradients across the Section'.* Department of Civil Engineering. The City University. London, UK.

Cooke G M E (1985). *'Fire Engineering of Tall Fire Separating Walls'.* Fire Research Station. Building Research Establishment. Herts, UK.

Deam BL (1993). *'NAFI TF-1 : A Design Procedure for Timber Stud Wall Framing - Part 1 : End Fixity and Lining Contributions.'* Confidential Report STR 5100/1. Building Technology Limited. Judgeford, New Zealand.

ECCS (1983). *'European Recommendations for the Fire Safety of Steel Structures - Calculation of the Fire Resistance of Load-bearing Elements and Structural Assemblies exposed to the Standard Fire.'* European Convention for Constructional Steelwork. Brussels, Belgium.

Hancock G J (1988). *'Design of Cold-Formed Steel Structures (To Australian Standard AS 1538-1988)'.* Australian Institute of Steel Construction. Sydney, Australia.

HERA (1990). *'Fire Protection Manual'.* New Zealand Heavy Engineering Research Association. Auckland, New Zealand.

Klippstein K H (1978). *'Preliminary Study on the Column-Strength of Cold-Formed Steel Studs Exposed to Elevated Temperatures.'* American Iron and Steel Institute. Washington, USA.

Klippstein K H (1980a). *'Behaviour of Cold-Formed Steel Studs in Fire Tests.'* American Iron and Steel Institute. Washington, USA.

Klippstein K H (1980b). *'Strength of Cold-Formed Studs Exposed to Fire.'* American Iron and Steel Institute. Washington, USA.

Lie T T (1992). *'Structural Fire Protection'.* American Society of Civil Engineers. New York, USA.

Mehaffy, J R 1991. *'Development of Fire Endurance Models for Wood Stud Walls - Progress Report'.* Forintek Canada Corporation.

Milke J (1988). *'Analytical Methods for Determining Fire Resistance of Steel Members'.* The SFPE Handbook of Fire Protection Engineering, pages 3/88-3/112. Society of Fire Protection Engineers. Quincy, MA, USA.

Petterson O, Magnusson S E, Thor J (1976). *'Fire Engineering Design of Steel Structures'.* Publication 50. Swedish Institute of Steel Construction. Stockholm, Sweden.

Rondo (1993). *'Design Manual for Steel Stud Systems in Non-Cyclonic Areas'.* Rondo Building Systems. Sydney, Australia.

SAA (1984). *'AS 1397 : Steel Sheet and Strip, Zinc-Coated or Aluminium Zinc Coated'.* Standards Association of Australia. North Sydney, NSW, Australia.

SAA (1990). *'AS 1530 : Part 4 : Fire Resistance Tests of Elements of Building Construction'.* Standards Association of Australia. North Sydney, NSW, Australia.

SAA (1988). *'AS 1538 : Cold-Formed Steel Structures Code'.* Standards Association of Australia. North Sydney, NSW, Australia.

SAA/SNZ (1994). *'Load and Resistance Factor Design of Cold-Formed Steel - Calibration of the AISI Design Provisions'.* Confidential paper for Committee BD/82 - Cold-Formed Steel Structures.

Schleich J B, Bouillette J P, Hass R, Preston R, Sandman T (1993). *'International Fire Engineering Design for Steel Structures : State of the Art'.* International Iron and Steel Institute. Brussels, Belgium.

SCI (1993). *'Building Design using Cold Formed Steel Sections: Fire Protection'.* SCI Publication P129. The Steel Construction Institute. Berkshire, UK.

SNZ(1978). *'NZS 3441 : Specification for Hot-Dipped Zinc-Coated Steel Coil and Cut Lengths'.* Standards New Zealand. Wellington, New Zealand.

SNZ (1989). *'MP9:1989, Fire Properties of Building Materials and Elements of Structure - Part 1'* Standards New Zealand. Wellington, New Zealand.

SNZ (1992a). *'NZS 4203 : General Structural Design and Design Loadings for Buildings.'* Standards New Zealand. Wellington, New Zealand.

SNZ (1992b). *'NZS 3404 : Steel Structures Standard.'* Standards New Zealand. Wellington, New Zealand.

Sterner E, Wickstrom U (1990). *'TASEF - Temperature Analysis of Structures Exposed to Fire.'* Fire Technology SP Report 1990:05. Swedish National Testing Institute. Boras, Sweden.

Thomas GC, Buchanan AH, Carr AJ, Fleishman CM, Moss PJ (1994). *'Light Timber Framed Walls Exposed to Compartment Fires'.* Proceedings, Pacific Timber Engineering Conference. Volume 2, pages 531-538. Timber Research and Development Advisory Council. Queensland, Australia.

Thomas GC (1994(a)). Personal communications with Geoff Thomas, PhD student, University of Canterbury. Christchurch, New Zealand.

Trahair N S (1977). *'The Behaviour and Design of Steel Structures'.* John Wiley and Sons. New York, USA.

Wade C A (1993). *'Summary Report on a Finite Element Program for Modelling the Thermal Response of Building Components Exposed to Fire'.* BRANZ Study Report No.51. Building Research Association of NZ. Judgeford, New Zealand.

Winstone Wallboards (1992a). *'Gib® Board Fire Rated Systems, 1992'.* Winstone Wallboards Limited. Auckland, New Zealand.

Winstone Wallboards (1992b). *'Gib® Board Stopping and Finishing Systems, 1992'.* Winstone Wallboards Limited. Auckland, New Zealand.

APPENDICES

APPENDIX A : Cold-Formed Steel Design

APPENDIX B : Typical TASEF Result File

APPENDIX A

COLD-FORMED STEEL DESIGN

A 1 Working Stress Design in accordance with AS 1538 (SAA, 1988).

A 1.1 Governing equations for axially loaded compression members (Clause 3.6, with particular reference to Clause 3.6.4.2 *Monosymmetric sections*):

Load factor (recommended), $\Omega = 1 / 0.6$

Imperfection parameter, $N = (1.25 - Q)QF_y / F_{oc}$

X-axis flexural buckling stress, $$F_{ox} = \frac{\pi^2 \times E}{(L_x / R_x)^2}$$

Y-axis flexural buckling stress, $$F_{oy} = \frac{\pi^2 \times E}{(L_y / R_y)^2}$$

Polar radius of gyration, $$R_{01} = \sqrt{\frac{I_x + I_y}{A} + x_0^{\,2}}$$

Flexural torsional buckling stress, $$F_{ob} = \frac{AR_{01}\sqrt{F_{oy}F_{oz}}}{Z_x}$$

Permissible stress (bending), $$F_{bx} = \left(0.55 - 0.10\frac{F_{ob}}{F_y}\right)F_{ob} \quad \text{for } F_{ob} \le F_y$$

$$F_{bx} = \left[0.95 - 0.5\sqrt{\left(\frac{F_y}{F_{ob}}\right)}\right]F_y \quad \text{for } F_{ob} > F_y$$

Torsional buckling stress, $$F_{oz} = \frac{GJ}{AR_{01}^{\,2}}\left(1 + \frac{\pi^2 EI_w}{GJL_z^2}\right)$$

Elastic buckling stress,

$$F_{oxz} = \frac{(F_{ox} + F_{oz}) \pm \sqrt{\left[(F_{ox} - F_{oz})^2 + 4F_{ox}F_{oz}\left(\frac{x_o}{R_{01}}\right)^2\right]}}{2\left[1 - \left(\frac{x_o}{R_{01}}\right)^2\right]}$$

Maximum permissible buckling stress (where F_{oc} is the smaller of F_{oy} and F_{oxz}),

$$F_a = \frac{QF_y}{\Omega}\left\{\left[\frac{1+(1+N)\frac{F_{oc}}{QF_y}}{2}\right] - \sqrt{\left[\left(\frac{1+(1+N)\frac{F_{oc}}{QF_y}}{2}\right)^2 - \left(\frac{F_{oc}}{QF_y}\right)\right]}\right\}$$

A 1.2 Governing equation for combined bending and compression (Clause 3.7, with particular reference to Clause 3.7.3 *Sections bent about a plane of symmetry*):

For $f_a / F_a > 0.15$,

$$\frac{f_a}{F_a} + \frac{C_{mx} f_{bx}}{F_{bx}\left[1 - \left(\frac{\Omega f_a}{F_{ox}}\right)\right]} \leq 1$$

where,

f_a is the axial stress equal to the applied load divided by the cross-sectional area
f_{bx} is the tensile stress as a result of bending about the X-axis
C_{mx} is a moment coefficient (0.85) in accordance with Clause 3.7.5

A 2 Limit State Design in accordance with BS 5950 : Part 5 (BSI, 1987).

A 2.1 Governing equations for members in compression (Section 6, with particular reference to Clause 6.2 *Flexural buckling* and Clause 6.3 *Torsional flexural buckling*):

X-axis flexural buckling load, $P_{ex} = \frac{\pi^2 \times EI_x}{L_x^2}$

Y-axis flexural buckling load, $P_{ey} = \frac{\pi^2 \times EI_y}{L_y^2}$

Perry coefficient, $\eta = 0.002\left(\frac{L_e}{R_e} - 20\right)$

Short strut capacity, $P_{cs} = QAP_y$

Polar radius of gyration, $R_o = \sqrt{\left(R_x^2 + R_y^2 + x_o^2\right)}$

Constant, $\beta = 1 - \left(\frac{x_o}{R_o}\right)^2$

Torsional buckling load, $$P_T = \frac{1}{R_o^2}\left(GJ + 2\frac{\pi^2 EI_w}{L_e^2}\right)$$

Torsional flexural buckling load, $$P_{TF} = \frac{1}{2\beta}\left\{(P_{ex} + P_T) - \left[(P_{ex} + P_T)^2 - 4\beta P_{ex} P_T\right]^{\frac{1}{2}}\right\}$$

Axial load, $$P_c = 0.5\left(\left[P_{cs} + (1+\eta)P_e\right] - \left\{\left[P_{cs} + (1+\eta)P_e\right]^2 - 4P_{cs}P_e\right\}^{\frac{1}{2}}\right)$$

A 2.2 Governing equation for combined bending and compression (Clause 6.4, with particular reference to Clause 6.4.3 *Overall buckling check)*:

$$\frac{F_c}{P_c} + \frac{M_x}{M_{cx}\left(1 - \frac{F_c}{P_{ex}}\right)} \leq 1$$

where

P_e is the minimum elastic flexural buckling load
P_y is the design strength
F_c is the applied axial load
M_x is the applied bending moment about the X-axis
M_{cx} is the moment capacity in bending about the X-axis

A 3 Limit State Design in accordance with LRFD Cold-Formed Steel Design Manual (AISI, 1991)

A 3.1 Governing equations for concentrically loaded compression members (Section C4, with particular reference to C4.2 *Doubly or singly-symmetrical sections subject to torsional or torsional-flexural buckling*):

X-axis flexural buckling stress, $$\sigma_{ex} = \frac{\pi^2 E}{\left(L_x / R_x\right)^2}$$

Y-axis flexural buckling stress, $$\sigma_{ey} = \frac{\pi^2 E}{\left(L_y / R_y\right)^2}$$

Torsional flexural buckling stress, $$\sigma_t = \frac{1}{AR_o^2}\left(GJ + \frac{\pi^2 EI_w}{L_t^2}\right)$$

Constant, $\beta = 1 - \left(\frac{x_o}{R_o}\right)^2$

Torsional flexural buckling stress, $F_e = \frac{1}{2\beta}\left[(\sigma_{ex} + \sigma_t) - \sqrt{(\sigma_{ex} + \sigma_t)^2 - 4\beta\sigma_{ex}\sigma_t}\right]$

For $F_e > F_y/2$, $F_n = F_y\left(1 - F_y / 4F_e\right)$

For $F_e \leq F_y/2$, $F_n = F_e$

Axial load capacity is smaller of, $P_n = AQF_n$, or

$$P_n = \frac{A\pi^2 E}{25.7\left(w/t\right)^2}$$

where,

F_n is the nominal buckling stress
t is the web thickness (unstiffened element)
w is the web flat width (unstiffened element)

A 3.2 Governing equation for combined axial load and bending (Section C5)

$$\frac{P_a}{\phi_c P_n} + \frac{C_{mx} M_a}{\phi_b M_{cx}\left(1 - \frac{P_a}{\phi_c P_{ex}}\right)} \leq 1$$

where,

P_a is the applied axial load
M_a is the applied bending moment
M_{cx} is the bending moment capacity about the X-axis
ϕ_c is a load factor (0.85)
ϕ_b is a bending moment factor (0.9)
C_{mx} is a compression member coefficient (0.85)
P_{ex} is the X-axis flexural buckling load equal to $A\sigma_{ex}$

A 4 Notation (undefined terms in Appendix A)

Section Properties

A	Cross sectional area of the section
Z_x	Section modulus (X-axis)
I_x	Section moment of area (X-axis)
I_y	Section moment of area (Y-axis)
I_w	Section warping constant
X_o	Section shear centre (X-axis)
J	Section torsion constant
Q	Section form factor
X_o	Section shear centre (X-axis)
R_x	Radius of gyration (X-axis)
R_y	Radius of gyration (Y-axis)
L_x	Effective length (X-axis)
L_y	Effective length (Y-axis)
L_z	Torsional effective length
L_e	Effective length about the critical (X or Y) axis

Steel Properties

F_y	Yield stress
E	Youngs modulus
G	Shear modulus

	A	B	C	D	E	F	G	H	I	J
1	DESIGN OF AXIALLY LOADED COMPRESSION MEMBERS (C-SECTION STUDS)									
2	IN ACCORDANCE WITH AS 1538 - 1988									
3										
4	INPUT DATA									
5										
6	Section Properties:					Material Properties:				
7										
8	Area (gross)		215	mm2		Yield stress Fy		450	MPa	
9	Area (net)		215	mm2		Youngs modulus E		200000	MPa	
10	Section modulus Zx		7130	mm3		Shear modulus G		80000	MPa	
11	Section modulus Zy		2190	mm3						
12	Moment of area Ix		364000	mm4		Load Factor		1.00		
13	Moment of area Iy		75000	mm4						
14	Warping constant Iw		1.63E+08	mm6		ITERATION				
15	Radius of gyration Rx		41.1	mm						
16	Radius of gyration Ry		18.7	mm		Lateral load UDL		0.20	kN/m/stud	
17	Shear centre Xo		23.9	mm		Initial eccentricity		6.00	mm	
18	Form factor Q		0.68			Iterate to get 1		1.00		
19	Torsion constant J		72	mm4						
20	Effective length Lx (H		3600	mm		UDL deflection		6.01	mm	
21	Effective length Ly		300	mm		Equivalent UDL (P)		0.13	kN/m/stud	
22	Effective length Lz		300	mm		Total eccentricity		16.00	mm	
23	Web thickness t		1.15	mm		Maximum stud load		17.91	kN	
24						Deflection limit L/240		15.00	mm	
25	CALCULATIONS									
26										
27	Omega			1.00						
28	Elastic buckling stress Fox			257	MPa					
29	Elastic buckling stress Foy			7670	MPa					
30	Polar radius of gyration Ro1			51	mm					
31	Torsional buckling stress Foz			6374	MPa					
32	Buckling stress Foxz (+)			8231	MPa					
33	Buckling stress Foxz (-)			255	MPa					
34	Foxz			255	MPa					
35	Smaller of Foy and Foxz is Foc			255	MPa					
36	Imperfection factor N			0.68						
37	Foc/QFy			0.83						
38	1+N			1.68						
39	Maximum permissible stress Fa			129	MPa					
40	Cmx			0.85						
41	Flex. tors. buckling stress Fob			10777	MPa					
42	Fbx			382	MPa					
43	Smaller of Fbx and 0.6*Fy			270	MPa					
44	fa/Fa+fbx/Fbx <=1			1						
45	Maximum stud load			17912	N					

Figure A1: AS 1538 - Spreadsheet calculation

	A	B	C	D	E	F	G	H	I
1	DESIGN OF AXIALLY LOADED COMPRESSION MEMBERS (C-SECTION STUDS)								
2	IN ACCORDANCE WITH BS 5950 : Part 5 : 1987								
3									
4	INPUT DATA								
5									
6	Section Properties:					Material Properties:			
7									
8	Area (gross)		215	mm2		Yield stress Fy		450	MPa
9	Area (net)		215	mm2		Youngs modulus E		200000	MPa
10	Section modulus Zx		7130	mm3		Shear modulus G		80000	MPa
11	Section modulus Zy		2190	mm3					
12	Moment of area Ix		364000	mm4		ITERATION			
13	Moment of area Iy		75000	mm4					
14	Warping constant Cw		1.63E+08	mm6		Lateral load UDL		0.20	kN/m/stud
15	Radius of gyration Rx		41.1	mm		Initial eccentricity		6.00	mm
16	Radius of gyration Ry		18.7	mm		Iterate to get 1		1.00	
17	Shear centre Xo		23.9	mm					
18	Form factor Q		0.68			UDL deflection		6.01	mm
19	Torsion constant J		72	mm4		Equivalent UDL (P)		0.18	
20	Effective length Lx (H		3600	mm		Total eccentricity		17.31	
21	Effective length Ly		1800	mm		Maximum stud load		23.79	kN
22	Effective length Lz		1800	mm		Deflection limit L/240		15.00	mm
23	Web thickness t		1	mm					
24									
25									
26	CALCULATIONS				X-axis	Y-axis		Critical	
27									
28	Elastic buckling load Pex				55441		N		
29	Elastic buckling load Pey					45693	N		
30	Polar radius of gyration Ro			51	mm				
31	Factor B			0.78					
32	Torsional buckling load Pt			78300	N				
33	Tors./flex. buckling load Ptf			43522	N				
34	Factor A			1.02					
35	Short strut capacity Pcs			65790	N				
36	El. flex. buckling load Pe				55441	43522	N		
37	Perry coefficient N				0.14	0.15			
38	Axial load Pc				42112	35664	N	35664	N
39									
40	Fc/Pc + Mx/Mc = 1			1					
41	Maximum stud load			23792	N				
42	Maximum stud load			23.79	kN				

Figure A2: BS 5950 : Part 5 - Spreadsheet calculation

	A	B	C	D	E	F	G	H	I
1	DESIGN OF AXIALLY LOADED COMPRESSION MEMBERS (C-SECTION STUDS)								
2	IN ACCORDANCE WITH LRFD COLD-FORMED STEEL DESIGN MANUAL (AISI)								
3									
4	INPUT DATA								
5									
6	Section Properties:					Material Properties:			
7									
8	Area (gross)		215	mm2		Yield stress Fy		450	MPa
9	Area (net)		215	mm2		Youngs modulus E		200000	MPa
10	Section modulus Zx		7130	mm3		Shear modulus G		80000	MPa
11	Section modulus Zy		2190	mm3					
12	Moment of area Ix		364000	mm4		Load factor P (0.85)		1.00	
13	Moment of area Iy		75000	mm4		Load factor M (0.9)		1.00	
14	Warping constant Cw		1.63E+08	mm6		Cmx (0.85)		1.00	
15	Radius of gyration Rx		41.1	mm					
16	Radius of gyration Ry		18.7	mm		ITERATION			
17	Shear centre Xo		23.9	mm					
18	Form factor Q		0.68			Lateral load UDL		0.20	kN/m/stud
19	Torsion constant J		72	mm4		Initial eccentricity		6.00	mm
20	Effective length Lx (H		3600	mm		Iterate to get 1		1.00	
21	Effective length Ly		1800	mm					
22	Effective length Lz		1800	mm		UDL deflection		6.01	mm
23	Flange thickness t		3	mm		Equivalent UDL (P)		0.12	
24	Flange width w		30	mm		Total eccentricity		15.66	
25						Maximum stud load		16.38	kN
26						Deflection limit L/240		15.00	mm
27									
28					X-axis	Y-axis			
29	CALCULATIONS								
30									
31	Elastic buckling stress Fex				257		N		
32	Elastic buckling stress Fey					213	N		
33	Polar radius of gyration Ro			51	mm				
34	Factor B			0.78					
35	Torsional buckling stress Ft			187	N				
36	Tors./flex. buckling stress Fe			146	N				
37	Nominal buckling stress Fn			146	N				
38	Design axial strength Pn1			21293	N				
39	Design axial strength Pn2			165134	N				
40	Design axial strength Pn			21293	N				
41	Design strength			21293	N				
42	Pa/Pn + Ma/Mnx = 1			1					
43	Maximum stud load			16383	N				
44	Maximum stud load			16.38	kN				

Figure A3: AISI 1991 - Spreadsheet calculation

APPENDIX B

TYPICAL TASEF RESULT FILE
(Including Input Data)

```
                    T A S E F   v 3.0   P C

                        Designed by Ulf Wickstr"m
                  Swedish National Testing and Research Institute (SP)
                          Tel int. +46 33 16 50 00

      Licenced user : University of Canterbury, NOT for commercial use

      TASEF is copyrighted by SP. The buyer is prohibited from
      making copies to a third party.

      SP is not liable for the results from TASEF, nor for their
      interpretation. The user must be aware of the limitations and
      assumptions of the model. It is the user's responsibility to
      assure that input data are appropriate and to check that the
      results are within reasonable limits.

TITLE OF RUN : 100mm LSF and 12.5mm Gib

GEOMETRY
********
MAXIMUM COORDINATES              XMAX= .1270          YMAX= .3000
MAXIMUM ELEMENT LENGTH           XBOX= .1270          YBOX= .3000

SUBREGIONS
NUMBER OF SUBREGIONS    5

SUBREGION DIAGONAL LIMITS

     XMIN         YMIN         XMAX         YMAX         FICTITIOUS AREA

   .0000        .0000        .1250E-01    .3000              F
   .1250E-01    .0000        .1350E-01    .2500              F
   .1350E-01    .0000        .1135        .2990              T
   .1135        .0000        .1145        .2500              F
   .1145        .0000        .1270        .3000              F


COORDINATES OF SPECIFIED X - LINES

  .3000E-02    .6000E-02    .9000E-02    .3800E-01    .6350E-01    .1015

  .1180        .1210        .1240


COORDINATES OF SPECIFIED Y - LINES

  .4000E-01    .8000E-01    .1200        .1600        .2000        .2400

NUMBER AND COORDINATES OF X - LINES

15 -     .0000        .3000E-02    .6000E-02    .9000E-02    .1250E-01
         .1350E-01    .3800E-01    .6350E-01    .1015        .1135
         .1145        .1180        .1210        .1240        .1270

NUMBER AND COORDINATES OF Y-LINES

10 -     .0000        .4000E-01    .8000E-01    .1200        .1600
         .2000        .2400        .2500        .2990        .3000
```

NUMBER OF NODES= 150 NUMBER OF ELEMENTS= 126

COUPLED NODES
****

MASTER	SLAVES
41	51
42	52
43	53
44	54
45	55
46	56
47	57
48	49 50 60 59 58
69	70
79	80
89	90
98	99 100 110 109 108
97	107
96	106
95	105
94	104
93	103
92	102
91	101

MATERIAL DATA
****

REGION NUMBER 1
STM2 THICKNESS 1.000

TEMP	CONDUCTIVITY
0.	.6000E+02
800.	.2700E+02
2000.	.2700E+02

TEMP	ENTHALPY	ENT/TEMP
0.	.0000E+00	.1085E+04
200.	.2169E+06	.1085E+04
400.	.4661E+06	.1165E+04
600.	.7581E+06	.1264E+04
700.	.9269E+06	.1324E+04
800.	.1192E+07	.1490E+04
1200.	.1766E+07	.1472E+04

REGION NUMBER 2
GYPSUM THICKNESS 1.000
Conductivity is kept constant after reaching maximum temperature

TEMP	CONDUCTIVITY	TEMP	ENTHALPY	ENT/TEMP
0.	.2500E+00	0.	.0000E+00	.1971E+03
70.	.2500E+00	100.	.1971E+05	.1971E+03
130.	.1300E+00	110.	.7484E+05	.6803E+03
300.	.1300E+00	140.	.1334E+06	.9529E+03
800.	.1800E+00	220.	.1846E+06	.8390E+03
1000.	.3500E+00	320.	.2031E+06	.6347E+03
1500.	.7750E+00	350.	.2086E+06	.5961E+03
4000.	.1000E+02	4000.	.1000E+07	.2500E+03

REGION NUMBER 3
SIMULATION THICKNESS 1.000
Conductivity is kept constant after reaching maximum temperature

TEMP	CONDUCTIVITY	TEMP	ENTHALPY	ENT/TEMP
0.	.1000E+03	0.	.0000E+00	.2500E+00
4000.	.1000E+03	4000.	.1000E+04	.2500E+00

REGION NUMBER 5
SIMULATION THICKNESS 1.000
Conductivity is kept constant after reaching maximum temperature

TEMP	CONDUCTIVITY	TEMP	ENTHALPY	ENT/TEMP
0.	.1000E+03	0.	.0000E+00	.2500E+00
4000.	.1000E+03	4000.	.1000E+04	.2500E+00

REGION NUMBER 6
GYPSUM THICKNESS 1.000
Conductivity is kept constant after reaching maximum temperature

TEMP	CONDUCTIVITY	TEMP	ENTHALPY	ENT/TEMP
0.	.2500E+00	0.	.0000E+00	.1971E+03
70.	.2500E+00	100.	.1971E+05	.1971E+03
130.	.1300E+00	110.	.7484E+05	.6803E+03
300.	.1300E+00	140.	.1334E+06	.9529E+03
800.	.1800E+00	220.	.1846E+06	.8390E+03
1000.	.3500E+00	320.	.2031E+06	.6347E+03
1500.	.7750E+00	350.	.2086E+06	.5961E+03
4000.	.1000E+02	4000.	.1000E+07	.2500E+03

```
INITIAL DATA
************
INITIAL TEMPERATURE= .160E+02
AMBIENT TEMPERATURE= .160E+02
STEFAN-BOLTZMANN CONSTANT= .567E-07
ABSOLUTE TEMPERATURE SHIFT= .273E+03

NODE GROUPS
***********
NODE GROUP  1
EMISSIVITY= .800
CONVECTION FACTOR= 1.00
CONVECTION POWER= 1.33
NODES    1    2    3    4    5    6    7    8    9   10

NODE GROUP  2
EMISSIVITY= .600
CONVECTION FACTOR= 1.00
CONVECTION POWER= 1.33
NODES   51   52   53   54   55   56   57   58

NODE GROUP  3
EMISSIVITY= .800
CONVECTION FACTOR= 1.00
CONVECTION POWER= 1.33
NODES   58   59   69   79   89   99   98

NODE GROUP  4
EMISSIVITY= .600
CONVECTION FACTOR= 1.00
CONVECTION POWER= 1.33
NODES   98   97   96   95   94   93   92   91

NODE GROUP  5
EMISSIVITY= .600
CONVECTION FACTOR= 2.20
CONVECTION POWER= 1.33
NODES  141  142  143  144  145  146  147  148  149  150

PRESCRIBED HEAT FLUX BOUNDARY
*****************************
NODE GROUPS AND TYPES OF BOUNDARIES

NODE GROUP  1 FIRE BOUNDARY
NODE GROUP  5 AMBIENT BOUNDARY

GENERATED/PRESCRIBED HEAT
*************************
NUMBER OF GENERATED/PRESCRIBED HEAT GROUPS =  0

VOIDS
*****
NUMBER OF VOIDS= 1
VOID NUMBER 1 IS SURROUNDED BY THE FOLLOWING NODE GROUP(S)  2  3  4
VOID NUMBER 1 IS SYMMETRICAL AROUND THE X-AXIS
```

```
TIME
****
MAXIMUM TIME=.800
MAXIMUM TIME INCREMENT=.100
CRITICAL TIME INCREMENT FACTOR=.800
MAXIMUM NUMBER OF TIME INCREMENTS=10000
NUMBER OF STEPS BETWEEN UPDATING OF CONDUCTION MATRIX=     1
 PRINT OUT TIMES    .00     .50E-01.10     .15     .20     .25     .30     .35
                   .40     .45     .50     .55     .60     .65     .70     .80
INTERFACE NODES
***************
-1 - FICTITIOUS NODE
 0 - INTERFACE NODE
 1 - HOMOGENEOUS NODE

           2  2  2  2  2  2  2  2  2  2

           2  2  2  2  2  2  2  2  2  2

           2  2  2  2  2  2  2  2  2  2

           2  2  2  2  2  2  2  2  2  2

           0  0  0  0  0  0  0  0  0  0

           0  0  0  0  0  0  0  0  0  0

          -1 -1 -1 -1 -1 -1 -1 -1  1  1

          -1 -1 -1 -1 -1 -1 -1 -1  1  1

          -1 -1 -1 -1 -1 -1 -1 -1  1  1

           0  0  0  0  0  0  0  0  0  0

           0  0  0  0  0  0  0  0  0  0

           6  6  6  6  6  6  6  6  6  6

           6  6  6  6  6  6  6  6  6  6

           6  6  6  6  6  6  6  6  6  6

           6  6  6  6  6  6  6  6  6  6

FIRE BOUNDARY TEMPERATURE
*************************
ISO STANDARD FIRE CURVE ASSUMED
FIRE DURATION: .80
```

```
****** TIME    .000 ****** INCREMENT NUMBER     1 *****************
FIRE TEMPERATURE    16.  ******    TIME INCREMENT LIMITING NODE    0

ENCLOSURE AIR TEMPERATURE
VOID NUMBER 1   TAIR=   0.

  16.   16.   16.   16.   16.   16.   16.   16.   16.   16.
  16.   16.   16.   16.   16.   16.   16.   16.   16.   16.
  16.   16.   16.   16.   16.   16.   16.   16.   16.   16.
  16.   16.   16.   16.   16.   16.   16.   16.   16.   16.
  16.   16.   16.   16.   16.   16.   16.   16.   16.   16.
  16.   16.   16.   16.   16.   16.   16.   16.   16.   16.
   0.    0.    0.    0.    0.    0.    0.    0.   16.   16.
   0.    0.    0.    0.    0.    0.    0.    0.   16.   16.
   0.    0.    0.    0.    0.    0.    0.    0.   16.   16.
  16.   16.   16.   16.   16.   16.   16.   16.   16.   16.
  16.   16.   16.   16.   16.   16.   16.   16.   16.   16.
  16.   16.   16.   16.   16.   16.   16.   16.   16.   16.
  16.   16.   16.   16.   16.   16.   16.   16.   16.   16.
  16.   16.   16.   16.   16.   16.   16.   16.   16.   16.
  16.   16.   16.   16.   16.   16.   16.   16.   16.   16.

****** TIME    .400 ****** INCREMENT NUMBER   951 *****************
  FIRE TEMPERATURE   805.  ******    TIME INCREMENT LIMITING NODE  150

 ENCLOSURE AIR TEMPERATURE
 VOID NUMBER 1   TAIR= 240.

 779.  779.  779.  779.  779.  778.  776.  776.  776.  776.
 683.  682.  682.  681.  680.  677.  670.  668.  667.  667.
 585.  585.  585.  583.  581.  575.  562.  559.  558.  558.
 488.  488.  487.  485.  481.  473.  455.  449.  448.  448.
 374.  374.  373.  370.  366.  355.  332.  322.  322.  322.
 374.  374.  373.  370.  366.  355.  332.  322.  322.  322.
   0.    0.    0.    0.    0.    0.    0.    0.  265.  265.
   0.    0.    0.    0.    0.    0.    0.    0.  223.  223.
   0.    0.    0.    0.    0.    0.    0.    0.  159.  159.
 129.  129.  128.  126.  123.  123.  130.  134.  134.  134.
 129.  129.  128.  126.  123.  123.  130.  134.  134.  134.
 100.  100.  100.   99.   98.   97.  100.  100.  100.  100.
  86.   86.   85.   85.   84.   84.   85.   86.   86.   86.
  75.   75.   75.   74.   74.   74.   74.   75.   76.   76.
  67.   67.   67.   66.   66.   66.   66.   67.   67.   67.
```

****** TIME .800 ****** INCREMENT NUMBER 1778 **********

FIRE TEMPERATURE 908. ****** TIME INCREMENT LIMITING NODE 150

ENCLOSURE AIR TEMPERATURE
VOID NUMBER 1 TAIR= 456.

889.	889.	889.	889.	889.	889.	888.	888.	888.	888.
815.	815.	815.	815.	815.	814.	811.	810.	810.	810.
724.	724.	724.	724.	723.	722.	716.	715.	714.	714.
631.	631.	631.	630.	629.	627.	619.	616.	616.	616.
519.	519.	519.	518.	517.	514.	503.	498.	498.	498.
519.	519.	519.	518.	517.	514.	503.	498.	498.	498.
0.	0.	0.	0.	0.	0.	0.	0.	465.	465.
0.	0.	0.	0.	0.	0.	0.	0.	451.	451.
0.	0.	0.	0.	0.	0.	0.	0.	421.	421.
401.	401.	400.	399.	399.	399.	403.	405.	405.	405.
401.	401.	400.	399.	399.	399.	403.	405.	405.	405.
286.	286.	285.	285.	284.	284.	288.	290.	290.	290.
191.	191.	190.	189.	189.	189.	193.	194.	195.	195.
113.	112.	112.	111.	111.	112.	114.	116.	117.	117.
94.	94.	93.	93.	93.	93.	95.	96.	96.	96.

MAXIMAL TEMPERATURES
ISO834
XMAX= .127 YMAX= .300

889.	889.	889.	889.	889.	889.	888.	888.	888.	888.
815.	815.	815.	815.	815.	814.	811.	810.	810.	810.
724.	724.	724.	724.	723.	722.	716.	715.	714.	714.
631.	631.	631.	630.	629.	627.	619.	616.	616.	616.
519.	519.	519.	518.	517.	514.	503.	498.	498.	498.
519.	519.	519.	518.	517.	514.	503.	498.	498.	498.
0.	0.	0.	0.	0.	0.	0.	0.	465.	465.
0.	0.	0.	0.	0.	0.	0.	0.	451.	451.
0.	0.	0.	0.	0.	0.	0.	0.	421.	421.
401.	401.	400.	399.	399.	399.	403.	405.	405.	405.
401.	401.	400.	399.	399.	399.	403.	405.	405.	405.
286.	286.	285.	285.	284.	284.	288.	290.	290.	290.
191.	191.	190.	189.	189.	189.	193.	194.	195.	195.
113.	112.	112.	111.	111.	112.	114.	116.	117.	117.
94.	94.	93.	93.	93.	93.	95.	96.	96.	96.

MAX-TIME .80 NUMBER OF TIME INCREMENTS 1778

FIRE ENGINEERING RESEARCH REPORTS

95/1	**Full Residential Scale Backdraft**	**I. B. Bolliger**
95/2	**A Study of Full Scale Room Fire Experiments**	**P. A. Enright**
95/3	**Design of Load-bearing Light Steel Frame Walls for Fire Resistance**	**J. T. Gerlich**
95/4	**Full Scale Limited Ventilation Fire Experiments**	**D. J. Millar**
95/5	**An Analysis of Domestic Sprinkler Systems for Use in New Zealand**	**F. Rahmanian**

School of Engineering
University of Canterbury
Private Bag 4800
Christchurch, New Zealand

Phone 643 366-7001
Fax 643 364-2758

FIRE ENGINEERING RESEARCH REPORTS

95/1	Full Residential Scale Backdraft	I B Bolliger
95/2	A Study of Full Scale Room Fire Experiments	P A Enright
95/3	Design of Load-bearing Light Steel Frame Walls for Fire Resistance	J T Gerlich
95/4	Full Scale Limited Ventilation Fire Experiments	D J Millar
95/5	An Analysis of Domestic Sprinkler Systems for Use in New Zealand	F Rahmanian
96/1	The Influence of Non-Uniform Electric Fields on Combustion Processes	M A Belsham
96/2	Mixing in Fire Induced Doorway Flows	J M Clements
96/3	Fire Design of Single Storey Industrial Buildings	B W Cosgrove
96/4	Modelling Smoke Flow Using Computational Fluid Dynamics	T N Kardos
96/5	Under-Ventilated Compartment Fires - A Precursor to Smoke Explosions	A R Parkes
96/6	An Investigation of the Effects of Sprinklers on Compartment Fires	M W Radford
97/1	Sprinkler Trade Off Clauses in the Approved Documents	G J Barnes
97/2	Risk Ranking of Buildings for Life Safety	J W Boyes
97/3	Improving the Waking Effectiveness of Fire Alarms in Residential Areas	T Grace
97/4	Study of Evacuation Movement through Different Building Components	P Holmberg
97/5	Domestic Fire Hazard in New Zealand	KDJ Irwin
97/6	An Appraisal of Existing Room-Corner Fire Models	D C Robertson
97/7	Fire Resistance of Light Timber Framed Walls and Floors	G C Thomas
97/8	Uncertainty Analysis of Zone Fire Models	A M Walker
97/9	New Zealand Building Regulations Five Years Later	T M Pastore
98/1	The Impact of Post-Earthquake Fire on the Built Urban Environment	R Botting
98/2	Full Scale Testing of Fire Suppression Agents on Unshielded Fires	M J Dunn
98/3	Full Scale Testing of Fire Suppression Agents on Shielded Fires	N Gravestock
98/4	Predicting Ignition Time Under Transient Heat Flux Using Results from Constant Flux Experiments	A Henderson
98/5	Comparison Studies of Zone and CFD Fire Simulations	A Lovatt
98/6	Bench Scale Testing of Light Timber Frame Walls	P Olsson
98/7	Exploratory Salt Water Experiments of Balcony Spill Plume Using Laser Induced Fluorescence Technique	E Y Yii
99/1	Fire Safety and Security in Schools	R A Carter
99/2	A Review of the Building Separation Requirements of the New Zealand Building Code Acceptable Solutions	J M Clarke
99/3	Effect of Safety Factors in Timed Human Egress Simulations	K M Crawford
99/4	Fire Response of HVAC Systems in Multistorey Buildings: An Examination of the NZBC Acceptable Solutions	M Dixon
99/5	The Effectiveness of the Domestic Smoke Alarm Signal	C Duncan

99/6	**Post-flashover Design Fires**	**R Feasey**
99/7	**An Analysis of Furniture Heat Release Rates by the Nordtest**	**J Firestone**
99/8	**Design for Escape from Fire**	**I J Garrett**
99/9	**Class A Foam Water Sprinkler Systems**	**D B Hipkins**
99/10	**Review of the New Zealand Standard for Concrete Structures (NZS 3101) for High Strength and Lightweight Concrete Exposed to Fire**	**M J Inwood**
99/12	**An Analytical Model for Vertical Flame Spread on Solids: An Initial Investigation**	**G A North**
99/13	**Should Bedroom Doors be Open or Closed While People are Sleeping? - A Probabilistic Risk Assessment**	**D L Palmer**
99/14	**Peoples Awareness of Fire**	**S J Rusbridge**
99/15	**Smoke Explosions**	**B J Sutherland**
99/16	**Reliability of Structural Fire Design**	**JKS Wong**
00/1	**Fire Spread on Exterior Walls**	**FNP Bong**
00/2	**Fire Resistance of Lightweight Framed Construction**	**PCR Collier**
00/3	**Fire Fighting Water: A Review of Fire Fighting Water Requirements (A New Zealand Perspective)**	**S Davis**
00/4	**The Combustion Behaviour of Upholstered Furniture Materials in New Zealand**	**H Denize**
00/5	**Full-Scale Compartment Fire Experiments on Upholstered Furniture**	**N Girgis**
00/6	**Fire Rated Seismic Joints**	**M James**
00/7	**Fire Design of Steel Members**	**K R Lewis**
00/8	**Stability of Precast Concrete Tilt Panels in Fire**	**L Lim**
00/9	**Heat Transfer Program for the Design of Structures Exposed to Fire**	**J Mason**
00/10	**An Analysis of Pre-Flashover Fire Experiments with Field Modelling Comparisons**	**C Nielsen**
00/11	**Fire Engineering Design Problems at Building Consent Stage**	**P Teo**
00/12	**A Comparison of Data Reduction Techniques for Zone Model Validation**	**S Weaver**
00/13	**Effect of Surface Area and Thickness on Fire Loads**	**H W Yii**

School of Engineering
University of Canterbury
Private Bag 4800, Christchurch, New Zealand

Phone 643 364-2250
Fax 643 364-2758